UCLouvain

epl

École polytechnique de Louvain

Conception of a bidirectional and wireless power transfer for satellite applications

Author: **Thomas BALDWIN**
Supervisor: **Marc BEKEMANS**
Readers: **Marc BEKEMANS, Emmanuel DE JAEGER, Quentin DELHAYE**
Academic year 2021–2022
Master [120] in Electrical Engineering

Abstract

Trough the years, satellites are becoming way more present around the earth. With this exponential increase, the risk of malfunction of some of them becomes unavoidable. It is in this context that on-orbit service will take place in a near future. This service will allow to replace some dysfunctional parts of satellites in order to fix them.

In this master thesis, a solution is explored concerning a way to replace a dysfunctional battery if needed. This solution needs to implement a wireless bidirectional power transfer between the battery and the main power bus of the satellite.

At first, the best topology is considered. Then, a detailed study is performed about this solution. In the end, the results of the implemented solution by simulation and prototyping are shown in order to validate the design.

Acknowledgements

This work would never have been possible if I had not had the precious help of several people who have followed and encouraged me throughout this project.

First of all, I would like to give my very heartfelt thanks to my supervisor, the Professor Marc Bekemans, for all the involvement, the innumerable advises and the trust he gave me.

I would also like to thank the whole team at Thales Alenia Space for their welcome, their time and their help.

Finally, I would like to share a special thank with my parents, who knew how to be always present when I needed it.

Contents

List of Figures

List of Tables

1 | Introduction

In a world where innovation is the key of future technologies developments, humankind is more and more looking towards space : the aim is to push forward the satellites capabilities and to make our lives safer and more comfortable, providing us with conveniences such as communication means or meteorology data, or even broadcast entertainment.

Almost no satellite ever sent in space is a dead piece of metal roaming in the deep cold of the interspace. Many of them are indeed carrying a lot of advanced equipments and share essential data with earth's users, and these equipments obviously require energy to operate.

To supply all the onboard electric devices, satellites are equipped with solar arrays that convert solar energy into electricity. However, there are times when the gathered energy is greater than the consumed one - and times when satellites need to continue to operate when the sun energy is out of reach. This is why they are also equipped with batteries, storing the energy in order to restore it later when required.

However, there are many drawbacks to the massive investments and launch of satellites. Due to extreme conditions and intrinsic fatigue of the components, all satellites can fall out of service due to a software, electronics or hardware problem (like mechanical wear or debris damages). Looking at the increase of space launches, it can be guessed that in the near future on-orbit services will emerge to replace or repair defective satellites assemblies, thus avoiding further technological wastes in space and reduce the financial and environmental impacts.

The aim of this master thesis is to anticipate this evolution by working on a subset of an interchangeable smart battery system for satellites that will be able to efficiently transmit power both ways between the battery and the satellite power bus with no physical connection. This thesis has been conducted in collaboration with Thales Alenia Space Belgium in order to be able to collaborate, benefit from their huge experience, get access to materials and laboratory in order to combine both theoretical and practical live measurements. Designing, building and characterizing a prototype of a Wireless Power Transfer (WPT) sub-system for satellites as proof of concept is the major achievement this thesis will cover.

This paper will give a thorough description of the steps that have been undertaken for the accomplishment of this work. It states all the context behind this project, follows the engineering path that was chosen and describes the final obtained results. In order to take the reader on a journey, a common thread goes through the writing, takes the path of the state of the art and reminds some theory, concludes on the choices and then incrementally applies improvements on the model in order to achieve the most successful final solution within the allotted time. Finally, improvement tracks are discussed.

First, an abstract on the spatial context in which the project register and all the specifications of the industrial need will be found in Chapter 2.

In Chapter 3, a State Of The Art of the existing wireless power transfer technologies will be depicted in order to achieve the best solution for the required specifications and some essential studies will be done on selected implementations.

In Chapter 4, the selected topology is analysed from a theoretical perspective in more details.

In Chapter 5, the practical design and the results that were achieved during this project are presented.

Finally, Chapter 6 will come back on the solution and elaborate on the results of this last and the perspectives of improvement.

2 | Global context and requirements

This chapter is a brief overview of the spatial context in which this thesis takes place. Indeed, space environment is very harsh compared to earth and satellites have specific requirements in order to operate as expected.

First, the environment and what it involves will be described, then, the global architecture of power units in satellites will be discussed for a better understanding of the main challenges and features for the final application design.

2.1 Spacial context

2.1.1 Working conditions

Space is the main environment where the satellites will operate for years or even for decades. However, the operating conditions are far from being harmless to electro-mechanic devices due to the following constraints [1]:

- **The launch:** During launch, equipment transported by the rocket will be subject to mechanic stress: vibrations can shatter sensitive parts of the equipments. Launch conditions tests on earth are required to overcome this.
- **Temperature:** Space temperatures range from extreme cold (hundreds of degrees below freezing), to hundreds of degrees above. The hardware must then be able to withstand high temperatures but also high variations in a small laps of time (e.g. temperature on the International Space Station can reach 130 °C when facing the sun and -160 °C when in complete dark).
- **Vacuum:** Electric devices in satellites do not have an efficiency of 100% resulting in heat losses. Due to the almost complete of vacuum, this heat can hardly be extracted by thermal convection.
- **Charged particles**: If a charge builds up that is too big for a material to withstand, discharge arcs called Electrostatic Discharge will take place. Depending on the discharge path, this can lead to electronic components or other systems damages.
- **Radiations:** Sun or other celestial bodies radiated emissions might cause important damages to electronic circuits or change memory-cells content of on board processors for example. They thus need to be protected from those external radiations.

2.1.2 Trajectories

Depending on the satellite mission and how it is designed, dedicated trajectories are selected. Those trajectories are called orbits and can be of different kinds. For Earth missions there is a path where the satellite does not orbit around Earth but which is still of interest, it is called a Lagrange orbit. This case is an exception given the fact that they navigate around the sun: on-orbit service is therefore currently impossible.

Around Earth orbits can be divided into five big categories [2][3], shown in Figure 2.1

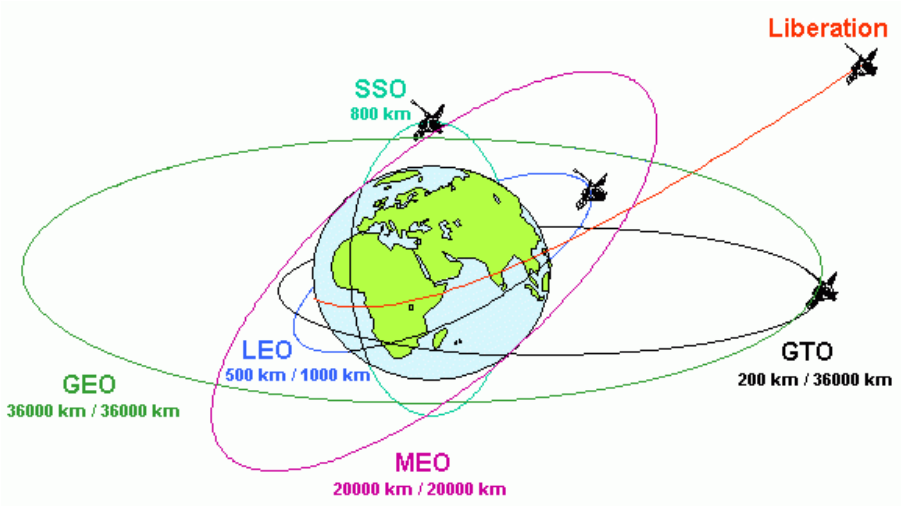

Figure 2.1: Satellites Earth orbits

- **Geosynchronous orbit** (GSO): Satellites in GSO circle follow Earth rotation synchronously. This requires 23 hours 56 minutes and 4 seconds, exactly the same time needed by the Earth to perform a complete rotation on itself. The satellite can also follow a path over the Equator. This orbit is called Geostationary orbit (GEO). Satellites in GSO come back at the same place in the sky at the same time each day but do not appear stationary contrary to GEO.
- **Low Earth orbit** (LEO): A low Earth orbit is an orbit that is relatively close to Earth's surface. It is normally at an altitude of less than 1000 km which is low compared to other orbits and do not need to follow a specific path contrary to GEO.
- **Medium Earth orbit** (MEO): Medium Earth orbit comprises a wide range of orbits anywhere between LEO and GEO. As LEO, it also does not need to take specific paths around Earth.
- **Polar orbit and Sun-synchronous orbit** (SSO): Satellites in polar orbits usually travel past Earth from north to south rather than from west to east, passing roughly over Earth's poles.
- **Transfer orbits and geostationary transfer orbit** (GTO): Transfer orbits are a special kind of orbit used to get from one orbit to another.

The orbit type is important before developing a satellite because the power management will be completely different from an orbit to another. For example, in a MEO, if the time needed to the satellite to fully "rotate" around the Earth is approximately 24 hours and, depending on the time of year, the satellite might experience short or no time of darkness each day.

In comparison, a satellite in a LEO configuration can perform the same rotation at a lower altitude in about 90 minutes with half of that in darkness. The amount of time without energy harvesting is quite short but it also means that during one half of the orbit the satellite must be able to recharge its battery enough for the rest of the orbit while functioning normally.

2.1.3 Power management in satellites

The under-laying requirements resulting from the satellite trajectories impact both the global energy management and power distribution system.

Power management in satellites can be represented as shown in the simplified Figure 2.2.

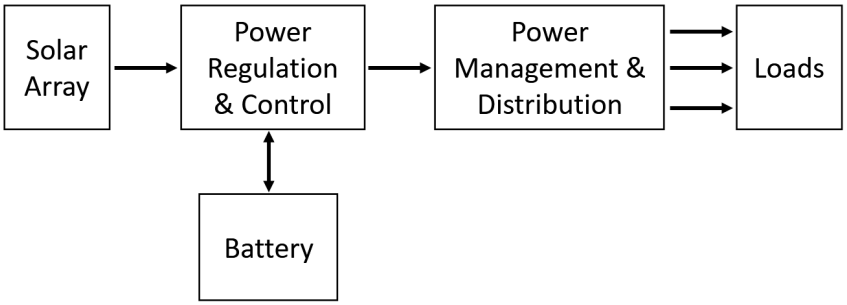

Figure 2.2: Design of Electrical Power Systems for Satellites

It is composed of:

- **Solar array(s)**, providing electricity converted from the sun energy;
- **A power regulation and control block** that manages the power flows in the satellite (e.g. charge and discharge of the battery, main bus voltage regulation, ...);
- **A Battery** that stocks electricity for periods of darkness and or high load consumption;
- **A power management and distribution** that manage the power distribution to the different loads (sensors, transmitters, ...).

2.1.3.1 Solar panels The electricity that will supply all the instrumentation in the satellite is harvested from the sun through solar arrays. These are composed of solar panels, themselves composed of solar cells [4].
All those cells, whose equivalent circuit can be found in Figure 2.3, can be placed in parallel or in series in order to reach the required bus voltage for the power and regulation module and have an efficiency of about 35%.

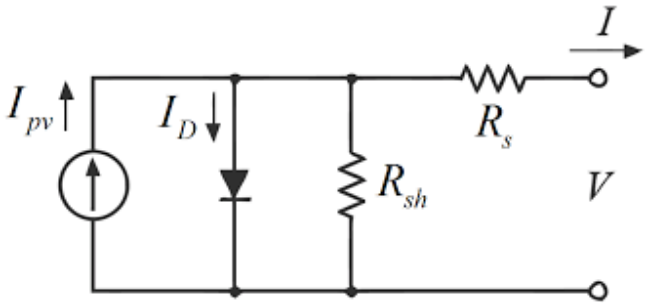

Figure 2.3: Equivalent circuit of a PV cell

The maximum available power out of a solar cell at a given moment only depends on its efficiency (at a given illumination). The above model shows a current source and a diode along with internal resistance. As a consequence, a solar cell exhibits an open-circuit voltage, resulting in a voltage but not current and similarly a short-circuit current at the cost of no output voltage. Those 2 limit cases obviously exhibits no power. The resulting power curve from the model is drawn in Figure 2.4:

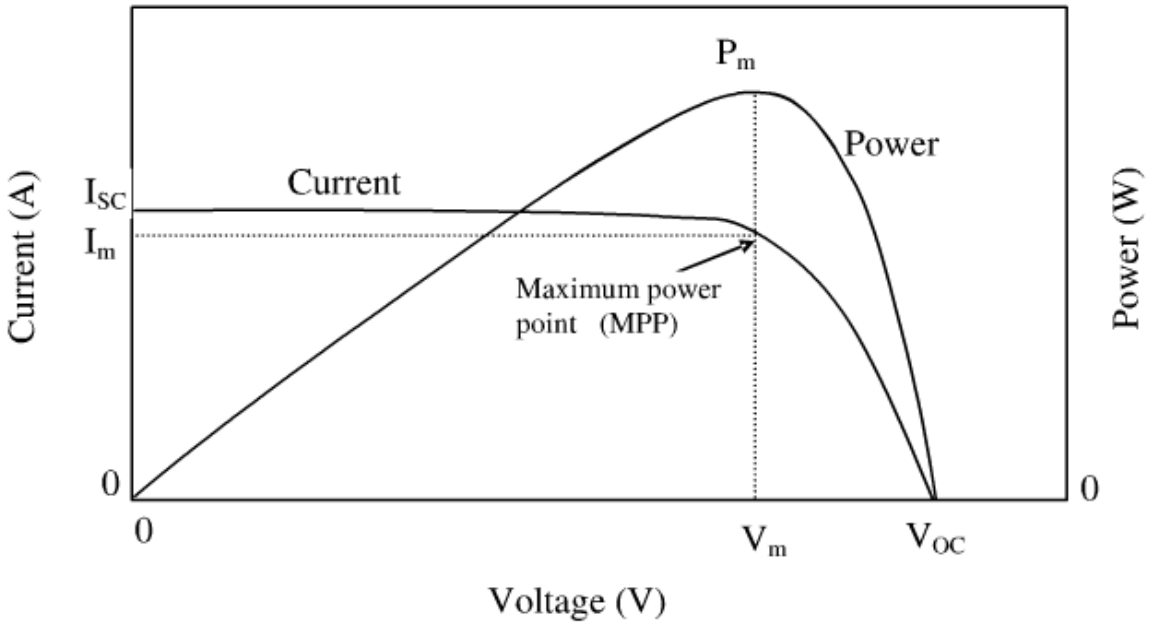

Figure 2.4: PV cell I-V curve and MPP

In order to control the amount of power produced by the solar cell, a brief look at the above I-V curve shows that for a given working (light) condition, a maximum power catch can only be achieved at a given point of the curve. The consequence is that the ouput voltage and current will vary for this to occur. The maximum power point (MPP) can be tracked in order to always harvest the maximum energy from the sun. Nevertheless this harvesting implies varying conditions at the input of the power regulation module, impacting the specifications of this module, detailed later.

2.1.3.2 Battery Batteries can be made of different technologies, but globally require the same charging schemes. Due to the chemistry, safe working areas must be obeyed [5].
The following situations will permanently damage the batteries:

- **Over & under charge-discharge** (i.e. voltage related)
- **Over-current**
- **Over-voltage**
- **Over & under temperature**

For a given battery pack, the above current, voltage, temperature limit values must be respected and dedicated control achieved, through a module generally called BMS (Battery Management System). The commonly used charging scheme is of CCCV type and is derived from the above requirements:

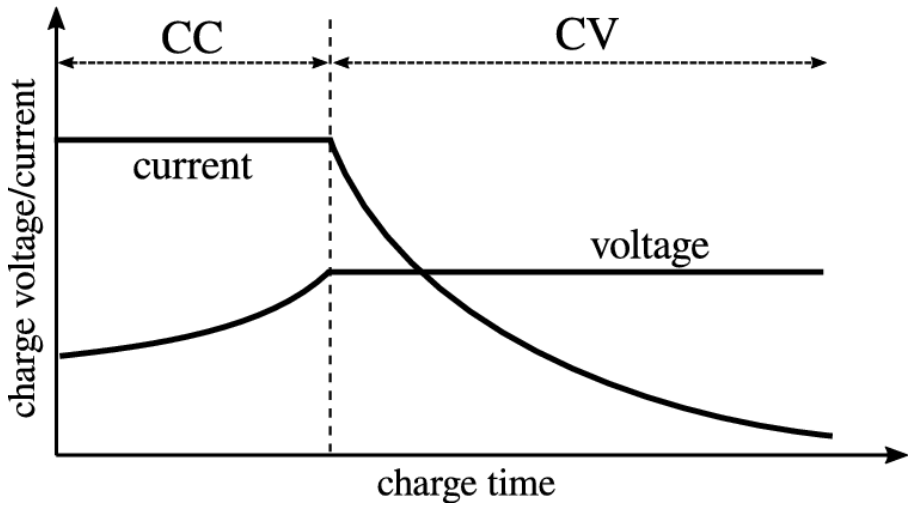

Figure 2.5: Constant current Constant voltage charging of batteries

In a CCCV, assuming the battery is not fully charged, it is initially charged at constant current (CC) in order to respect the maximum charge current constraint. When the battery is nearly full, its voltage reaches the maximum allowed value, and the current is reduced in order to respect the maximum voltage constraint. Thermal management and trickle charge is out of this scope.

2.1.3.3 Loads and power-management Available energy within the satellite is consumed by various loads. These loads and the energy sources must be controlled in order to achieve the satellite targeted operation. The power-management and distribution system ensures the global management.

2.1.3.4 Power regulation and control From the previous sub-systems descriptions, it appears that there will be a lot of power variations (power coming from the solar array(s) and from or to the battery). This is why a power regulation and control block is essential in order to regulate the power coming from the solar array, the power exchanged with the battery and the power transmitted to the loads.

2.2 Industrial impact

Now that the constraints and subsets have been briefly addressed, the needs of industrial demand will be analyzed in order to respond to the encountered problems and conclude on the technical requirements of the solution.

As a reminder, the purpose of this thesis is to anticipate the prospective on-orbit services. Service that will have as objective to fix broken satellites in space by offering the opportunity to replace a defective battery for example.

It is in this context that a different method to transfer power between the battery and power controller of the satellite **wirelessly** (without wired connection) will be studied. This needs to be achieved **in both directions**: from the battery to the main power bus during dark or high load periods and from the main power bus to the battery during high sunshine times where production is greater than consumption.

2.2.1 Full sub-system Specifications

A simplified diagram of the complete satellite, based on the previous writings, can be expressed like this:

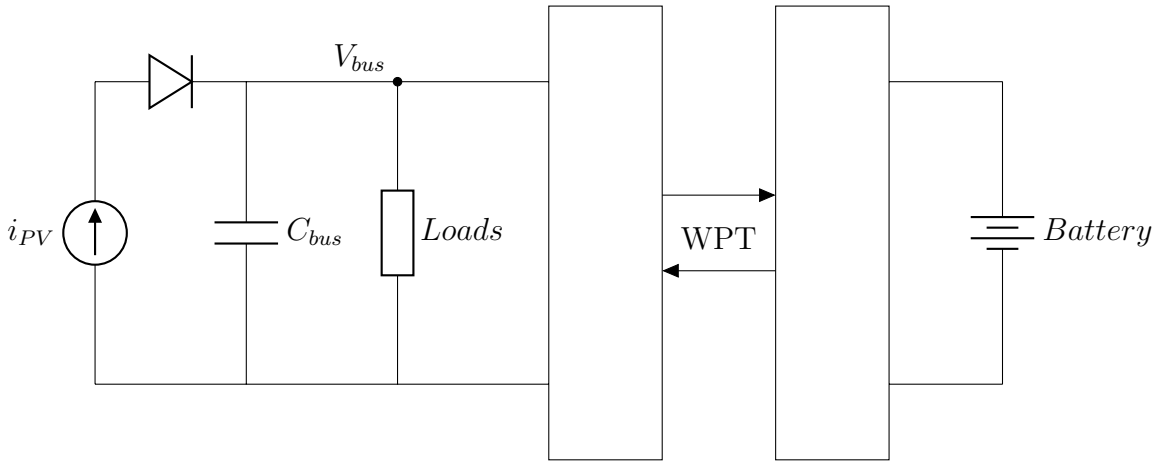

Figure 2.6: Simplified architecture

The major requirements for the entire satellite build are:

- Bidirectional Wireless Power Transmission (WPT);
- Main power bus voltage regulation;
- Battery protection;
- Under Voltage Protection of the battery (UVP);
- Battery disabling during the orbiting and replacement maneuver.

A detailed view of the battery sub-assembly coupler in the above diagram is then:

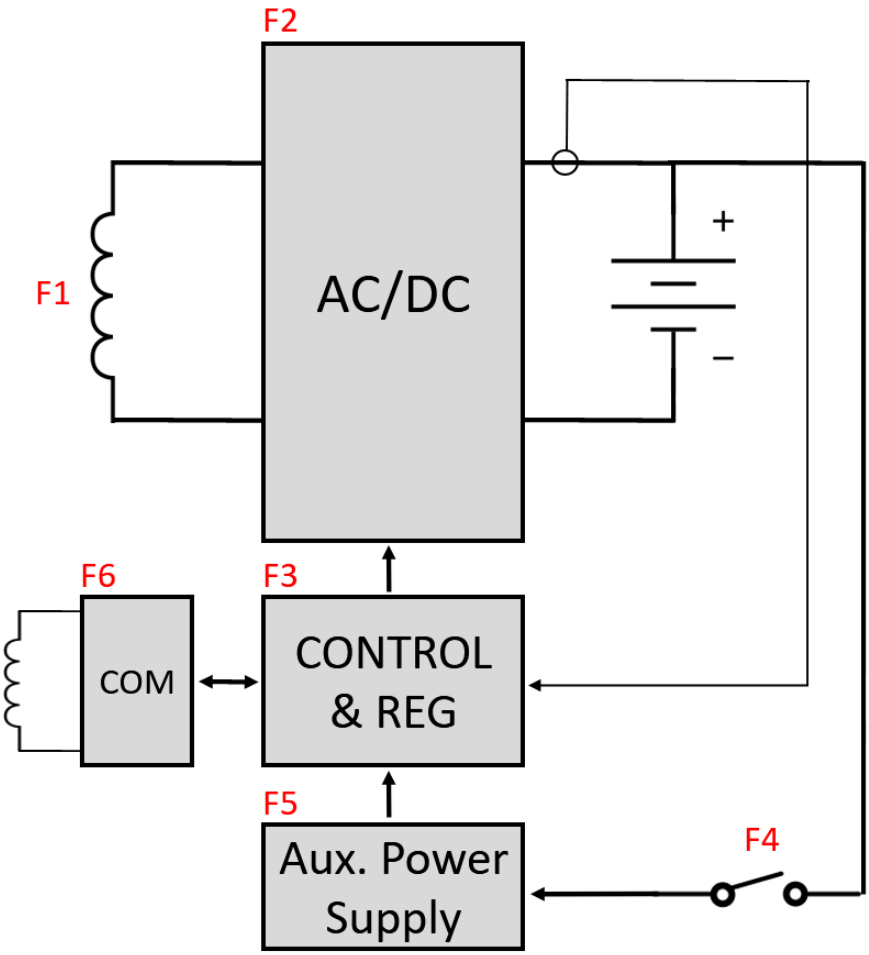

Figure 2.7: Detailed receiver side

Where the main functions that need to be implemented are:

- F1: Wireless Coupling for bidirectional WPT;
- F2: Voltage regulation;
- F3: Control & Regulation of the WPT;
- F4: Proximity switch to disconnect the battery during the launch from earth to its placement on the satellite;
- F5: Auxiliary power supply;
- F6: Communication with Power Regulation & Control on main satellite side.

2.2.2 Power Transfer sub-system requirements

This thesis investigates the wireless power transfer based on realistic objectives driven by the following constraints and facts:

- Off-the-shelf available space-grade components at Thales Alenia Space;
- Bench instruments limits;
- Trade-off between simulations and available time for experiments;

- Lead-time of printed circuit board and its assembly;
- Prototype debugging;
- Improvements;
- Measurements.

Based on the previous points, a datasheet-like specification (Table 6.1) of the system to be developed can be expressed:

	Minimum	**Maximum**
Power exchanged [W]	50	250
Bus voltage [V]	50	150
Battery voltage [V]	0	50
Output current [A]	2	5
Frequency of operation [kHz]	50	150
Efficiency [%]	90	-

Table 2.1: WPT specifications

In further reading we will focus on the contactless energy transfer as follows:

First, a state of the art will be achieved in order to select the best technology for the project. After this, the selected architecture will be studied and designed in order to perform simulations and prototyping. In the end, measurements and comparison will be shown to see the pertinence of the selected architecture related to the constraints evoked.

3 State of the art of contacless power transfer

The technology of wireless power transmission can eliminate the use of wires and sometimes batteries, thus improving an electronic device by increasing its mobility and versatility when interconnecting wires are not possible, not convenient or hazardous. The most known WPT application is known to almost anybody as the Qi standard [6] used nowadays in order to charge a cell phone from a charger or even to exchange power with another cell phone.

3.1 Principle and classification

WPT [7] is the transmission of electrical energy without wires as a physical link. In a wireless power transmission system (see Figure 3.1) the transmitter is directly connected to an energy source. To transmit this energy, this latter is converted into a time-varying electromagnetic field in order to be propagated trough the coupling device (or media). On the other side, a receiver captures the transmitted power and transmits it to an electrical load.
Each WPT topology has its own power converting circuit, its own coupling device or media and its own operating frequency. This leads to huge variations in achievable distance, nominal power transmitted and efficiency as it will be detailed here under.

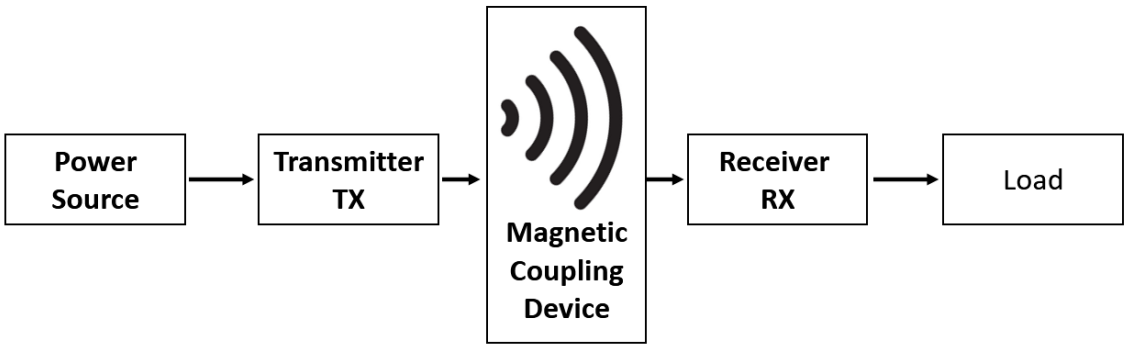

Figure 3.1: Principle of wireless power transfer

WPT can be classifed following two aspects:

- Achievable power and range;
- Underlaying technology.

Wireless power techniques can be classified [8] (Figure 3.2) into two main categories based on the ratio between the antenna diameter (and thus the radiation pattern) and the range of transmission: Non-Radiative Near-Field (NRNF) and Radiative Far-Field (RFF) WPT.

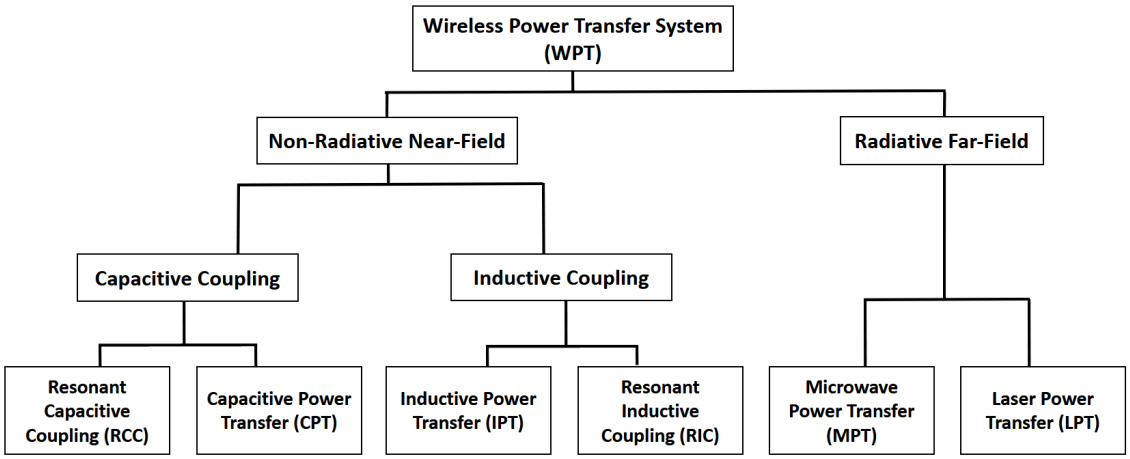

Figure 3.2: Classification of WPT

Comparison of the achievable power transferred and the achievable range for each technology can be depicted:

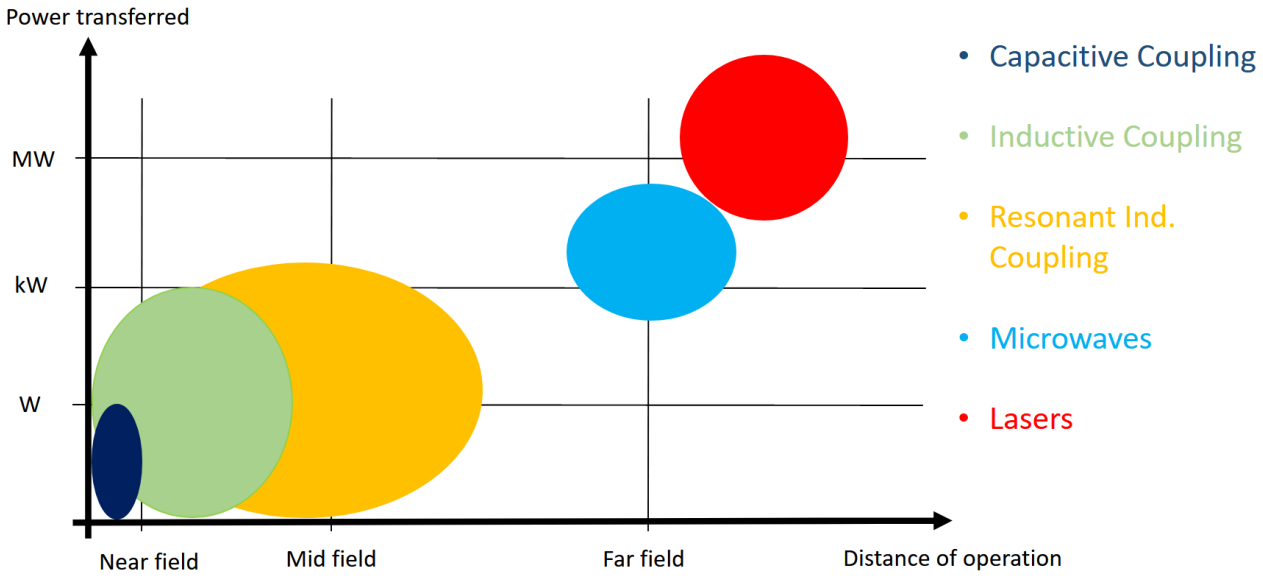

Figure 3.3: Comp

For the ease of comprehension, only the main topologies will be presented in the following subsections. A more detailed comparison can be found in Appendix A.

3.1.1 Non-Radiative Near-Field

First, the NRNF encompass all the power transfers where the receiver is located at a maximum of up to 10 times the coupling device diameter ($d_{Range} \leq 10 \cdot D_{Device}$). We call it non-radiative because if no coupling device is placed in the range of the transmitter, no power will be transmitted.

The NRNF can then be divided into two categories: capacitive or inductive couplings.

3.1.1.1 Capacitive coupling: Capacitive Coupling Wireless Power Transfer (CCWPT) is the transfer of alternating electrical signals or energy from one segment of a circuit to the other using a capacitor (Figure 3.4). The electrical field between the capacitor plates as coupling provides a medium for the ac signals while blocking the dc energy.

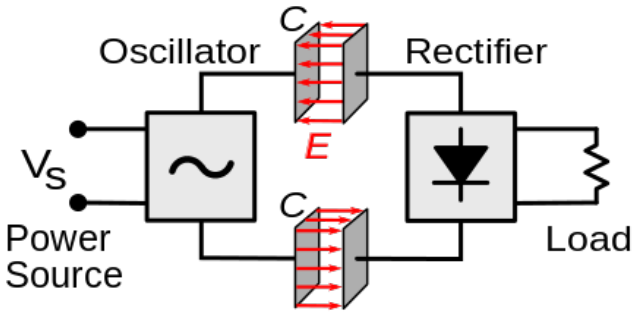

Figure 3.4: Capacitive coupling

This field is non-radiative, meaning the energy stays within a short range from the transmitter and that no energy is propagated by the transmitter if there are no receiver device. Furthermore, the strength of this electric field decays quadratically with the distance as it can be seen with a derivation of Coulomb's law where the electric field at a certain distance is expressed in function of a particle charge:

$$\overrightarrow{E} = \frac{1}{4\pi \cdot \epsilon_0} \cdot \frac{q}{r^2} \tag{3.1}$$

This means that if the distance between the two plates is much higher than the plate diameter, only a very small amount or sometimes none of the transmitted power will be received. In order to increase the efficiency and the range of the CCWPT, some compensation inductors can be added in series with the capacitors to create a resonance. It is called the resonant capacitive coupling.

The main advantages of CCWPT are the low cost of the topology and low eddy current losses in neighboring metals. This topology is used in many short range and low power applications such as integrated circuits or biomedical devices in order to achieve digital control signals isolation.

3.1.1.2 Inductive Coupling: Inductive power transfer first converts energy into a magnetic field in order to exploit induction between two coils that are used as coupling devices as it can be seen in Figure 3.5. In this case, transmitting and receiving coils form a transformer. As for the CCWPT, it is also a near-field WPT, meaning that if no coil is present in order to receive the energy, no power flows from the transmitting coil.

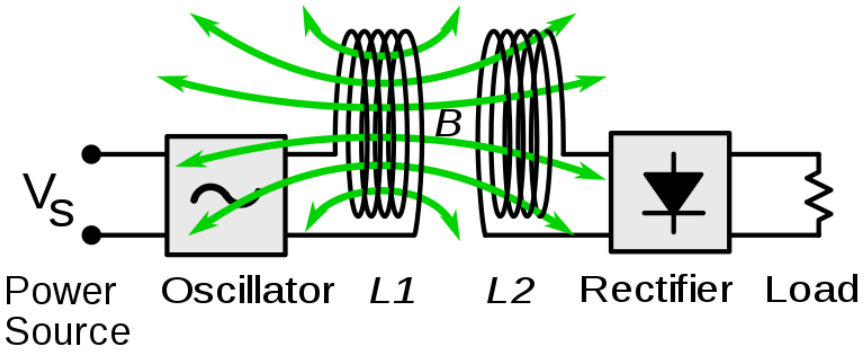

Figure 3.5: Generic block diagram of an inductive wireless power system

A more detailed study about this topology will be done in Section 3.3. The same resonance principle can be used in order to improve the efficiency and the range (detailled in Section 3.4).

Inductive coupling is the oldest and most widely used wireless power technology. It is used in many applications like cell phones, electric toothbrush, biomedical devices or even in bigger power demanding applications like the charge of electric vehicles.

3.1.2 Radiative Far-Field

On the other side, RFF techniques encompass all other power transfers where the transfer distance is greater than 10 times the coupling device diameter ($d_{Range} > 10 \cdot D_{Device}$) and can easily transmit power up to several kilometers or above. In order to reach these high distances, RFF convert the primary energy into electromagnetic waves at extremely high frequencies (up to several hundreds of GHz) with the help of antennas or lasers.

These techniques are called Radiative because there is no need of a receiver to have power flowing trough the transmitter due to the radiation of electromagnetic waves. Nevertheless, even if they can transport energy at longer distances, they must be aimed precisely at the receiver to work efficiently.

The RFF can be divided into two categories: micro-power transfer and laser power transfer.

3.1.2.1 Microwave: The microwave power transmission uses radio waves with wavelengths ranging from about one meter to one millimeter in order to transmit power at longer distance. To do so, it uses the electromagnetic radiation by using antenna as coupling devices as in Figure 3.6.

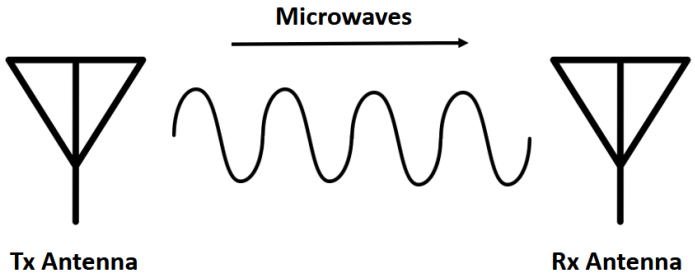

Figure 3.6: Microwave Power Transfer

Microwave technology has been proposed for the transmission of energy from orbiting solar power satellites to Earth or to supply mobile phones for example. Even if there seems to be a lot of potential in this technology and even if it has the advantage of being more directional, there are still a lot of drawbacks. To name a few: there are a lot of power losses due to microwave propagation, humans and other electrical systems may be exposed to excessive microwave radiation, and environmental changes due to the receiver movement may cut the link.

3.1.2.2 Lasers: In a laser power transmission, the source power is transmitted by converting electricity into a laser beam that is oriented towards a photovoltaic cell that converts this energy to electricity as shown in Figure 3.7

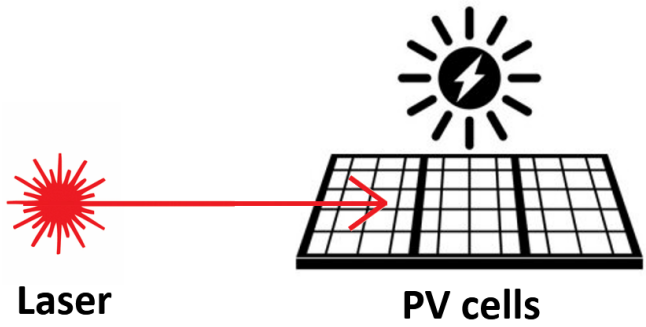

Figure 3.7: Laser Power Transfer

This technology has been mainly used for military and aerospace applications but nowadays still exhibits too much drawbacks to be used in other applications. Indeed, lasers can be harmful for humans and animals, conversion of light into electricity is not very efficient at the moment, and the laser can easily be disturbed by the weather, atmospheric absorption and objects in its trajectory.

3.2 Comparison

By referring to the specifications of the application in Chapter 2.2 and comparing them to the specifications of each WPT technology, the optimal power transfer technique can be chosen for

our application.

RFF technologies such as microwave and lasers can be discarded due to the complexity and the low technology readiness level. Furthermore, the overall efficiency and cost are not adequate for our requirements.

Similarly, CCWPT usable power range restricted to a few hundred's of milliwatts makes it inadequate for our application, despite its simplicity and robustness.

Inductive coupling is the wireless technology that best suits our requirements. Moreover, inductive coupling is the oldest and most widely used industry wireless power transfer technology. It is thus the most likely to be seen in space applications where all systems need to be extensively tested as a proof of durability. This WPT technology will be selected and its underlying theory detailed.

3.3 Inductive coupling WPT

Now that the WPT technology has been selected, the following subsections will explore in more details the working principle of the inductive coupling and the different ways of implementations which are most used. After this, the same work will be performed for the case of resonant inductive coupling.

But first, a brief introduction to the switching elements that are key elements in ICWPT implementations will be done just below.

3.3.1 Electronic switches

As seen in previous sections, the WPT requires AC voltages, it thus needs to use DC/AC inverters and AC/DC rectifiers in order to achieve the power transfer. This section will browse the basics of switches that are used in switching applications [9] [10].

The switch [10] is one of the main component of power electronics switching devices such as DC/DC converters. Those switches are primarily used to control the flow of electrical energy between the energy source and the load, and to do so with great precision, with extremely fast switching times, and with low dissipated power.

In an ideal switch (represented in Figure 3.8a), there are no loses due to dissipation. If the switch in ON, there is no voltage developed and if the switch is OFF, there is no current flowing (see Figure 3.8b). However, the characteristic of a real switch is not as ideal (see Figure 3.8c).

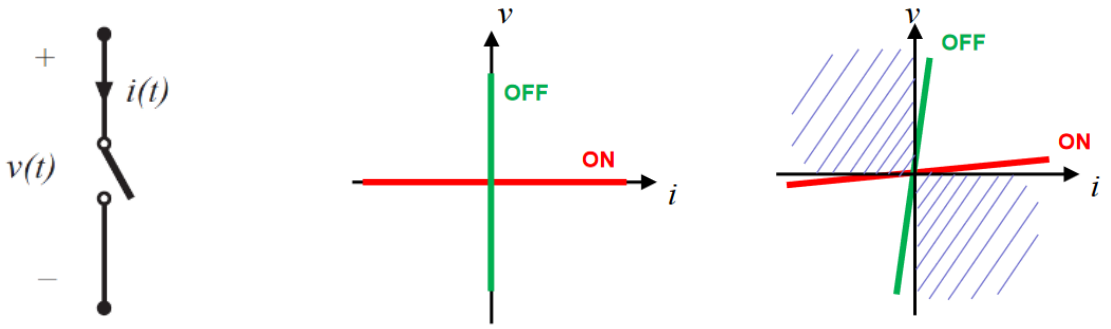

(a) Switch symbol (b) Ideal switch characteristic (c) Real switch characteristic

Figure 3.8: Main figure caption

These non-idealities involve two different kind of losses [11] in the switch as schematized in Figure 3.9:

- Conduction losses: These are losses due to the current (Joule effect) when the switch is ON. They can be estimated via the following formula:

$$P_{conduction} = R_{ON} \cdot I_{ON} \tag{3.2}$$

  Where R_{ON} is the equivalent resistance of the switch when this latter is ON.

- Switching losses: These are losses linked to the simultaneous presence of voltage and current during short moment at switching (when the switch opens or closes) and they are

proportional to the switching frequency. They can be estimated as follows:

$$P_{switching} = \int_{T_1}^{T_2} V_{ON} \cdot I_{ON} \, dt \tag{3.3}$$

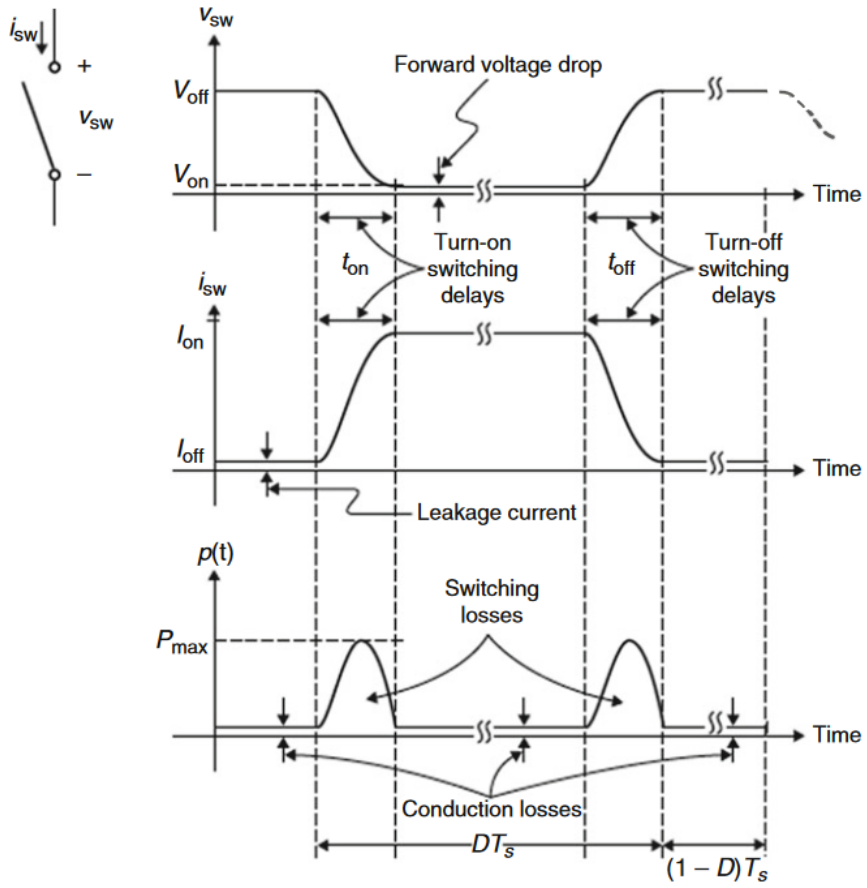

Figure 3.9: Losses in a real switches

In real applications, those switches can be implemented via a multitude of elements. Nevertheless, the two that will be used are the diode, that is a passive switch, and the transistor that is an active switch (meaning it requires a power source to perform its function where the passive switch does not).

3.3.2 Transformer as cornerstone

In inductive coupling, the power is transferred from a transmitter to a receiver by the mean of a magnetic field like in Figure 3.5 presented above. Two coils (transmitting and receiving) are used together to create and capture the field and together form a transformer as shown in Figure 3.10.

The main objective of a power transformer is to transfer electric energy from a primary side to a secondary side with a magnetic coupling between two or more windings.

The transformer can either increase or decrease the voltage in order to suit the wanted application via the transformer equation 3.4; e.g., raise the voltage from electric generators so that the electric power can be transmitted over long distances by minimizing the current losses, or

to reduce the voltage to operate lower voltage circuits.

$$\frac{u_1}{u_2} = \frac{n_1}{n_2} = k \tag{3.4}$$

Where n_i is the number of turns in coil i and k is the turn ratio of the transformer.

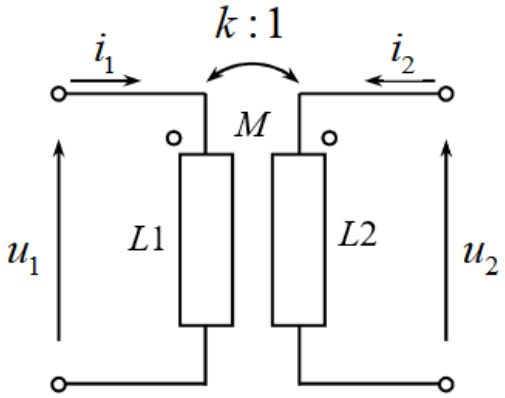

Figure 3.10: Ideal transformer schematic

Just below, a more mathematical approach is performed for a better comprehension of this power transmission.

3.3.2.1 Basic (ideal) principle: By applying AC current on the transmitter coil (L1), it induces an oscillating magnetic field inside the coil by Ampere's law :

$$I = \oint \frac{\overrightarrow{B}}{\mu_0} \cdot \overrightarrow{dl} \tag{3.5}$$

Where μ_0 is the vacuum permeability.
The amount of magnetic field picked up by the receiving coil (L2) is called the flux and is proportional to the receiving area and to the magnetic field:

$$\phi = \int \int_S \overrightarrow{B} \cdot \overrightarrow{dS} \tag{3.6}$$

Then, a variable flux in a coil induces an alternating electromotive force (EMF) voltage at the coil's extremity by Lenz-Faraday's law :

$$\epsilon = \oint \overrightarrow{E}\overrightarrow{dl} = \frac{\delta\phi}{\delta t} \tag{3.7}$$

Finally, this alternating voltage creates an alternating current in the receiver in presence of a load.

3.3.2.2 Mutual inductance and coupling coefficient: A transformer with individual winding inductances L_1 and L_2 has mutual inductance **M** between the windings. The mutual inductance can be defined as a measure of the mutual induction between two magnetically linked circuits, given as the ratio of the induced electromotive force in the secondary coil to the rate of change of current producing it in the primary coil.

If the two coils are close to each other, the mutual inductance will take a high value. Similarly, if the two coils are separated by a large distance, the mutual inductance between them will decrease as the flux generated by L_1 and intercepted by L_2 is smaller.

The mutual inductance can be expressed as follows:

$$M = \frac{N_2 \cdot \phi_{21}}{I_1} = \frac{N_1 \cdot \phi_{12}}{I_2} \tag{3.8}$$

The coupling coefficient **k** of the transformer can also be expressed as follows:

$$k = \frac{M}{\sqrt{L_1 \cdot L_2}} = \sqrt{1 - \frac{L_s}{L_1}} \tag{3.9}$$

Where $L_S = L_1 - M^2/L_2$.

This coefficient is equal to the fraction of magnetic flux through the transmitter coil L_1 that passes through the receiver coil L_2 when this second coil is open circuited. If the two coils are on the same axis and close together, almost all the magnetic field is intercepted and the efficiency can be high ($> 90\%$). If the two coils are too far away from each other, the amount of power transferred will decrease heavily and the system efficiency will drop drastically.

Finally, it can be said that the amount of power which can be transferred in the transformer increases with the coupling coefficient **k** where **M** is the mutual inductance between the two coils.

In order to increase the coupling, ferrite cores are usually added to the transformer's coils to confine the magnetic field. This lead to a reduction of the leakage flux and of the interferences, increasing the efficiency, but adds losses in the magnetics depending on the hysteresis cycle. Those loses are however lower than the efficiency gain.

3.3.3 Basic topologies

Various topology have been developed. Nevertheless, we will focus on the two topologies worth of interest for our application:

- Single active bridge (SAB)
- Dual active bridge (DAB)

3.3.3.1 Single Active Bridge: Figure 3.11 shows the schematic of an isolated DC/DC converter called Single Active Bridge (SAB) [12][13] which is the easiest implementation of inductive coupling. It is composed of two bridges coupled through a transformer. The input bridge on the left is a full-bridge while the output bridge on the right is a diode bridge rectifier.

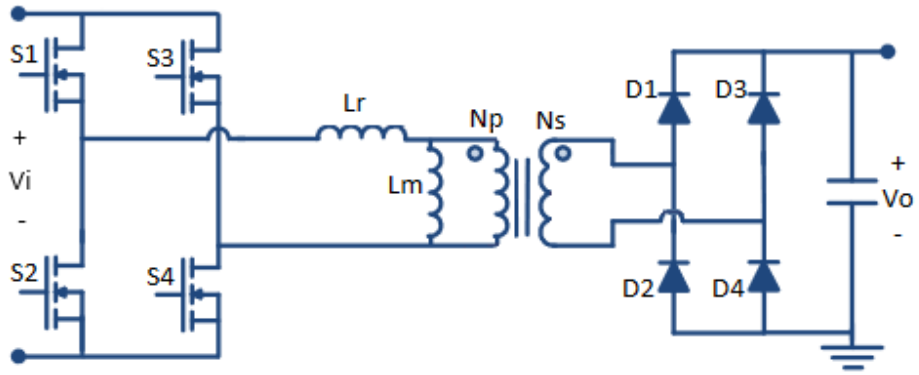

Figure 3.11: Single Active Bridge schematic

Its operating principle is the following: a square voltage source is applied on the primary of the transformer, inducing an AC current in the primary that will be induced in the secondary via the inductive coupling effect introduced in Section 3.3. This current will be rectified in the secondary through a diode bridge rectifier, leading to a positive average of active power transferred.

The converter has two possible states within the power delivery operation:

At first, as shown in Figure 3.12a, the primary inductor is excited with a positive voltage, so the current flows in the positive direction in the inductor and through the diodes D_1 and D_4 at the output bridge, powering the load.

The second state is when the primary winding is excited with a negative voltage. The current flow shown in Figure 3.12b is then negative in the secondary inductor and flows through diodes D_2 and D_3 at the output bridge, always powering the load.

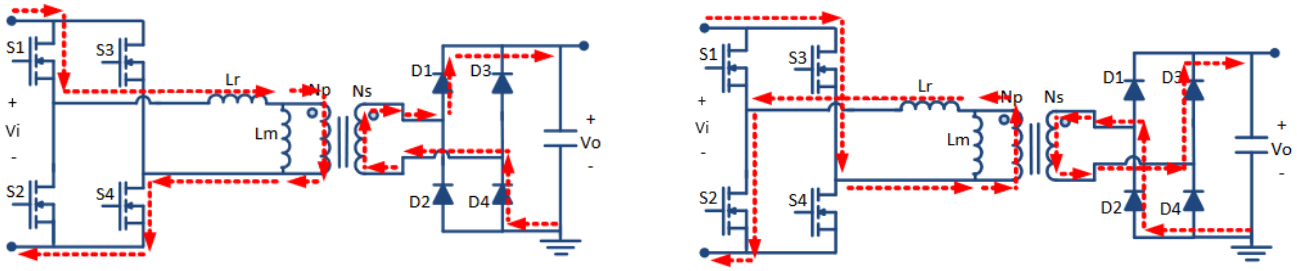

(a) Positive inductor voltage

(b) Negative inductor voltage

Figure 3.12: Modes of operation of the SAB

The voltage and current waveforms in both side are represented in the following figure (with ideal drive, without dead time):

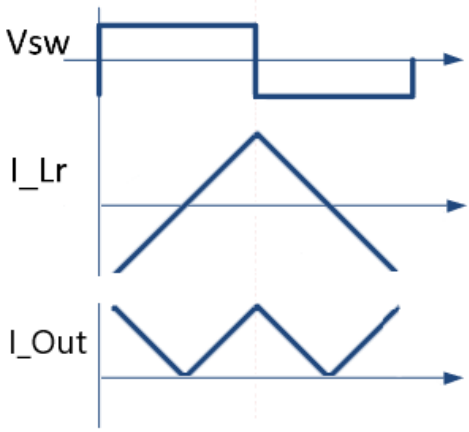

Figure 3.13: Waveforms in the SAB

However, even if this topology is already widely used and easy to implement, it does not provide a bidirectional power transfer as required (see Chapter 2.2) unless it is connected in a back to back configuration.

This back to back configuration results in doubled solution size, reduced robustness due to increased components bill of material (MTBF), higher cost and higher control complexity due to the dual converter usage.

3.3.3.2 Dual Active Bridge: In order to resolve the just described drawnbacks of the SAB, an improved architecture has been adapted over years known as the Dual Actrive Bridge (DAB) [14][15]. The SAB is improved by replacing the output uni-directional non-controlled full bridge diode rectifier with an active controlled full bridge, making the architecture symmetric. The main architecture of the DAB represented in the following figure 3.14 allows more flexibility by controlling the voltages and allows an efficient digital control by modifying the phase shift between the two full-bridges as it will be detailed in a future Section.

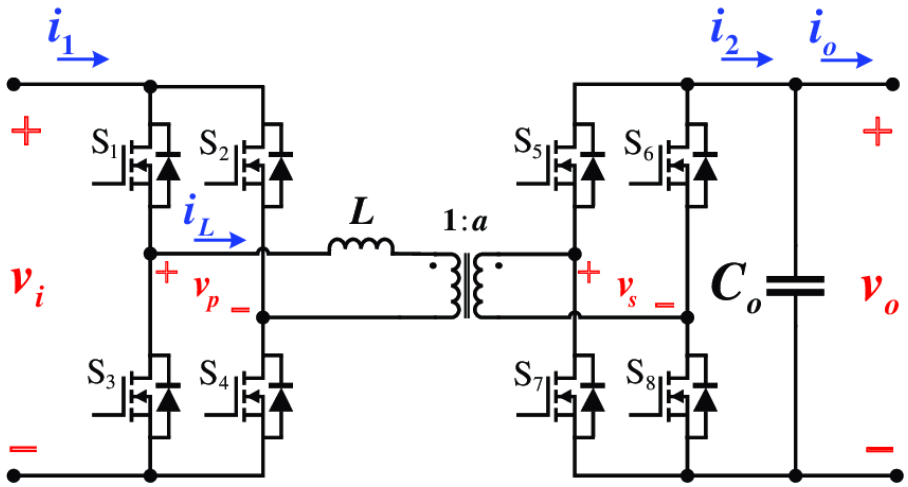

Figure 3.14: Dual Active Bridge schematics

In a single-phase DAB, primary and secondary bridges are controlled simultaneously. All switches operate at 50% duty cycle. The diagonal switches turn on and turn off together so

that the output of each bridge is a square wave (v_p and v_s in Figure 3.15).

The switching sequence is divided into four specific moments due to the phase shift between primary and secondary voltages of the transformer. Those four moments induces four intervals in the inductor current.

During interval one, switches Q1 and Q4 at the primary side and switches Q6 and Q7 at the secondary side conduct current. The voltage at the inductor terminal is then $v_p = V_i$ and $v_s = -V_o$. The slope of the inductor current is given by the following equation:

$$\frac{di_L}{dt} = \frac{v_i + v_o}{L} \tag{3.10}$$

During interval two, the primary side does not change so switches Q1 and Q4 remain turned on, but at the secondary, the switches Q6 and Q7 turn OFF. After a small dead time to avoid short circuits, Q5 and Q8 are turned ON to conduct current.

The voltage at the inductor terminal is then $v_p = V_i$ and $v_s = V_o$. The slope of the inductor current is now given by the following equation:

$$\frac{di_L}{dt} = \frac{v_i - v_o}{L} \tag{3.11}$$

During interval three, this time the switches at the secondary side remain ON while the switches at the primary change. Indeed, switches Q1 and Q4 turn OFF and switches Q2 and Q3 turn ON after a small dead time. In this interval, the voltage across the primary is $v_p = -V_i$ and $v_s = V_o$. Hence, the current ramps down with a negative slope as shown in the next equation:

$$\frac{di_L}{dt} = -\frac{v_i + v_o}{L} \tag{3.12}$$

During the last interval, switches Q2 and Q3 keep conducting current at the primary side. At the secondary, switches Q6 and Q7 turn back ON after switches Q5 and Q8 have been turned OFF and a small dead time has elapsed.
The inductor voltage is finally equal to $v_p = -V_i$ and $v_s = V_o$ and its current slope can be described as follows:

$$\frac{di_L}{dt} = -\frac{v_i - v_o}{L} \tag{3.13}$$

Figure 3.15 shows the gate signals controlling the switches opening and closing on each side where α is the phase shift between the primary and the secondary control signals. V_p and V_s represent the voltage on the primary and secondary windings of the transformer (so the voltage at the inductor terminals). Finally, I_L represents the inductor current.

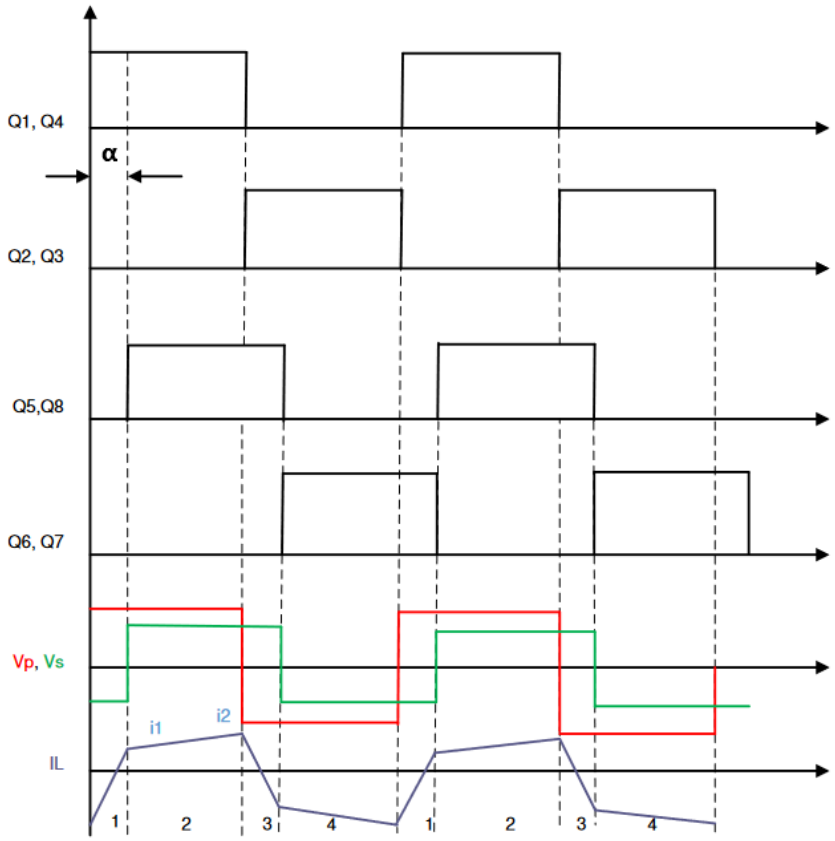

Figure 3.15: Gate Signals, Transformer Primary (v_p) and Secondary (v_s) Voltages, and Inductor Current

3.4 Improvement: Resonant inductive coupling

Ordinary inductive coupling can only achieve high efficiency when the coils are very close together. Resonant inductive coupling increases the efficiency by using a resonant circuit (see Figure 3.16) that can achieve higher efficiency at greater distance.

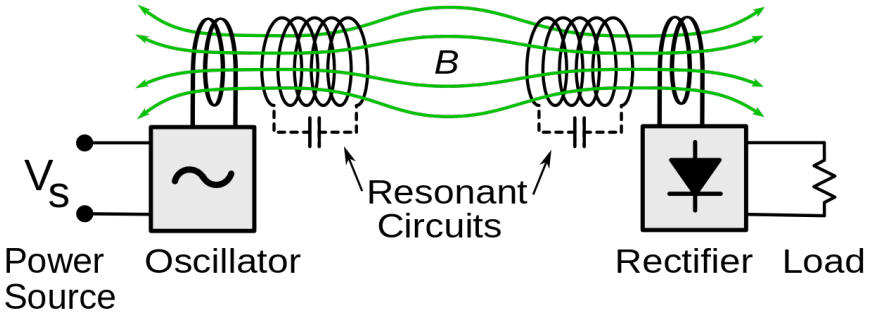

Figure 3.16: Generic block diagram of a resonant inductive wireless power system

3.4.1 Principle

Resonant inductive coupling is a form of inductive coupling in which power is transferred by magnetic fields between two resonant circuits, one in the transmitter and one in the receiver. Each resonant circuit consists of an inductor and a capacitor resonating together. By resonating at the same frequency, it greatly increases the coupling and the power transferred.

Intuitively, resonance can be described as follows : when a resonant system operates in steady state, the amount of energy necessary to keep the system in this state is strongly reduced because it is easily able to store and transfer energy between its components. If the energy is suddenly cut off, the system will continue to operate close to the previous state for some time while shedding only a small amount of energy at each step.

For example, in the case where a resonant converter is used instead of a basic converter, the resonant one includes the natural commutation of power switches, resulting in low switching power dissipation and reduced component stresses. This leads to a better efficiency and a greater range for power transmission.

3.4.2 SAB application

Figure 3.17a shows the resonant version of the SAB in Figure 3.11 [16]. This time, a capacitor C_r is added in order to resonate with the parasitic leakage inductor L_r of the transformer. Further explanation about this phenomena will be given in Section 4.3.

Due to the resonance, the current in the inductor is now sinusoidal if the switching frequency is equal to the resonant frequency.
The currents at different locations in the converter are represented in Figure 3.17b:

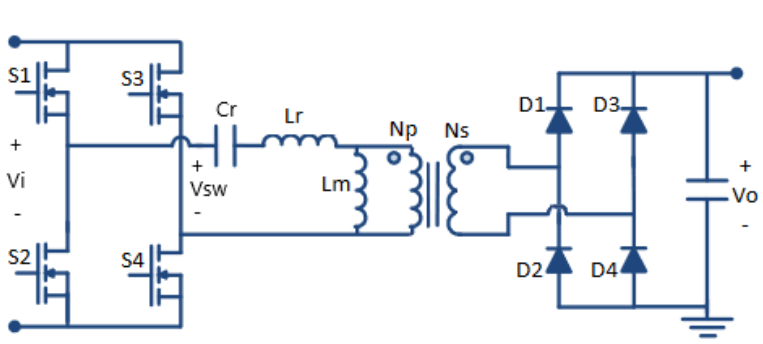

(a) Resonant SAB schematic

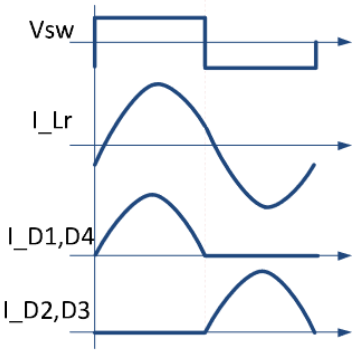

(b) Waveforms in the resonant SAB

Figure 3.17: Resonant Single Active Bridge

3.5 Conclusion

As conclusion of this section, it appears that the topology that will be studied for this work will be the DAB as it presents more advantages than the SAB at the expense of more complexity. This will be confirmed after the design and subsequent measurements.

The following Chapter aims to study in depth the DAB topology and its behaviour in order to make simulations and implement it with a prototype.

4 | Dual Active Bridge Analysis

As stated above, this Chapter will analyse the physics behind the DAB topology [17][18]. Furthermore, explanations on the resonance implementation and its benefits for the DAB will be given.

4.1 Mathematical model

The time-based working principle analysis of the DAB has been detailed in Section 3.3.3.2. Nevertheless, a more detailed analysis is required in order to lay-down the theory for the global prototype sizing and tuning. The DAB model with phase shift AC control can be expressed in the frequency domain as in Figure 4.1, the transformer acting globally as an inductor. In this model, the phase between voltage sources E_1 and E_2 controls the transferred power from one source to the other via an inductive link.

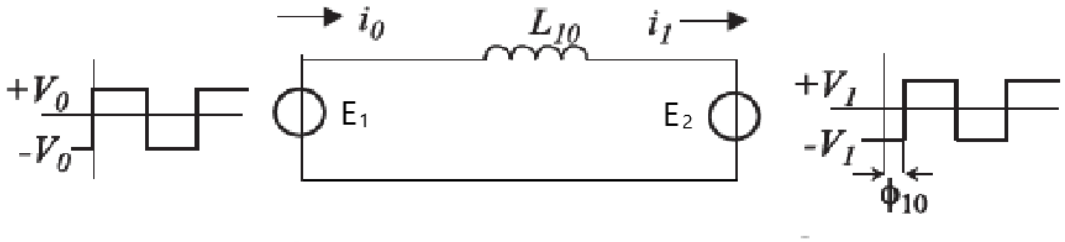

Figure 4.1: Phase shift AC topology

With the use of an inductive link between the source, both voltage and current phasors can be controlled in order to modify the power exchanged on the link.
Indeed, as in Figure 4.2, the average active power exchanged is defined by the relative position of the current and voltage phasors. Three different use-cases can be identified:

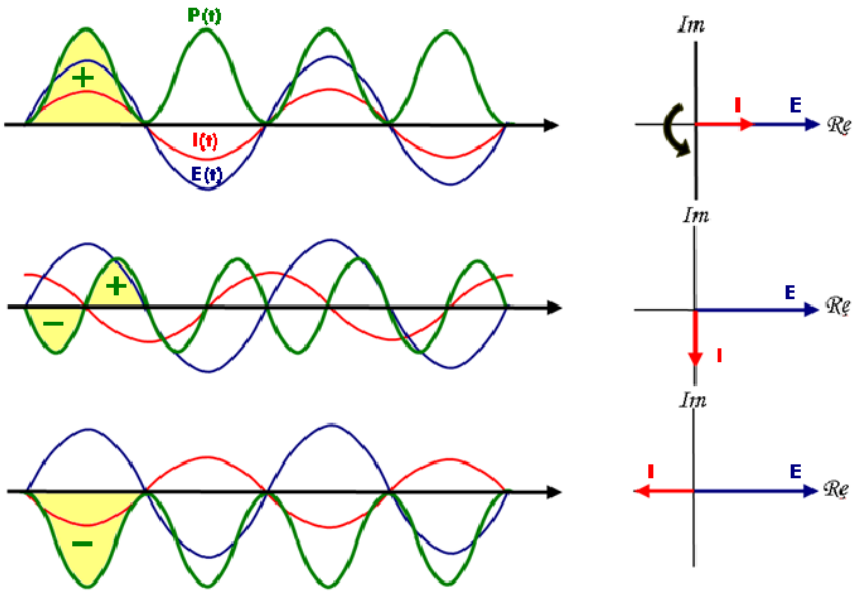

Figure 4.2: Phasors control

- If the current is in phase with the voltage, the active power exchanged is always positive (flowing from source E_1 to source E_2).
- If the current is at 180° from the voltage, the active power is always negative (flowing from source E_2 to source E_1).
- If the current and the voltage are 90° out of phase, the average active power is null and no power is exchanged.

4.1.1 Sinusoidal

Now that the working principle has been presented, lets assume only the first fundamental of the square sources will be taken into account in order to express the power transmission with phasors. The first fundamental of a square being a sinusoid, the new equivalent circuit is represented in Figure 4.3a.

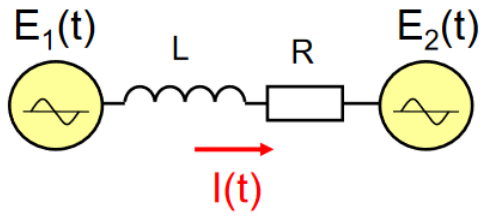

(a) Equivalent model with sinusoidal sources

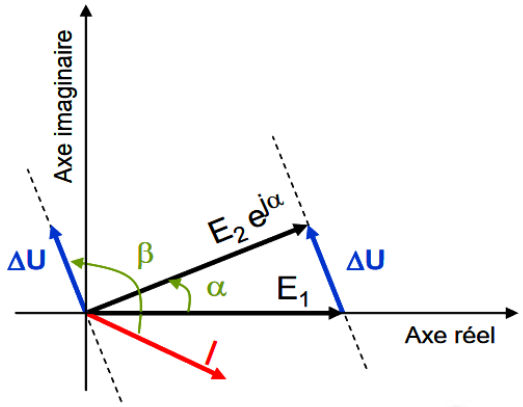

(b) Phase diagram

Figure 4.3: Power exchange between two AC sources

Assuming the two sinusoidal sources have as magnitudes respectively E_1 and E_2 and if the phase shift between the two is equals to α and that $\omega L >> R$ (the parasitic elements are neglected in order to simplify the analysis and will be introduced back later), the complex power exchanged by the source E_1 can be expressed as follows:

$$S_1 = P_1 + j \cdot Q_1 \tag{4.1}$$
$$S_1 = E_1 \cdot I \tag{4.2}$$
$$S_1 = E_1 \left(\frac{E_1 - E_2 e^{j\alpha}}{j\omega L} \right) \tag{4.3}$$
$$\tag{4.4}$$

Where **P** is the active power and **Q** is the reactive power.

By introducing the Euler's formula in Equation 4.4:

$$S_1 = \frac{E_1 \cdot E_2}{\omega L} \cdot sin(\alpha) + j \left(\frac{E_1 \cdot E_2}{\omega L} \cdot cos(\alpha - \frac{E_1^2}{\omega L}) \right) \tag{4.5}$$

The active **P** and reactive **Q** power exchanged by E_1 can then be expressed as:

$$P_1 = \frac{E_1 \cdot E_2}{\omega L} \cdot sin(\alpha) \qquad Q_1 = \frac{E_1 \cdot E_2}{\omega L} \cdot cos(\alpha) - \frac{E_1^2}{\omega L} \tag{4.6}$$

It can be seen that those equations are the parametric equation of a circle. Indeed, if the two voltages E_1 and E_2 are equal, the equations can be represented as shown in Figure 4.4.

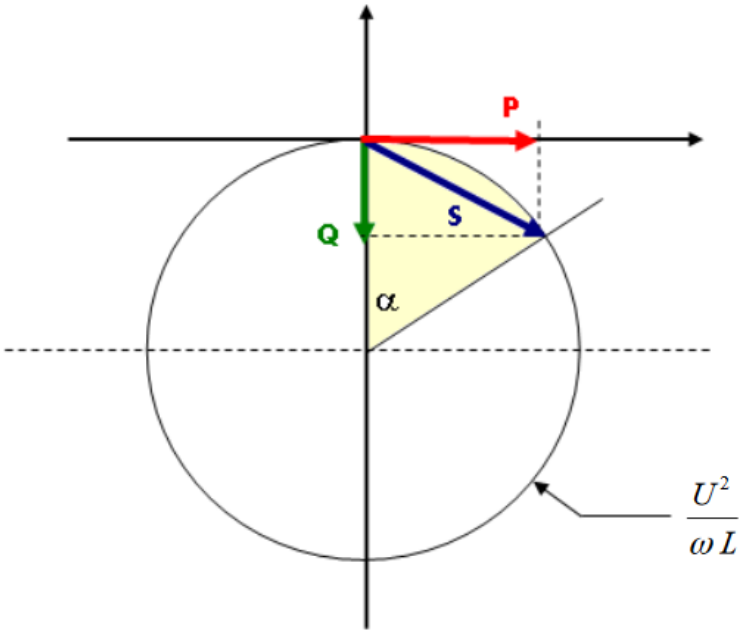

Figure 4.4: Power circle if voltages are equal

As a function of the phase shift α between the two power sources, the power exchanged by the source E_1 can be either positive (E_1 lagging E_2) or negative (E_1 leading E_2).

With this circle, it can also be seen that the maximum of amount active power which can be transmitted is achieved when the phase shift between the sources is of 90°.

Indeed, the different powers can be plotted in function of the phase shift α as in the following Figure 4.5. It can clearly be seen that the maximum of active power exchanged is achieved at 90°.

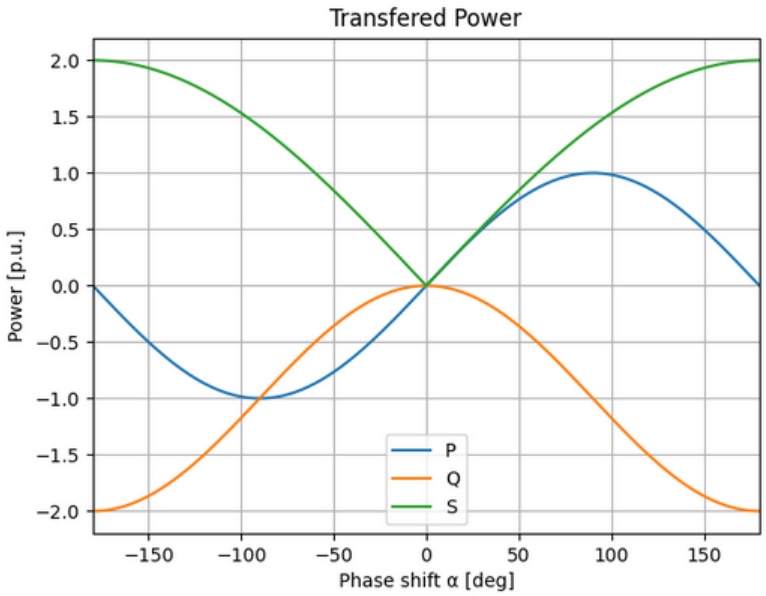

Figure 4.5: Power in function of α

Nevertheless, increasing the active power results in an increase of the reactive power and thus of the losses due to the reacting current. Beyond 90° of phase shift, the active power is reduced while the reactive power still increases.

Finally, it can be said that this power transfer is a trade-off between the maximal transmitted power and the efficiency as less active power involves less reactive power.

4.1.2 Square drive model

This sinusoidal model can be improved upon in order to analyse the relevance of this model when the sources are square waves. The new equivalent model can be seen in Figure 4.6, also including the required AC/DC conversion after the second source in order to rectify the current in order to exhibit a DC voltage to the load.

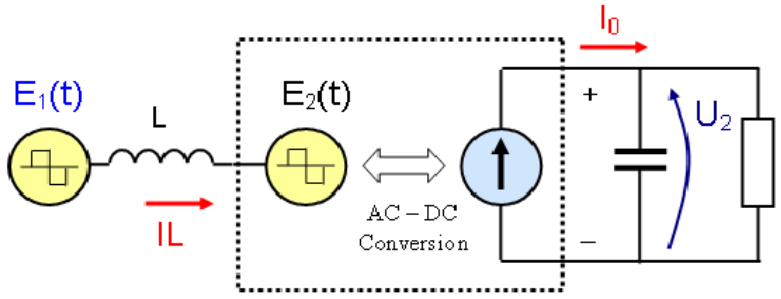

Figure 4.6: Equivalent model with square sources and AC/DC transformer at output

If the two voltage sources have a different phase, the waveforms can be represented as in Figure 4.7 showing voltage and current across the inductor along with the rectified current by the AC/DC converter.

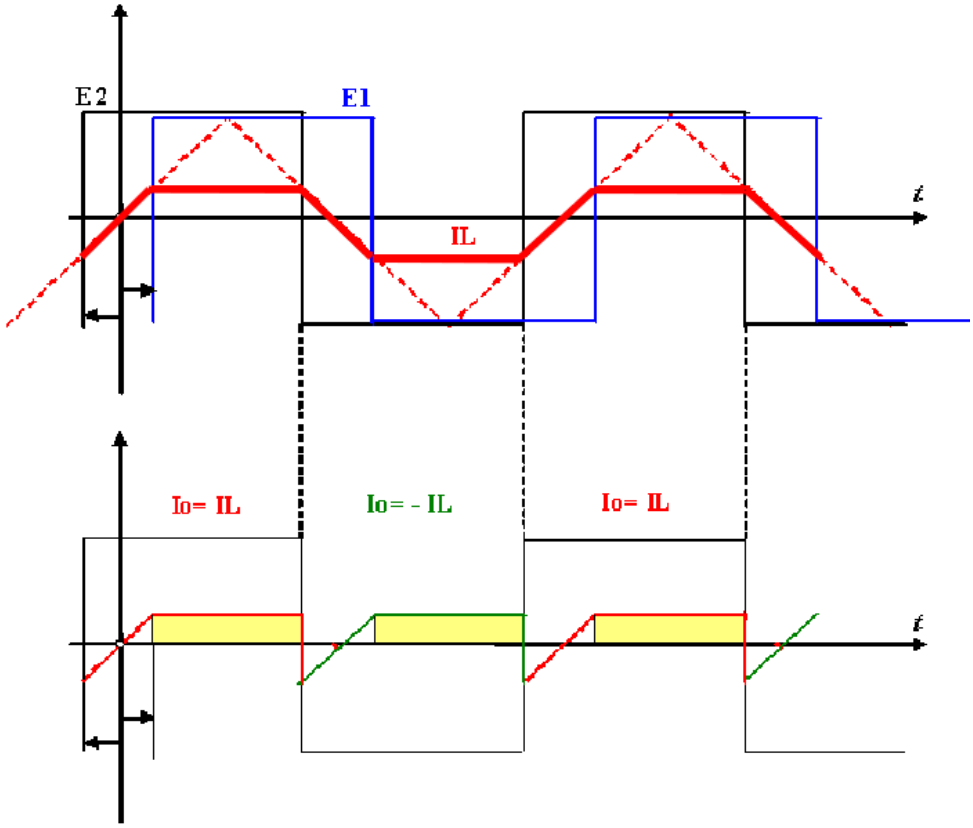

Figure 4.7: Voltage and current waveforms

The exchanged power can be expressed by integrating the rectified current waveform and multiplying this latter by the second source voltage:

$$P = \frac{E_1 \cdot E_2}{\omega L} \cdot \alpha \left(1 - \frac{|\alpha|}{\pi}\right) \tag{4.7}$$

The first harmonic RMS amplitude of a square compared to its initial amplitude is equal to:

$$|E| \cdot \frac{4}{\sqrt{2} \cdot \pi} \tag{4.8}$$

Introducing equation 4.8 in equation 4.6, the exchanged power becomes:

$$P = \frac{E_1 \cdot E_2}{\omega L} \cdot \frac{8}{\pi^2} \cdot sin(\alpha) \tag{4.9}$$

The comparison between square wave source and its sinus approximation finally can be drafted, showing the sinusoidal approximation fits pretty well the real computations (see Figure 4.8) with the above assumptions.

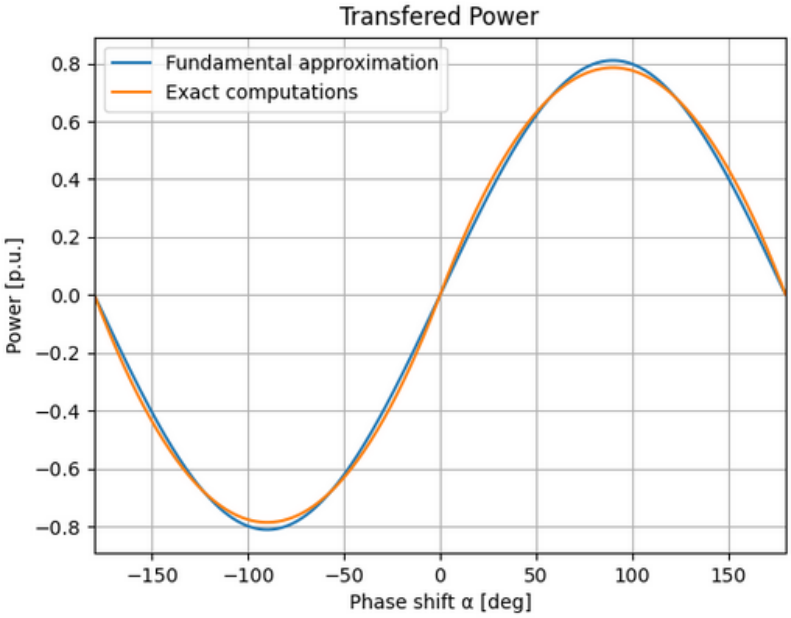

Figure 4.8: Real vs approximation

4.2 Transformer

In this Section, a theoretical analysis of the transformer used in the DAB will be studied [19] [20].

The main objective of a transformer is to transfer electric energy from a primary side to a secondary side with a magnetic coupling between two or more windings.

The transformer can either increase or decrease the voltage in order to suit the wanted application; e.g., raise the voltage from electric generators so that the electric power can be transmitted over long distances by minimizing the current losses, or to reduce the voltage to operate lower voltage circuits.

The transformer will be used in order to achieve the WPT by inductive coupling introduced in Section 3.3. In order to be able to achieve system simulations, to compare it to the theoretical models, and in order to construct a working prototype, an existing transformer core has been used and modified (see Section 5.1).

This transformer having no known datasheet, this chapter has for objective to introduce the equivalent model of the real transformer and to characterize the parameters of this latter via different trials and for different air gap configurations.

4.2.1 Theoretical model

Figure 4.9 represents the complete equivalent circuit of a single phase transformer.

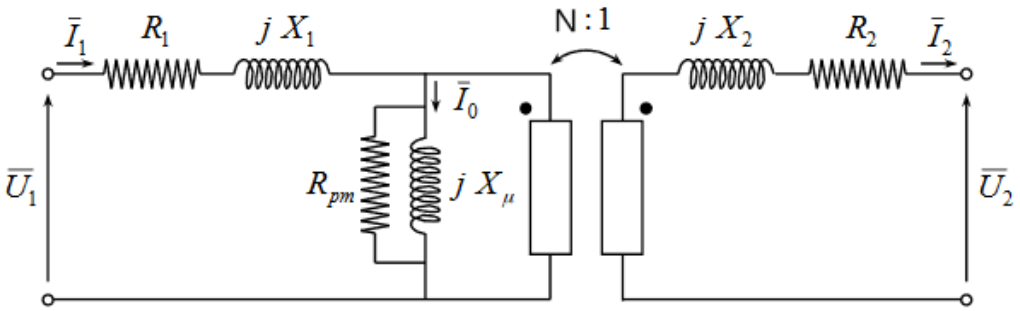

Figure 4.9: Equivalent circuit of a single phase transformer

Here is a list of the different elements composing the equivalent circuit:

- R_1 and R_2: are the equivalent resistance of the transformer's windings and thus create the Joules losses in the transformer.

  Indeed, the resistance of a material can be expressed as follow:

  $$R = \frac{\rho l}{S} \tag{4.10}$$

  Where ρ is the resistivity of the material, l is its length and S is the surface of the material crossed by the current.

  This latter can be diminished by the use of Litz Wires (see Section 4.2.2)

- X_1 and X_2: are the leakage inductances representing the amount of flux generated by the windings that flows outside the magnetic circuit.

  Indeed, all of the flux that is generated by L_1 cannot be "caught" by the secondary winding L_2. A small amount of this flux just flows outside as in Figure 4.10

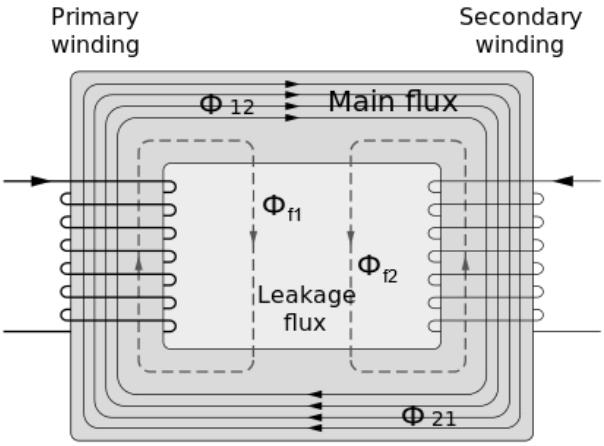

Figure 4.10: Coupling coefficient k measurements

- X_μ: represents the magnetizing current flowing into the ferrites because ferromagnetic materials do not have an infinite magnetic permeability.

  The magnetic field in the material can be expressed as follows:

$$\oint \overrightarrow{H}\overrightarrow{dl} = N \cdot i = n_1 \cdot i_1 + n_2 \cdot i_2 \tag{4.11}$$

  Where n_i is the number of turns of the side **i** of the transformer.

  In the case of no load at the secondary side, involving $i_2 = 0$, the field **H** does not stay equal to zero, involving a current $i_1 \neq 0$ that is the magnetizing current.

- R_{pm}: represents the iron losses of the transformer being the sum of hysteresis losses [21] and Eddy currents losses [22].

  Hysteresis losses come from the non ideal B-H curve of the magnetic material. When the flux density increases, it does not follow the same path as when it decreases. In the case of an alternating flux density, the losses are then equal to the area between the two paths (Figure 5.18a).

  Eddy currents are created when the flux density varies inside the ferrite as opposition to this flux variations. They are thus Joule losses in the material. One way to reduce those losses is to laminate the material in order to reduce the surface and the losses (Figure 5.18b).

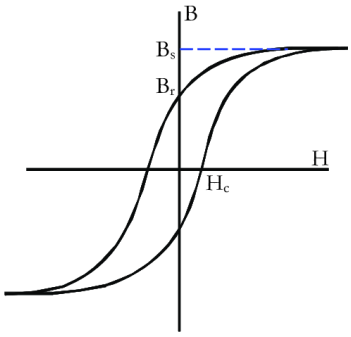

(a) Hysteresis effect

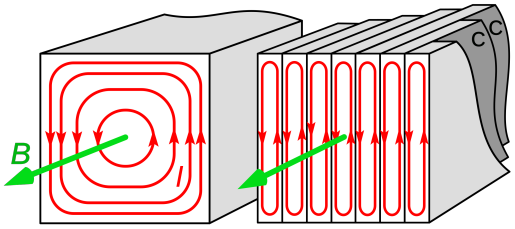

(b) Eddy current effect

Figure 4.11: Iron losses effects

$$P_{iron} = P_{hyst} + P_{eddy} \tag{4.12}$$

Where:

$$P_{hyst} = \eta \cdot f \cdot B_{max}^2 \cdot V \tag{4.13}$$

With η, the Steinmetz hysteresis coefficient which depends on the material, f, the frequency, B_{max}, the density of highest flux and V, the magnetic material volume in m^3.

$$P_{hyst} = K_e \cdot f^2 \cdot B_{max}^2 \cdot V \tag{4.14}$$

With K_e, the eddy current constant.

Those last losses are always present and only depend on the operating frequency and on the supply voltage.

- N: the transformer turns ratio.

$$N = \frac{n_1}{n2} = \frac{U_1}{U_2} = -\frac{i_1}{i_2} \tag{4.15}$$

4.2.2 Litz Wire:

As stated earlier, the resistance of the windings R_1 and R_2 exhibit Joule losses of the wires and Litz wires configuration [23] can be used in order to decrease these losses. Please note Litz configuration also exhibits lower leakage inductance.

Indeed, there are in the coils eddy-current losses that occur due to high frequencies. These are due to skin and proximity effects.

- **Skin effect:**

The skin effect is the tendency of an alternating current to become distributed within a conductor such that the current density is bigger near the surface of the conductor and decreases exponentially with greater depths in the conductor. The alternating current generates an alternating flux, that generates itself Eddy-currents. Due to this, the current in the center of the conductor is reduced, while the current near the surface is increased as illustrated in Figure 4.12. While the mean current is the same and losses are quadratic to the current, global losses are much higher.

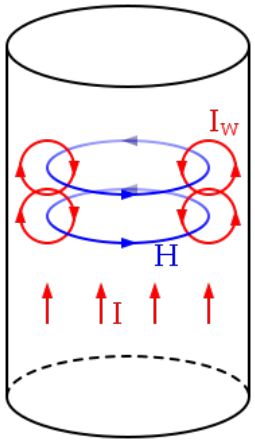

Figure 4.12: Skin effect representation

The current is almost exclusively flowing in a equivalent region called skin-depth, determined with the following formula:

$$\delta = \frac{1}{\sqrt{\pi \cdot \mu_0 \cdot \sigma \cdot f}} \tag{4.16}$$

Where μ_0 is the void permeability, σ is the material conductivity and f is the frequency. The smaller the surface, the bigger the equivalent resistance and Joule losses.

For example, at 100 kHz (which is near our application frequency), the skin-depth of copper is equal to 0.22 mm.

- **Proximity effect:**

The proximity effect is the concentration of the current to a smaller region in a conductor due to current flowing in neighbouring conductors as in Figure 4.13.

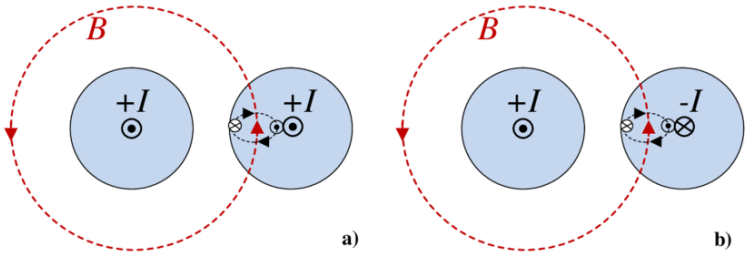

Figure 4.13: Proximity effect representation

The Eddy-currents induced by proximity effect are not symmetric with respect to the center of the conductor as the magnetic field of neighbouring conductors is not constant with the distance.

To avoid those effects, the Litz wire is made of multiple wires, grouped and twisted together as in Figure 4.14. They are constructed so that each of the individual wire has a diameter way smaller than the skin effect: $D_{wire} << \delta$.

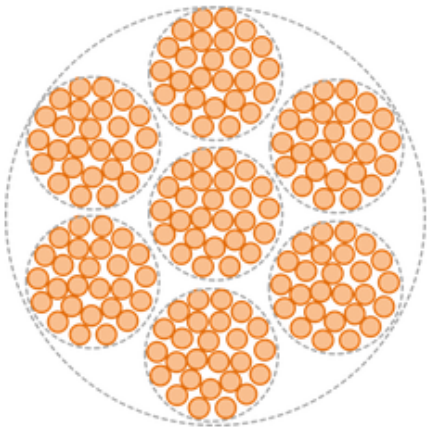

Figure 4.14: Litz wire possible configuration

4.3 Improvements

As stated earlier, resonance can be used in order to improve the WPT performances. In addition to the energy transfer efficiency improvement, resonnance enables soft switching. As a reminder, turning on or off a switching device results in power losses if both current and voltages are not null, this is called hard-switching (see Section 3.3.1).

4.3.1 Resonant tank

In order to achieve the resonance effect, an inductor-capacitor circuit will be used. Different solutions can be applied, involving different inductor-capacitor combinations (e.g. LLC, CLC, CLLLC, ...) [24][25][26][27].

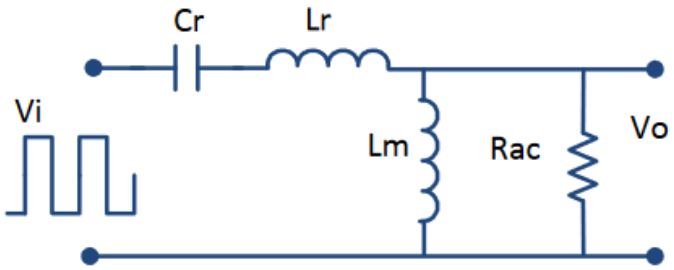

Figure 4.15: LLC equivalent circuit of the transformer

For this project, the chosen resonant tank will be a LLC one (see schematic in Figure 4.15) where a capacitor will be added in series with the transformer in order to resonate with the leakage inductor of the transformer. Finally, the LLC one has been selected as it is one of the most popular and easiest to implement topology and because it also requires few components and board area.

For all computations, the equivalent resistance of the transformer wires will be neglected as it is way smaller than the reflected load R_{ac}.

The gain of the LLC stage can be expressed as:

$$G \equiv \frac{V_o}{V_i} = \frac{Z_1}{Z_1 + Z_2} \tag{4.17}$$

Where:

$$Z_1 = \frac{1}{j\omega C} + j\omega L_r \qquad Z_2 = \frac{R_{ac} \cdot j\omega L_m}{R + j\omega L_m} \tag{4.18}$$

To ease readability and plotting, the following variables can be introduced in equation 4.17:

- $Q = \dfrac{\sqrt{\frac{L_r}{C_r}}}{R_{ac}}$ The filter quality factor

- $f_r = \dfrac{1}{2\pi\sqrt{L_r \cdot C_r}}$ — The filter resonant frequency
- $F = \dfrac{f_s}{f_r}$ — The ratio between switching and resonant frequency
- $L = \dfrac{L_r + L_m}{L_r}$ — The ratio of total primary inductor to the resonant inductor

Finally, the gain expression of the LLC circuit is the following:

$$G = \frac{F^2(L-1)}{\sqrt{(L \cdot F^2 - 1)^2 + F^2(F^2-1)^2 \cdot (L-1)^2 \cdot Q^2}} \tag{4.19}$$

The G gain of the LLC circuit in Figure 4.15 can be plotted in function of **F**, the ratio between switching and resonant frequency, and for different values of quality factor **Q**. For plots in Figure 4.16, **L** factor is introduced to be 3.5 as it is approximately the ratio obtained in the transformer available for the prototype (this is explained at the prototyping chapter).

However, this value can have a big impact on the whole WPT performances. Indeed, in function of the need, the **L** value can be defined at the transformer design in order to have a better efficiency or a better regulation control. This can be summarised in the following table:

Low L value	**High L value**
Higher boost gain	Higher magnetizing inductor
Narrower frequency range	Lower magnetizing circulating current
⇒ **More flexible regulation**	⇒ **Higher efficiency**

Table 4.1: Effects of L

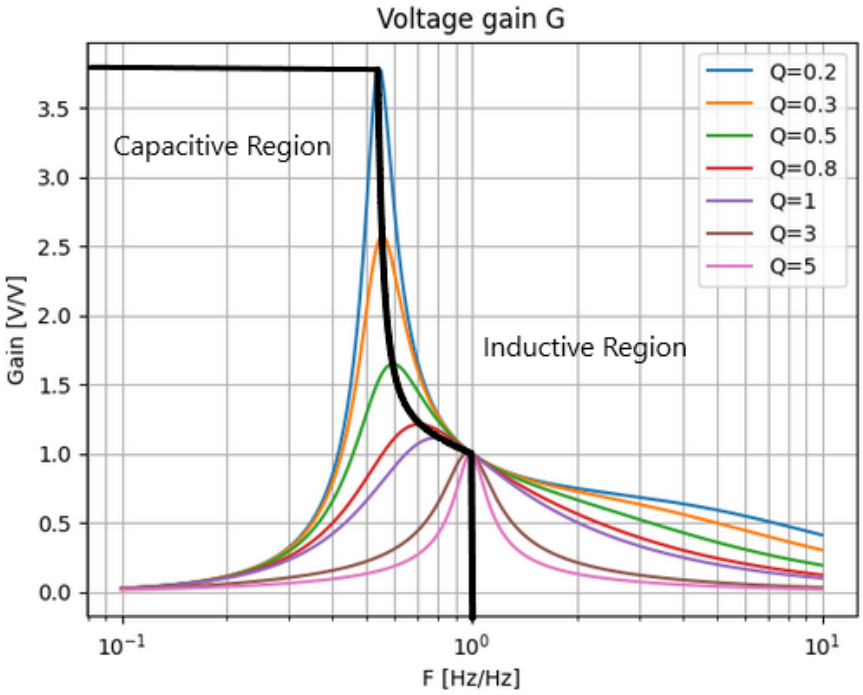

Figure 4.16: Gain of the LLC circuit in function of the normalized frequency

In Figure 4.16, low Q curves belong to lighter load operation (when the output resistance is high). on the other hand, high Q curves belong to heavier loads (when the output resistance is small).

It can be seen that all the different curves cross at the exact same point where $F = 1$ and $G = 1$.

The inductive to capacitive transition can be drawn: the black line represents the switchover between the capacitive behavior on the left and the inductive on the right.

The required working region is inductive in order to achieve Zero-Voltage Switching (detailed in the next Section). Indeed, in the capacitive region, the current leads the voltage resulting in the switching device current changing of direction before this latter turns off. Current is thus forced to go trough the body diode of the MOSFET and results in hard switching, generating losses, negative transient voltage and high frequency ringing creating EMI (Electro-magnetic interference - unwanted conducted and radiated noise).

4.3.2 Soft Switching

Resonance is one of the techniques used in order to achieve soft switching [28]. It is used to turn on and off power switching devices at zero voltage or current by using a resonance phenomenon. With resonance, the switching losses become very small because either voltage or current is zero or close to zero at the time of switching.

Switching at zero-voltage crossing is called Zero-Voltage Switching (ZVS) whereas switching at zero-current crossing is called Zero-Current Switching (ZCS).

Hard switching exhibits a considerable overlap between voltage and current waveforms. Whereas soft switching helps reducing losses in the power switching devices. In addition, it also efficiently reduces switching harmonic content and transient noise due to reduction of current and

voltage fast raises and decays.

Figure 4.17 shows a comparison between hard switching without any resonance and soft switching in the presence of resonance.

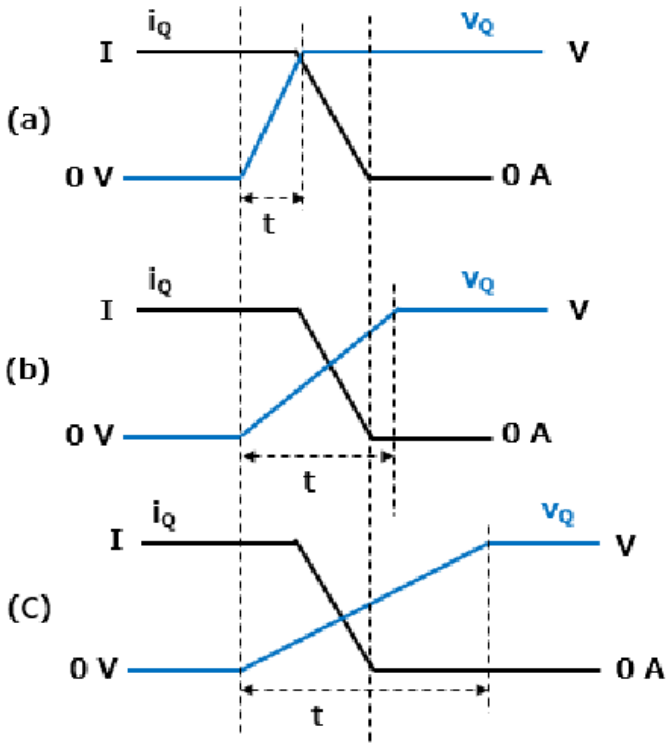

Figure 4.17: ZVS example

From top to bottom, subfigure (a) shows waveforms without any resonance while subfigure (b) and (c) show waveforms with a resonant effect in function of the capacitor size (b used a small capacitor while a used a big capacitor).

It can be seen that with resonance, the slopes of the current and voltage are reduced and that the switching power lost (represented by the integral of the current times the voltage during the switching time) is greatly reduced.

However, one major drawback of the resonance is the commutation time. Indeed, this latter is bigger with a resonant effect, it can thus limit the switching frequency.

5 | Practical Design

Since different concepts and elements composing the final application have been discussed and described, the two circuits that will be tested and compared will be analysed in this chapter.

As stated in Section 3.3, the selected topologies are the SAB and the DAB. Those topologies will be compared on different aspects:

- Ease of implementation
- Maximal transferred power
- Efficiency
- Ease of control

Moreover, a resonant variant as introduced in Section 3.4 of each topology will also be studied to see if it helps in decreasing the losses to boost the efficiency.

5.1 Transformer

The transformer is one of the key piece of the prototype. As stated earlier, this last was reused from an old project realised by Thales Alenia Space.

This Section aims to show the work that has been done around this transformer in order to characterize this last experimentally and to integrate it to the simulations and the prototype [20][29].

5.1.1 Lab measurements

Now that the equivalent model has been defined in Section 4.2.1, the values of the different parameters can be extracted from different measurements that will be performed for three air gap sizes of 2, 3 and 5 mm.

In this subsection, the simplified equivalent transformer in Figure 5.1 will be presented, then each of the trial and their aim will be described. Then, the results of the measurements in each situation will be resumed.

NOTE: The frequency measurements will not allow to define the iron losses R_{pm} due to the evolution of this last in function of the frequency. This equivalent resistance will thus be neglected by assuming it is extremely high and can be seen as an open circuit.

By applying the transformer transfer function, the equivalent circuit in Figure 4.9 can be simplified by moving the primary side series element (R_1 and jX_1) to the secondary side by applying a $1/k^2$ factor.

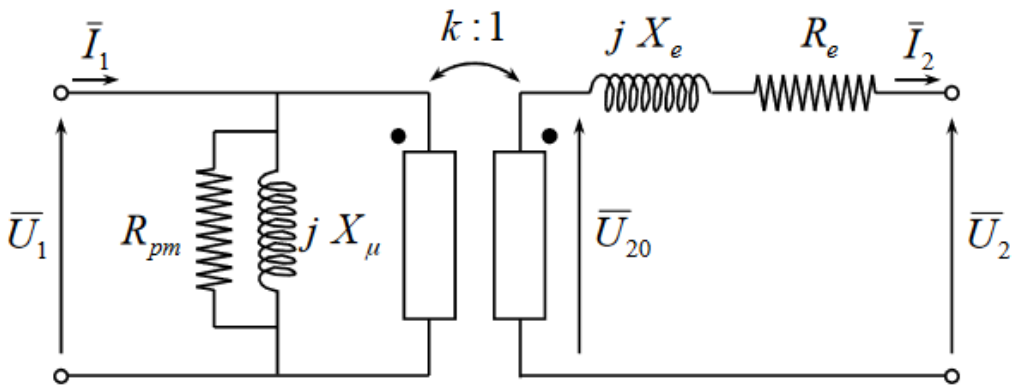

Figure 5.1: Simplified equivalent of a single phase transformer

The result is represented in Figure 5.1 and the new series element can be expressed as follow:

$$R_e = R_2 + \frac{R_1}{k^2} \qquad\qquad jX_e = j(X_2 + \frac{X_1}{k^2}) \tag{5.1}$$

Here are the different measurements that have been performed.

5.1.1.1 4-wires sensing (Kelvin probe): In order to measure the winding impedance, a 4-wires setup has been used. With a 4-wire connection, the objective is to have different wires to deliver the measurement current and to sense the voltage drop induced by the impedance.

This offers advantages: the voltage sensing is achieved regardless of the current-injection cables influence. If we assume the voltage sensing electronics has an almost infinite impedance, the associated cable and contact impedance has absolutely no influence on the measurements. These sensing and sourcing cables are directly connected to the legs of the impedance to be measured, achieving an almost perfect measurement.

This method is relatively helpful here due to the very small value of winding resistance for example.

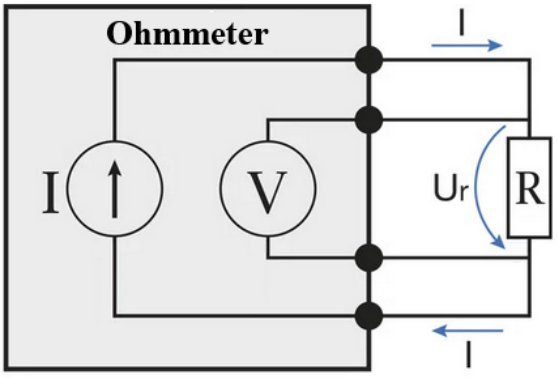

Figure 5.2: 4-wires trial schematic representation

5.1.1.2 Magnetizing inductance The no-load measurement results in measuring the magnetizing inductance of the transformer (primary winding). As it can be seen in Figure 5.3, when the transformer secondary is not loaded, the inductance seen from the primary side is only the magnetizing inductance if R_{pm} is neglected.

$$L_{measure} = jX_{\mu} = L_m \tag{5.2}$$

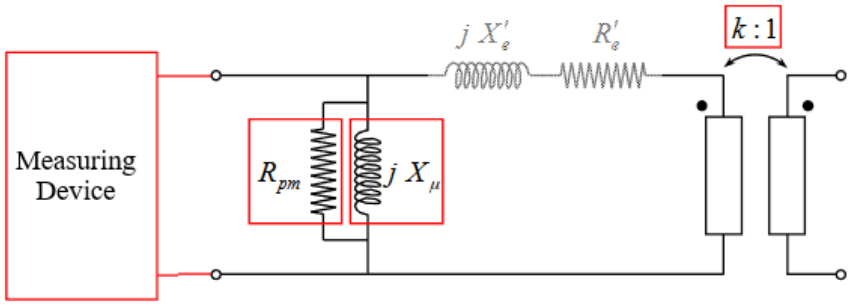

Figure 5.3: No-load trial schematic representation

5.1.1.3 Leakage inductance In the short-circuit setup, we can observe in Figure 5.4 that the magnetizing inductance is shorted when we connect the secondary wires. Thanks to this, the measured value is only equal to the leakage inductance if the winding resistance is neglected.

$$L_{measure} = jX'_e = L_f \tag{5.3}$$

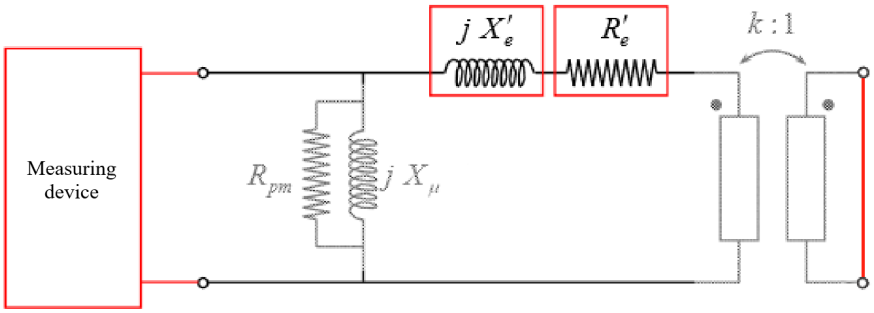

Figure 5.4: Short-circuit trial schematic representation

5.1.2 Final model

As a reminder, the frequency response of the coil will exhibit a behavior like in Figure 5.5 [30]: inductive behavior at low frequency, and capacitive behavior (parasitic capacitances, ...) at higher frequency.

In this graph, f_0 is the resonant frequency, value for which the impedances are equal: $Z_C = Z_L$

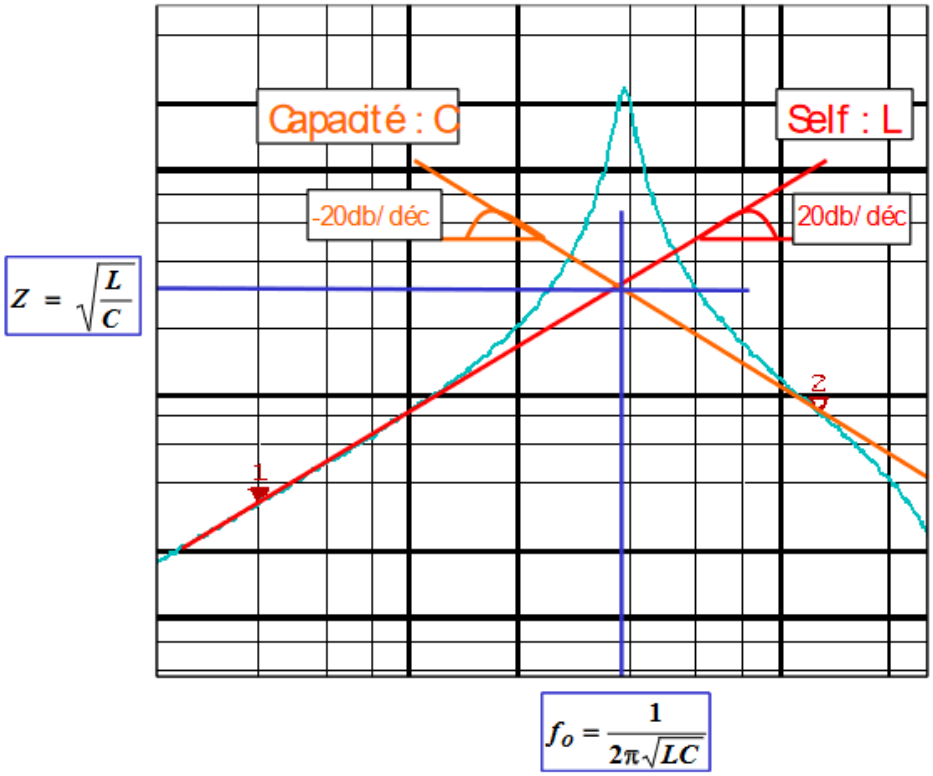

Figure 5.5: Impedance vs frequency

Figure 5.6 shows the frequency response of the transformer in the case of a no-load setup with an air gap of 3 mm.

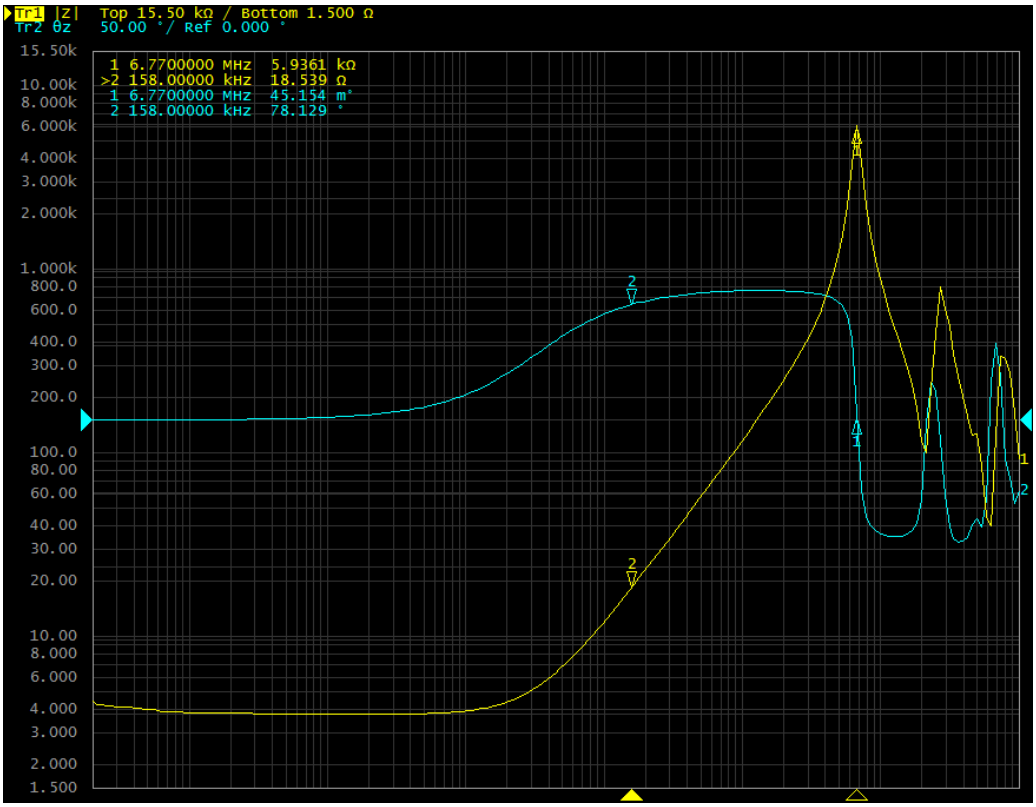

Figure 5.6: Measurement done in a no-load trial with a 3mm air gap

From this graph, the inductance value can be extracted.
Indeed, the impedance can be expressed as follows:

$$Z = \omega \cdot L \tag{5.4}$$

At 158 kHz, we have the following relation (measurement instrument related):

$$1\Omega = 1\mu H \tag{5.5}$$

The inductance value can thus easily be identified by from the impedance value at 158 kHz and is equal to 18.54 μH. If required, the value of the distributed parasitic capacitance could also be extracted from the resonant frequency introduced in Figure 5.5.

The following tables summarizes all the results of the different measurements:

		Leakage Inductance [µH]	**Magnetizing inductance [µH]**
Air gap [mm]	2	4.34	20.45
	3	5.04	18.54
	5	6.16	14.49

Table 5.1: Coil inductance

	Primary Coil	**Secondary Coil**
Resistance [mΩ]	123	131

Table 5.2: Coil resistance

The coupling coefficient **k** (introduced in Section 3.3.2) of the transformer in function of the air gap size can be plotted in Figure 5.7. As a reminder, higher is the coupling coefficient, lower is the leakage flux flowing out of the transformer and better is the efficiency.

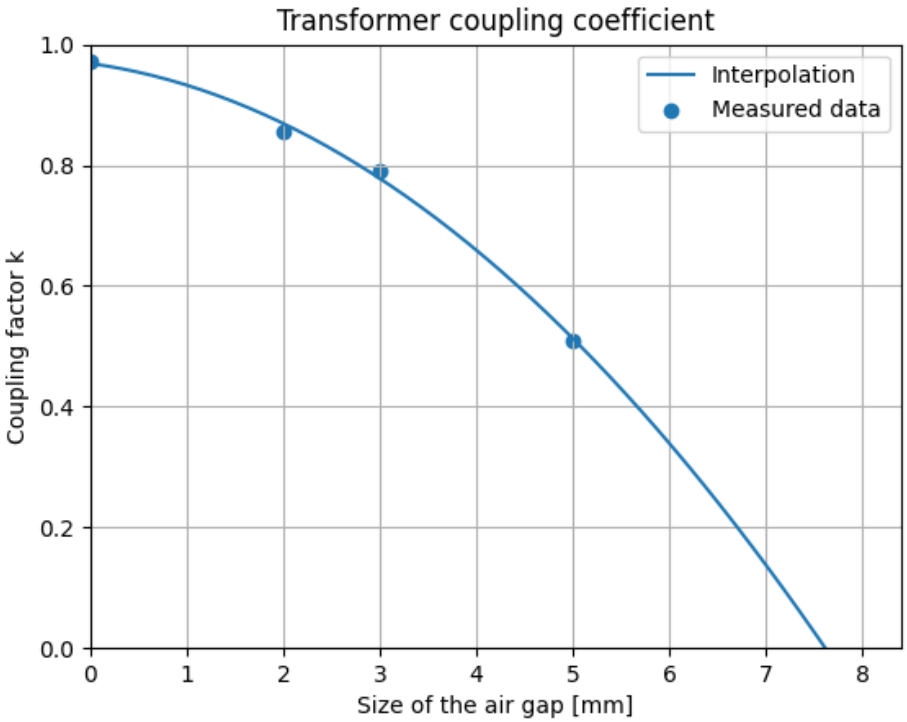

Figure 5.7: Coupling coefficient k measurements

5.1.3 Build it

5.1.3.1 Air gap: In order to have consistent results and the best efficiency for the WPT, a mechanical adapter was designed in order to obtain a constant and well known air-gap. The target is to keep the two coils exactly aligned to each other, minimizing the leakage flux.

Three different 3D printed parts have been designed with a different air gap of 2, 3 and 5 mm in order to observe the evolution of the results with a variation of the coils distance resulting in inductance and maximum flux density modifications.

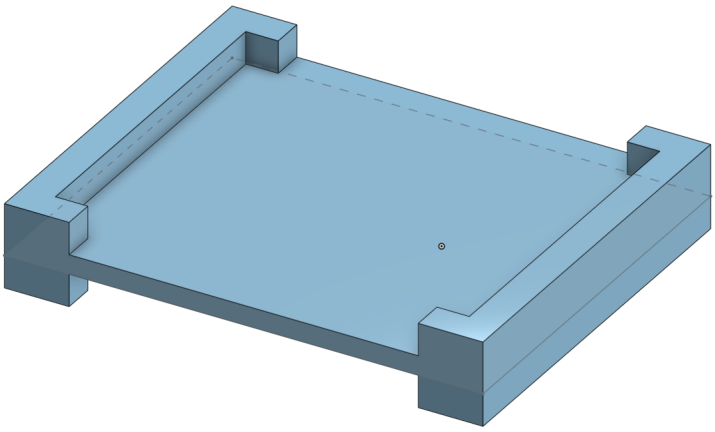

Figure 5.8: 3D overview of the constant air gap piece

Here is the final result when the two windings and the E-core ferrites are assembled:

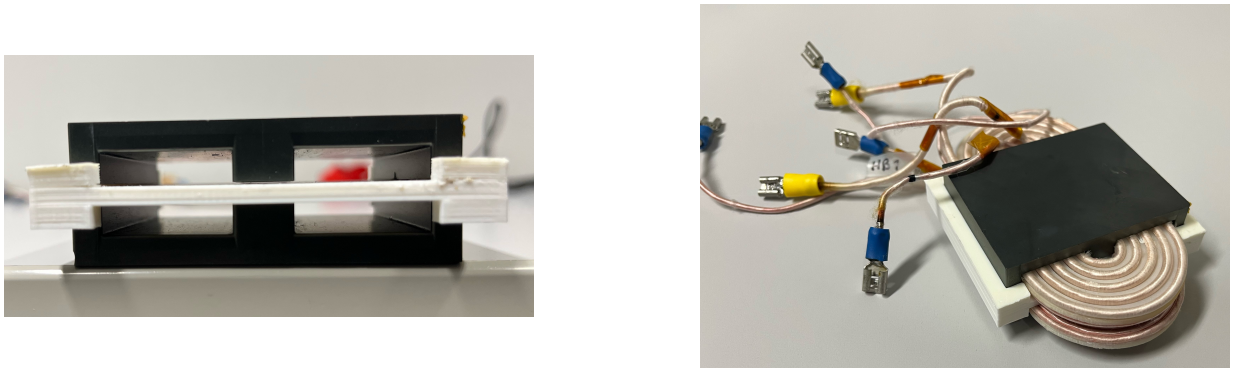

Figure 5.9: Transformer with printed air gap

The ferrite material can be found in Appendix B.1.

5.1.4 Air-gap influence

Before designing the DAB prototype, an evaluation has been performed in order to observe the evolution of efficiency on the power transfer in a SAB in function of the air-gap size of the transformer.

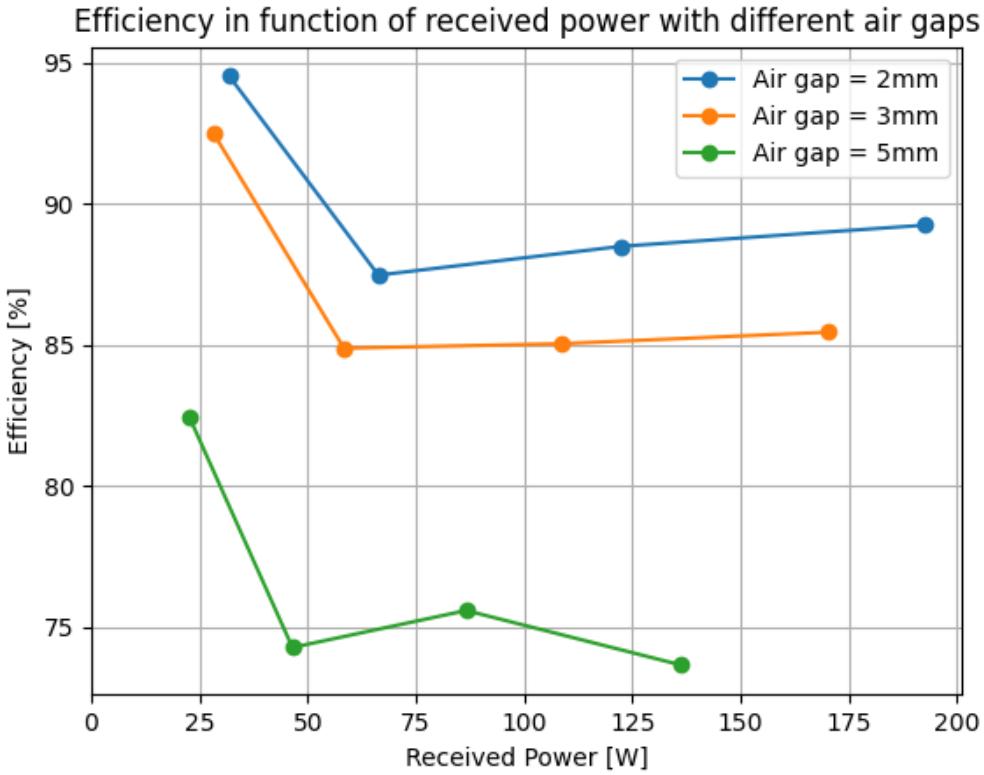

Figure 5.10: Air-gap influence

As explained in previous sections, when the air gap is bigger, the leakage inductance is also bigger and the magnetizing inductance is smaller. The impact is a lower efficiency of the transmission as less flux of the first coil is intercepted by the secondary coil as it can be seen in Figure 5.10.

5.2 SPICE simulations

The purpose of this Chapter is to introduce the simulation results of the DAB topology in order to design the circuit to the expected behaviour.

5.2.1 DAB

Figure 5.13 shows the DAB part of the simulated circuit. It takes back the two full bridge connected by the equivalent model of the transformer seen in Section 5.1.

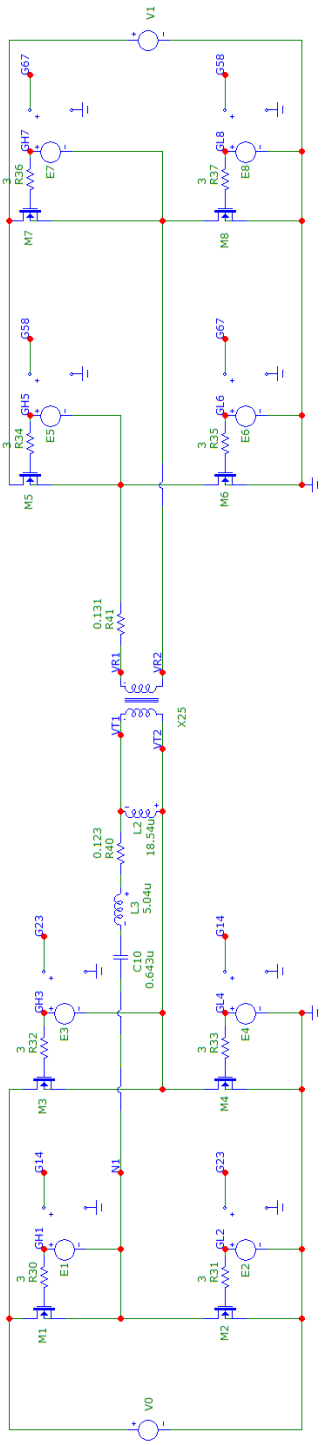

Figure 5.11: Dual Active Bridge schematic

5.2.2 Logic drive

The PWM signals required to control the transistors need to be created. Two different signals are required in order to drive the transistors of the input bridge: 180° out of phase for each half leg. Similarly two other signals for the secondary half bridge have the same purpose but can be shifted compared to the primary bridge.

As a transistor is not a perfect switching device and cannot switch instantly, dead-times have to be introduced in order to avoid cross-conduction in each half-bridge leg resulting in huge power losses. During this dead time, the currents continue to flow to the body diode of each transistor, also resulting in power losses. In order to create this dual function control, a **NE555** industry standard component was used in the asynchronous mode in order to create a saw-tooth [31]. This saw-tooth will be compared to some threshold in order to generate square waves that may be out of phase from -90° to 90°. After this, some R-C filters are used in order to create the mandatory dead-time.

The circuit that has been implemented is illustrated in Figure 5.12.

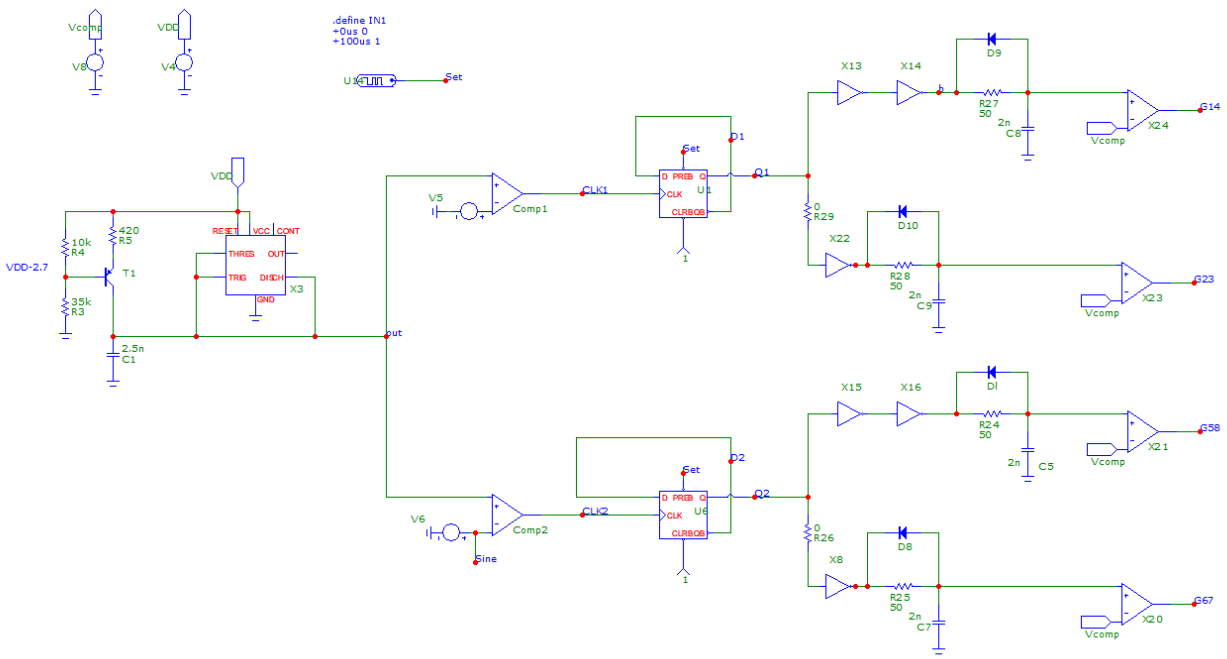

Figure 5.12: Logic-drive schematics

5.2.3 Results

The important waveforms of the signal generation can be inspected in Figure 5.13. In this Figure, the following signals are plotted: generated saw tooth (V(out)); PWM signals of each bridge (V(Q1/Q2)); and the sinusoidal signal in charge of the phase-shift between primary and secondary PWM signals(V(sine)).

For a better understanding of the simulation results, the sine wave is an image of the applied phase-shift between the primary and secondary bridges. On a half period of this signal, the phase shift goes from -90° to 90°. During the second half period, the phase shift turns back to -90°.

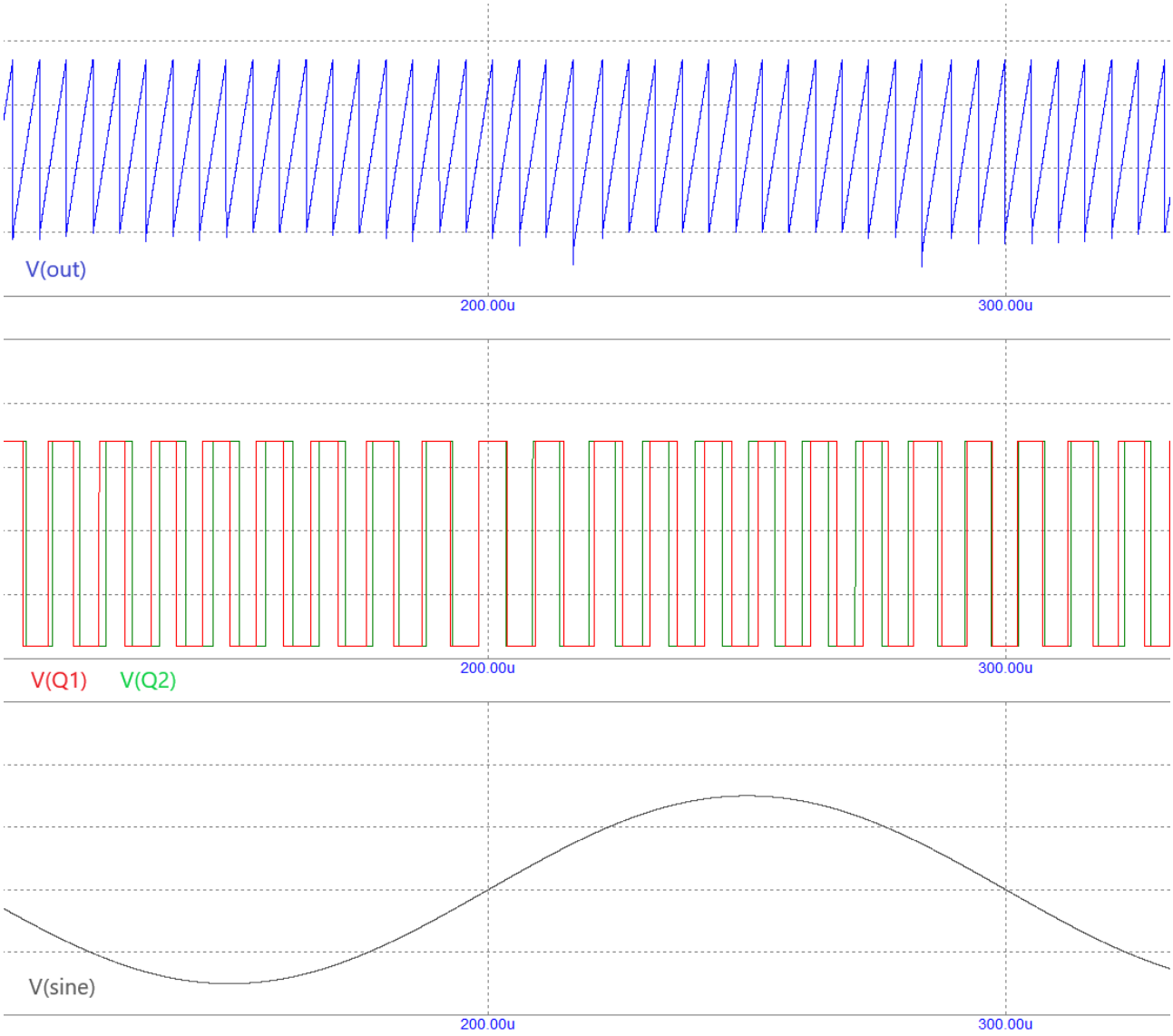

Figure 5.13: Gate driver schematics

Finally, the two following Figure 5.11 and Figure 5.14 plot the power transfer results respectively without and with resonance. We can observe the input and output power versus the phase-shift. We clearly observe the symetric bi-directional behavior of the DAB as expected.

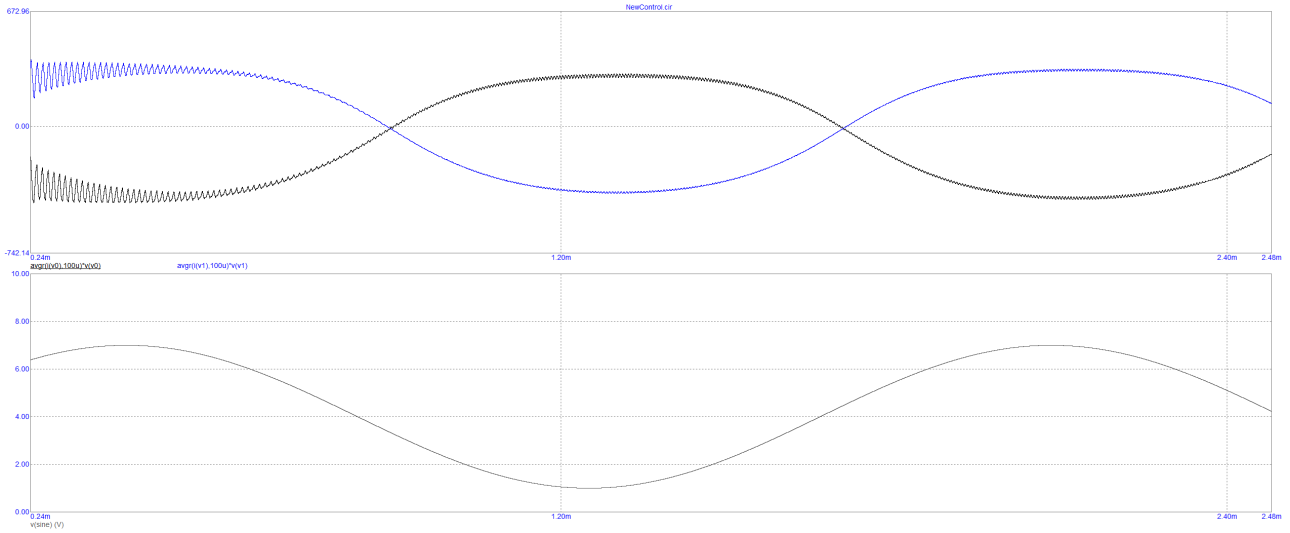

Figure 5.14: DAB power input-output vs phase-shift angle

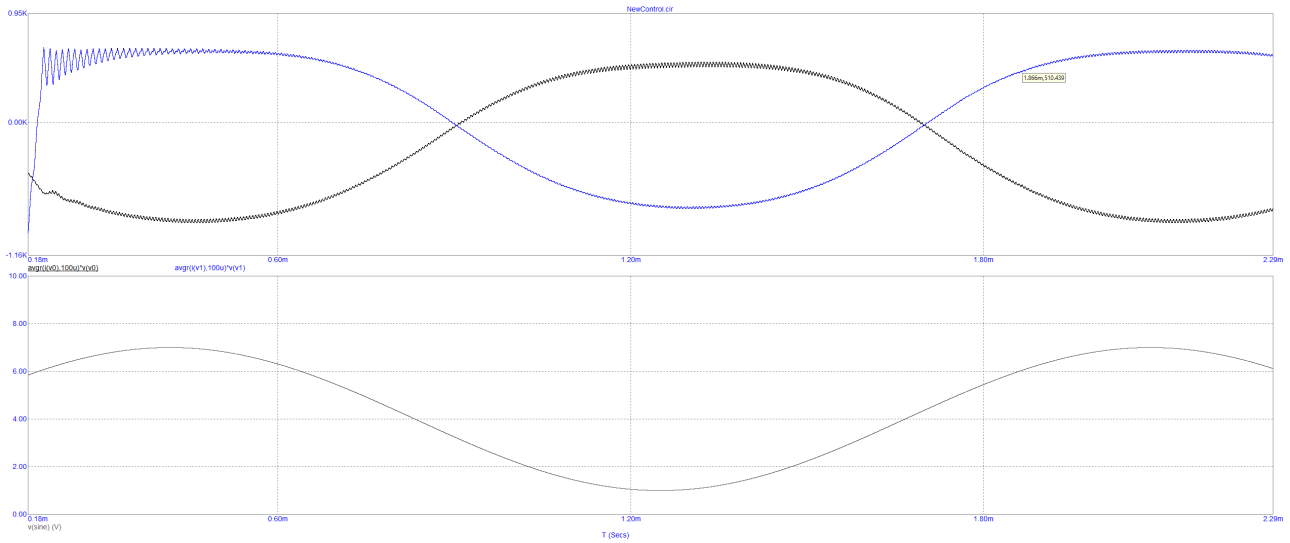

Figure 5.15: RDAB power input-output vs phase-shift angle

NOTE: As a personal feeling, the simulations, although important for comprehension and efficient design are not the most interesting part of projects like this one. Indeed, simulations come with a lot of trouble. Sometimes, the selected component is not available, the computations are very slow, they are a lot of simulation convergence problems.

5.3 Prototype

The objective of this Chapter is to present the prototype that has been realized and the related results of the different tests that have been performed. To this end, the results of the studied Dual Active Bridge will be compared with the results of a Single Active bridge to try to emphasise on the advantages and drawbacks of each architecture. Moreover, the results of the resonant variant of the DAB will also be shown.

5.3.1 Switching electronics

With the specifications of chapter 2.2, it can be seen that the transistors needs to withstand working voltages up to 50V. To realize the prototype, N-channel mosfets transistors manufactured by *Infineon* have been reused from the component stock of Thales Alenia Space (see Figure 5.16a). The specifications of those latter are in the following table and their datasheet can be found in Appendix B.

	V_{DS} $[V]$	I_D $[A]$	$R_{DS(ON)}$ $[m\Omega]$
Value	200	88	10.7

Table 5.3: Transistor specifications

Those transistors are not the most optimal for the range of voltage that will be used but they are way sufficient to prove the good behaviour of the DAB. Transistor voltage sizing has to take into account the working voltage of the DC rails and add the transients voltages due to the switching and parasitics, along with a safety margin. With increased voltage specification, a given technology exhibits a higher active channel resistance. Also an increased current specification leads to a bigger transistor and gate capacitor resulting in losses in the gate driver introduced below.

Each transistor needs to be driven by a device able to charge and discharge the gate capacitance. Two aspects can be observed: current drive capability and floating gate operation. The above mosfet are of type N because they exhibit a lower on-resistance. However the gate voltage has to be higher than the source voltage in order for the channel to be conductive even if their source is at the most positive DC rail. For these reasons, a gate driver component has to be used. Again, a standard module from Thales Alenia Space was reused with the following reference: *Kit master motherboard for low voltage drives scalable power demoboard* and also manufactured by *Infineon* (see Figure 5.16b).

(a) Half-bridge with two *IPB107N20N3 G* transistors

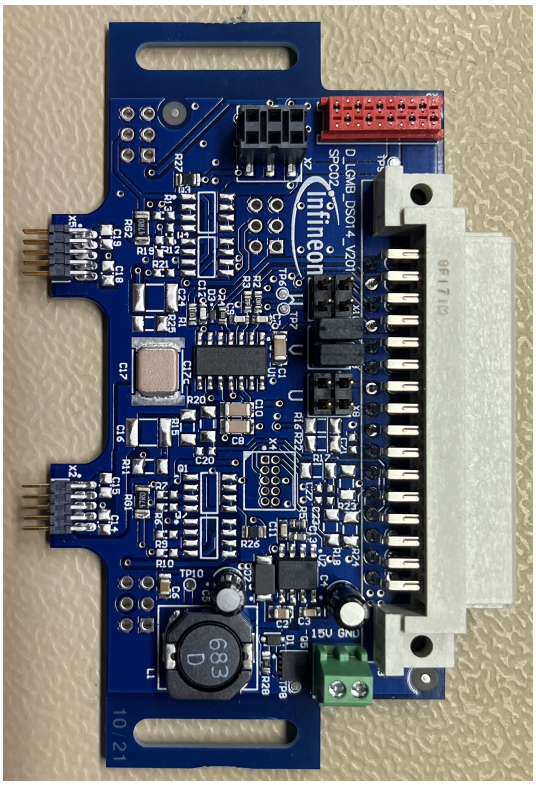

(b) Mother board with Gate drivers

Figure 5.16: Prototype electronics composants

For reference, the internal schematic of a gate driver is the following:

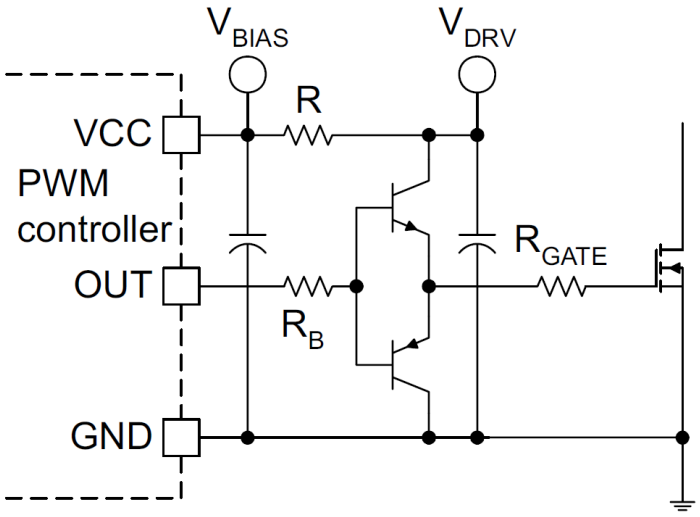

Figure 5.17: Gate driver schematics

5.3.2 PCB

As stated above, the gate-driver takes the PWM generated signals as input. A Printed Circuit Board (PCB) has been designed with Eagle and assembled in order to translate the bench signal generator to the required levels for the gate-driver and also introduce a configurable dead-time. The output of the PCB is 4 clocks in order to drive each pair of transistor (PCB schematics can be found in Appendix A.4.

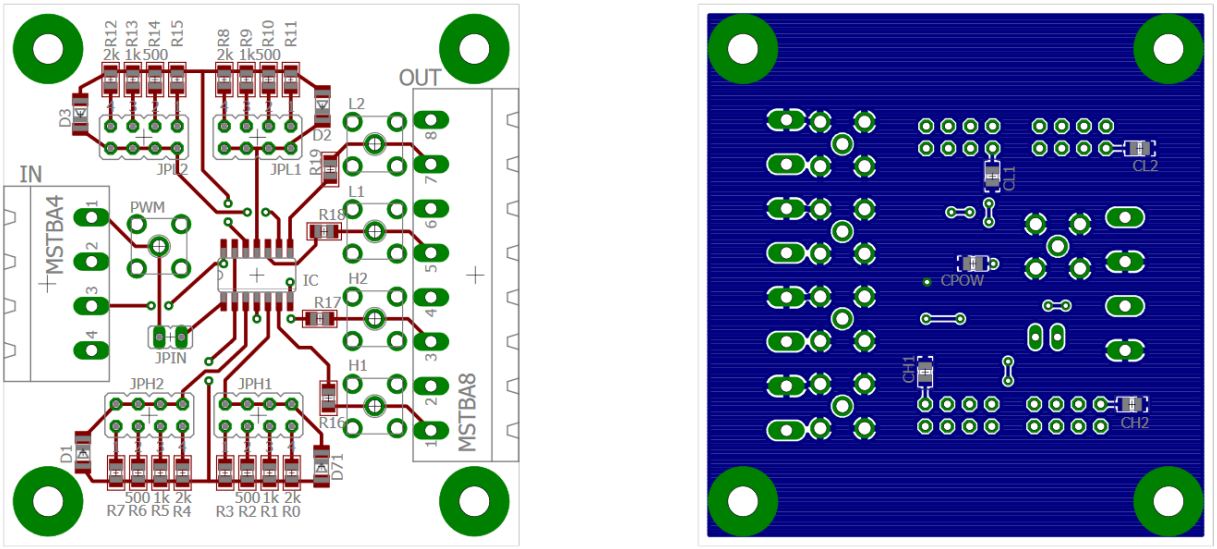

(a) Hysteresis effect

(b) Eddy current effect

Figure 5.18: Interface PCB

5.3.3 Complete setup

The following pictures depict both the global test setup and the top-view of the complete DAB assembly.

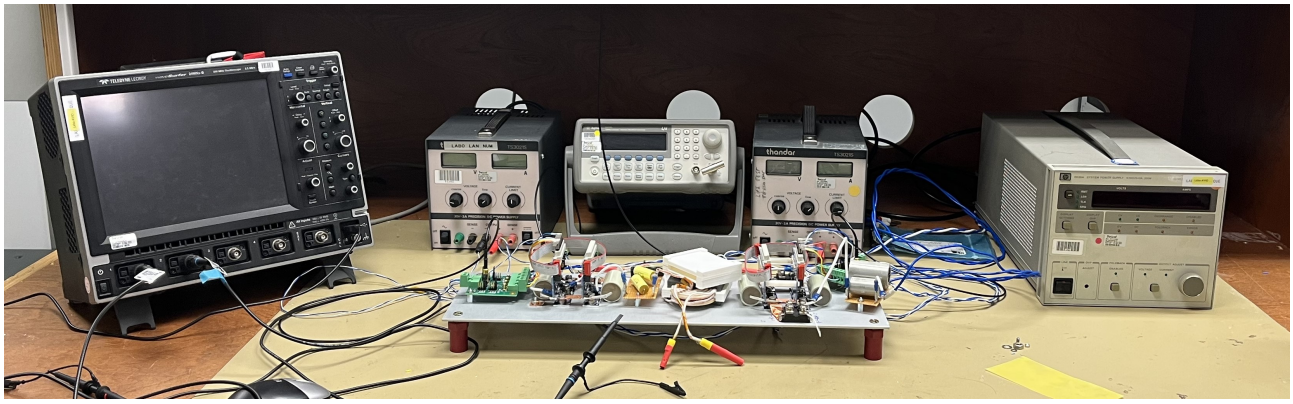

Figure 5.19: Test setup environment

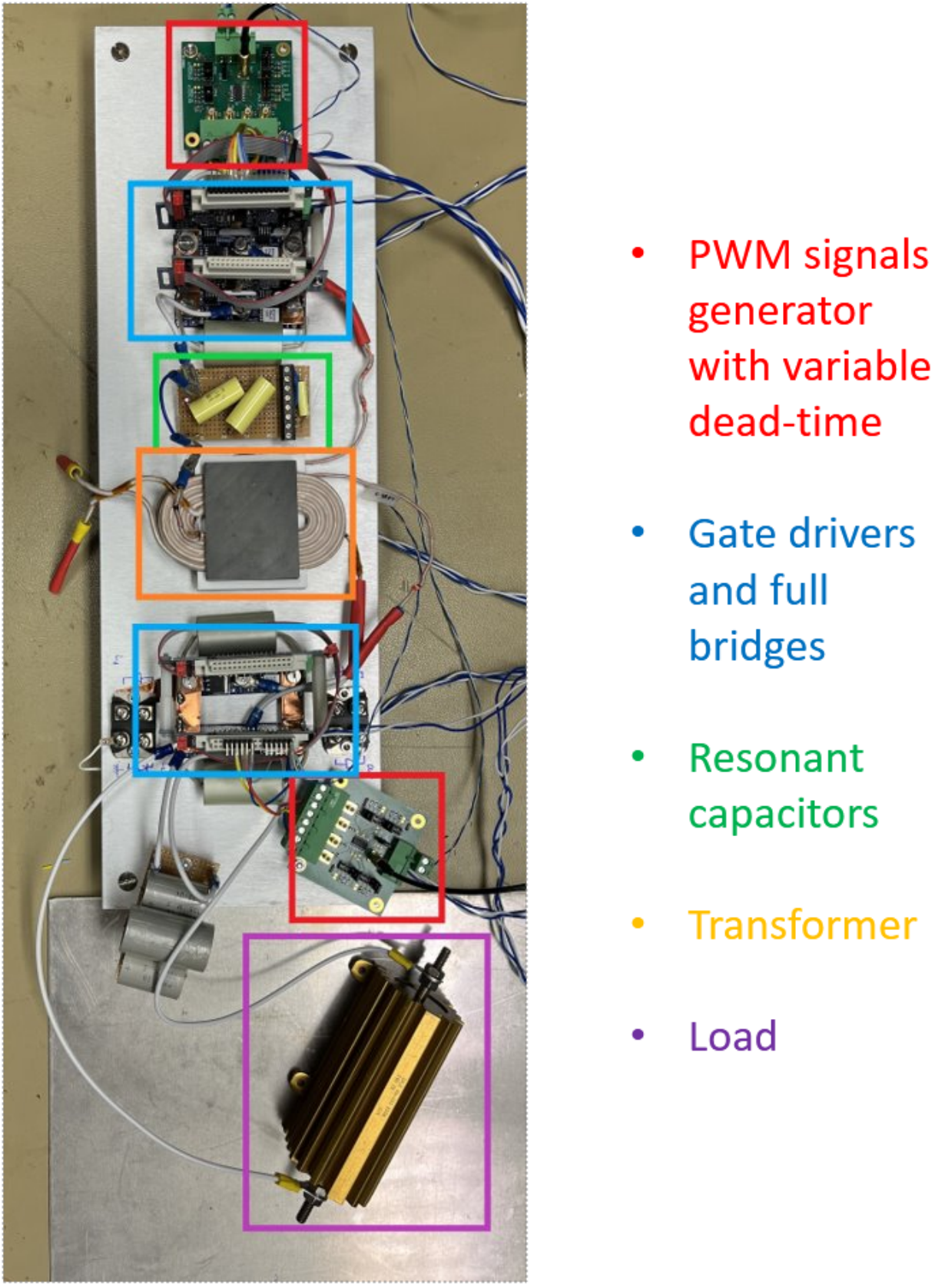

Figure 5.20: Final prototype of the resonant DAB

5.3.4 Debugging

This section will present the different tests that have been performed on the prototype in order to make it functional.

At first, the prototyped PCB had to be debugged in order to inspect if the different clock signals where correctly generated, with the correct dead-times. The output signals of the PCB is shown in Figure 5.21

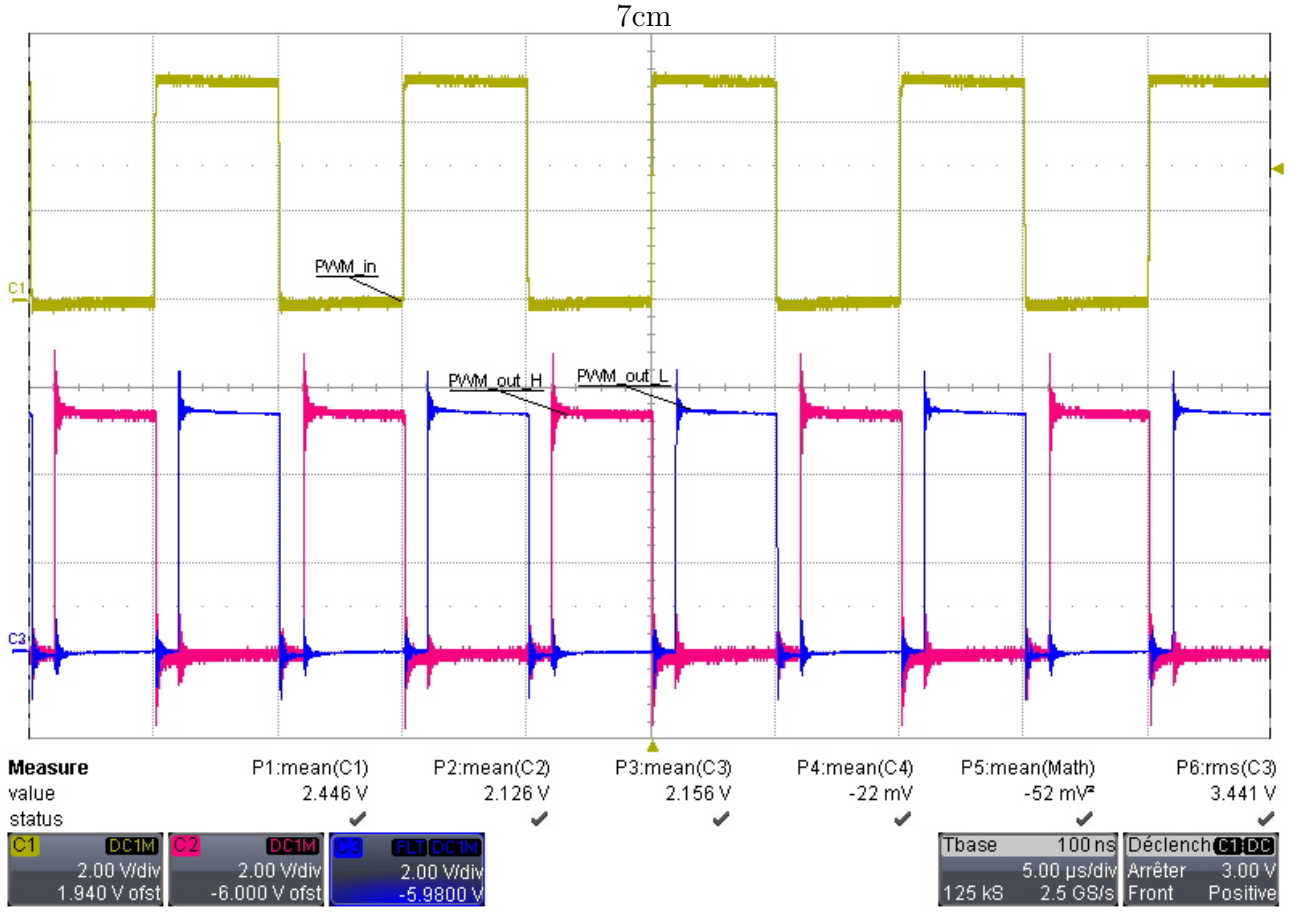

Figure 5.21: Logic control signals

A test was then performed as if the prototype was a SAB i.e. a full bridge on the primary side and a diode rectifier at the secondary side with the transformer between them. This is done disabling the secondary bridge drive and bypassing this last with diodes, resulting in a simple diode bridge. This test was performed in order to demonstrate the good behaviour of the gate drivers and of the full bridge at the primary side. As such, no resonance was introduced.

The corresponding waveforms are shown in the Figure 5.22:

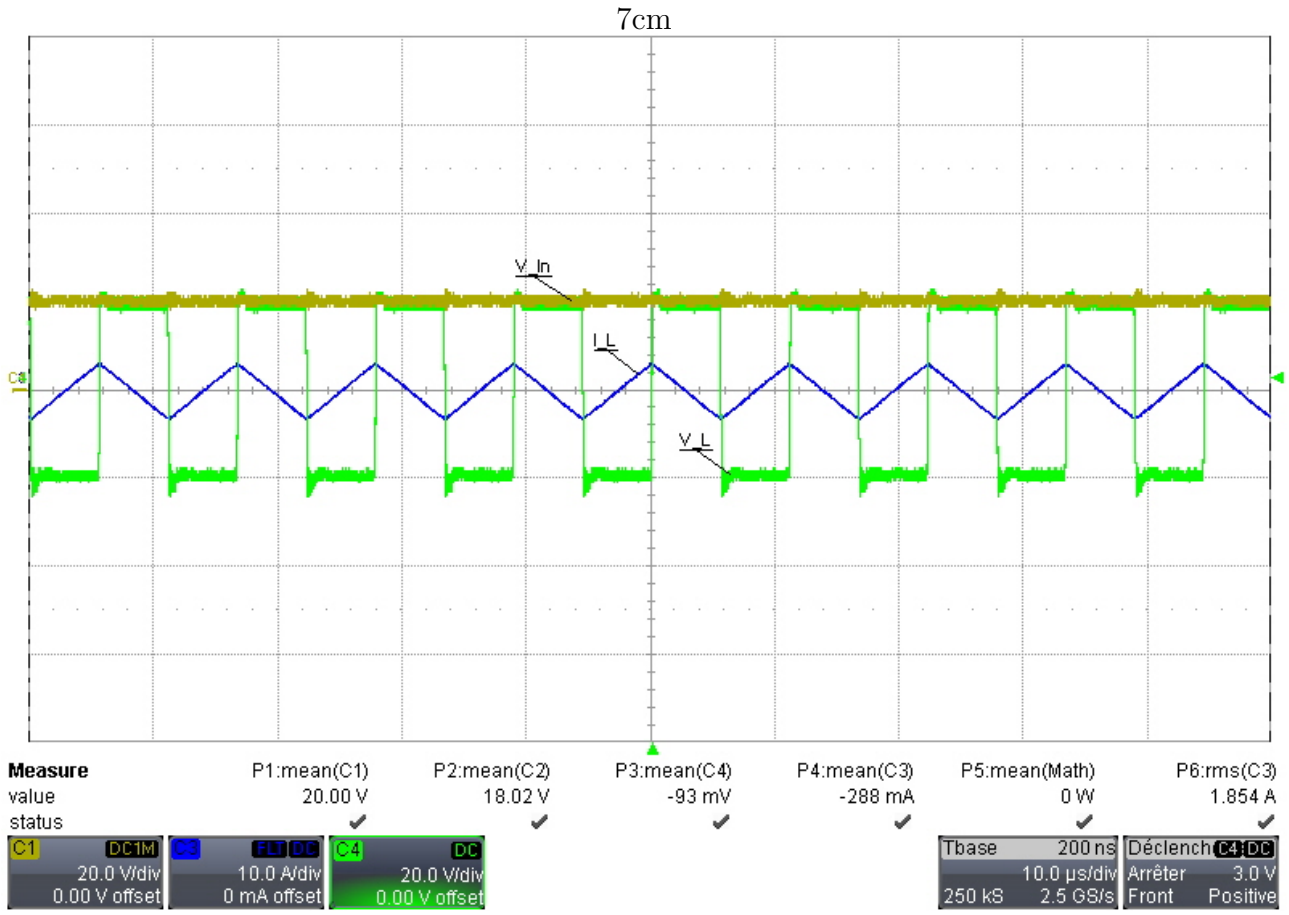

Figure 5.22: SAB waveforms

It can be seen that the transformer primary act as predicted as an inductance. The current is in a tooth saw shape due to the square voltage applied on the transformer primary side.

The third setup aimed to proof the good behaviour of the DAB mode. For this, the second full bridge (on the secondary side) control was added in order to achieve a controlled WPT in function of the phase shift between the control signals. The different waveforms are depicted in Figure 5.23.

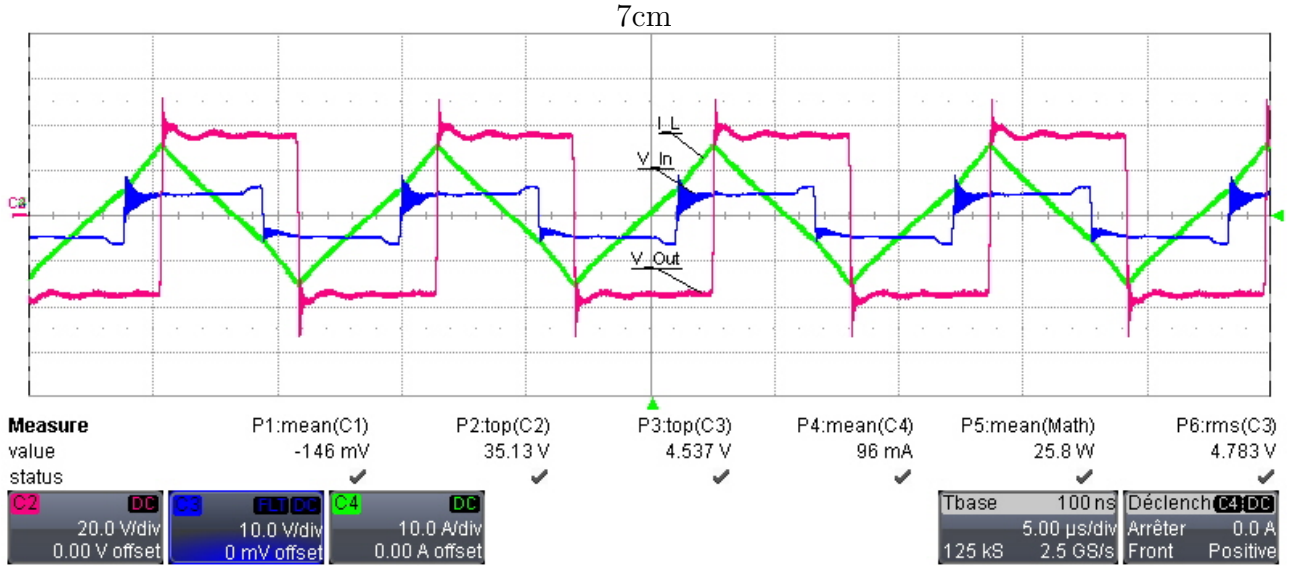

Figure 5.23: DAB waveforms

The phase shift between the two sources is clearly visible in Figure 5.23. The inductor current also exhibits the theoretical behaviour predicted with the four different phases explained in Section 3.3.3.2.

5.3.5 Tuning/improvement: resonance

In order to improve the efficency, capacitors have been added in order to achieve the final resonant DAB. As a reminder, the purpose of resonance is to improve the efficiency of the WPT, notably by introducing ZVS.

In order to explain the tuning process, the two next Figures show the waveform of the inductor current and primary side voltage. In Figure 5.24, the switching frequency is equal to the resonant frequency. It can be seen that in this configuration, the switching is not performed when the inductor current value is null resulting is switching losses. It can be observed that the purely inductive behavior of the non-resonant setup of Figure 5.23 exhibits a linear pure inductive current slope, while the (untuned) setup of Figure 5.24 shows a sinusoidal primary current. The crossing between voltage and currents is not occurring at zero current.

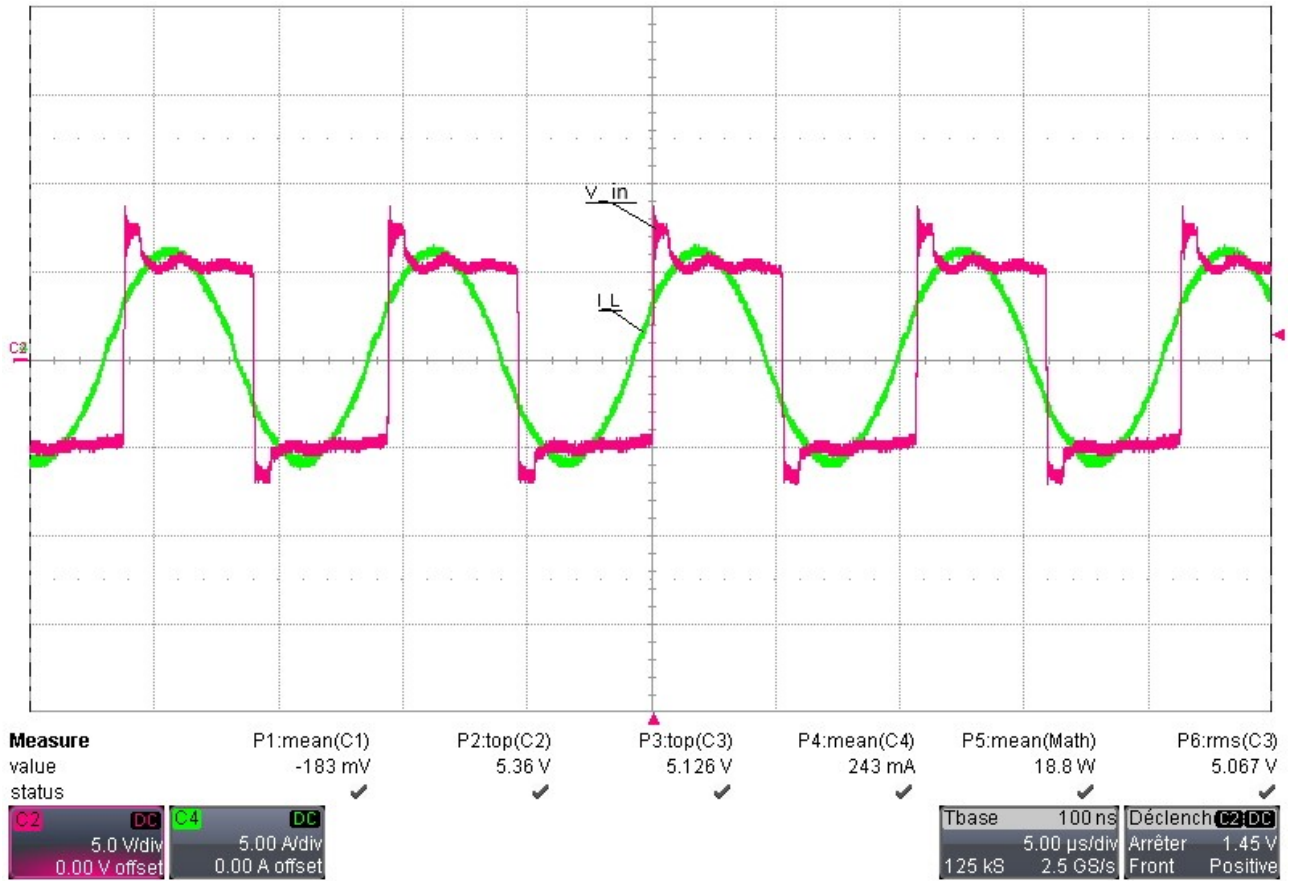

Figure 5.24: RDAB waveforms when $f_s = f_r$

In order to tune DAB resonance, the system need to adapted by modifying the switching frequency in order to obtained a tuned system. In Figure 5.25, the switching frequency is slightly raised, resulting in current and voltage crossing the X axis at the same moment: resonant tuned DAB with ZVS is achieved (RDAB).

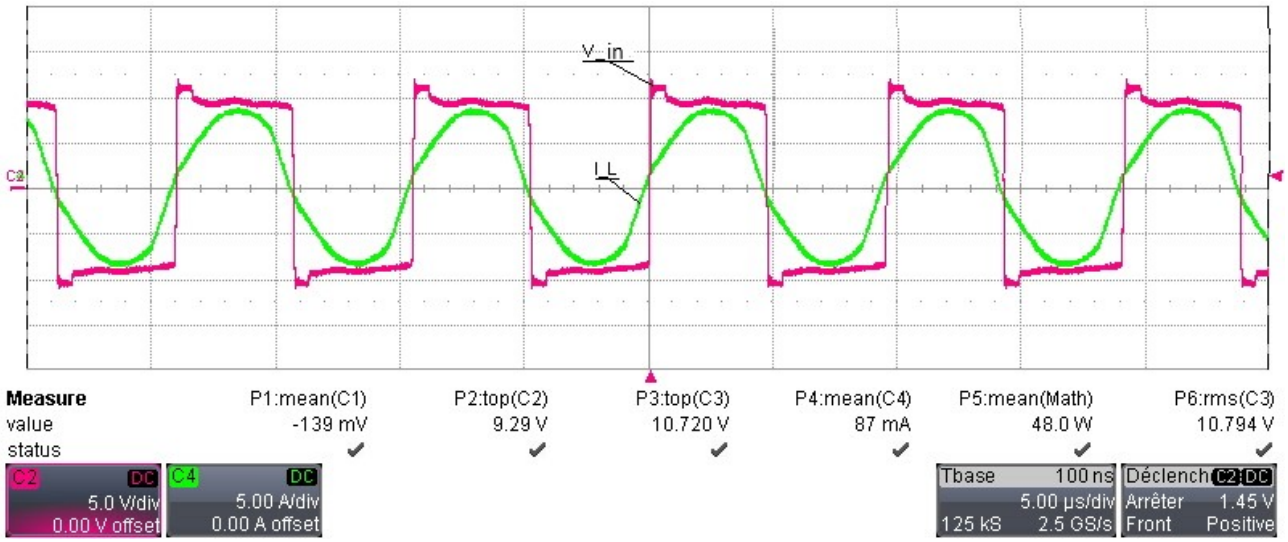

Figure 5.25: RDAB waveforms when $f_s > f_r$

5.4 Measurements

This section will present the different results obtained with the DAB and RDAB typologies. All the measurements were achieved in order to perform a transfer from a source to an active load as a proof of concept. Due to the lack of active source able to dissipate power, the bi-directional transfer was not tested without inverting the system in and out terminals (as already stated, the complete symmetry of the overall prototype and architecture ensure this will be the case). Nevertheless, a quick test has been achieved reversing the input and output terminals of the system at mid-power and confirms the bidirectional behavior. No further tests have been performed in order not to destroy the prototype if an unforeseen behavior occurred.

5.4.1 DAB

In the first test with the simple DAB, the received power in function of the phase-shift can been plotted with an input voltage equal to the output voltage of 20V.

It can be noticed that the curve in Figure 5.26 follows the behaviour expected (see Section 4). If a bi-directional prototype was tested, the curve in the other transfer direction is assumed to be the exact same one as below having undergone a central symmetry around (0,0).

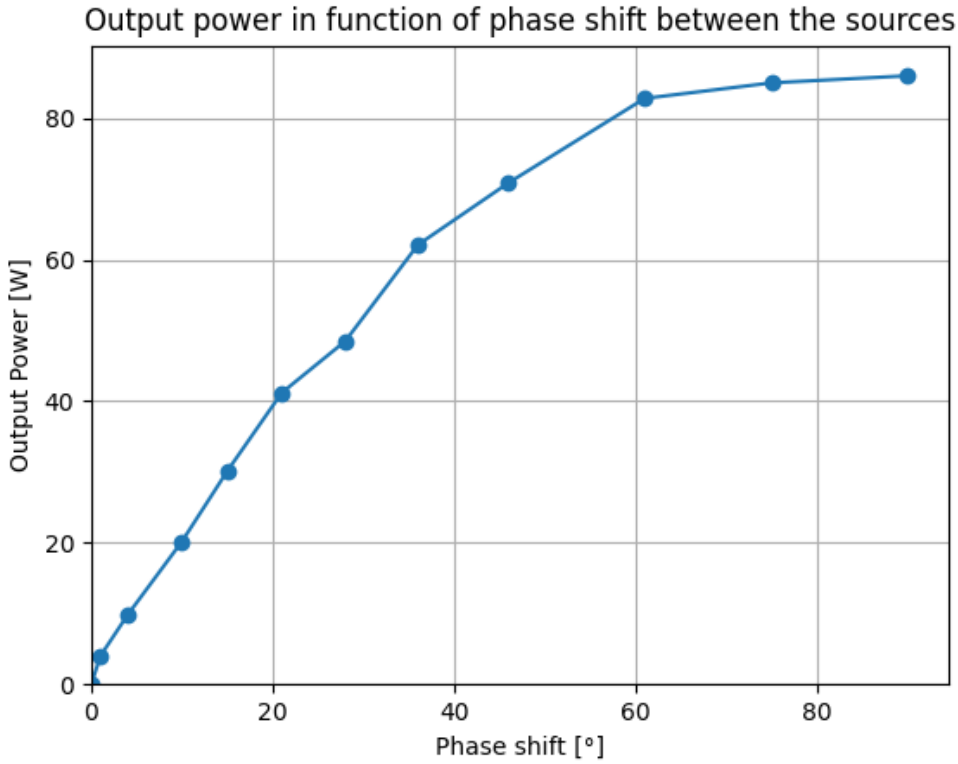

Figure 5.26: DAB power vs phase-shift (Vin=Vout=20V)

The simple DAB without any resonance measurements can be plotted in order to compare the efficiency of the power transfer with a constant input bus voltage (20V) and a variable output bridge voltage (ranging 20 to 50V). Results are shown in Figure 5.27.

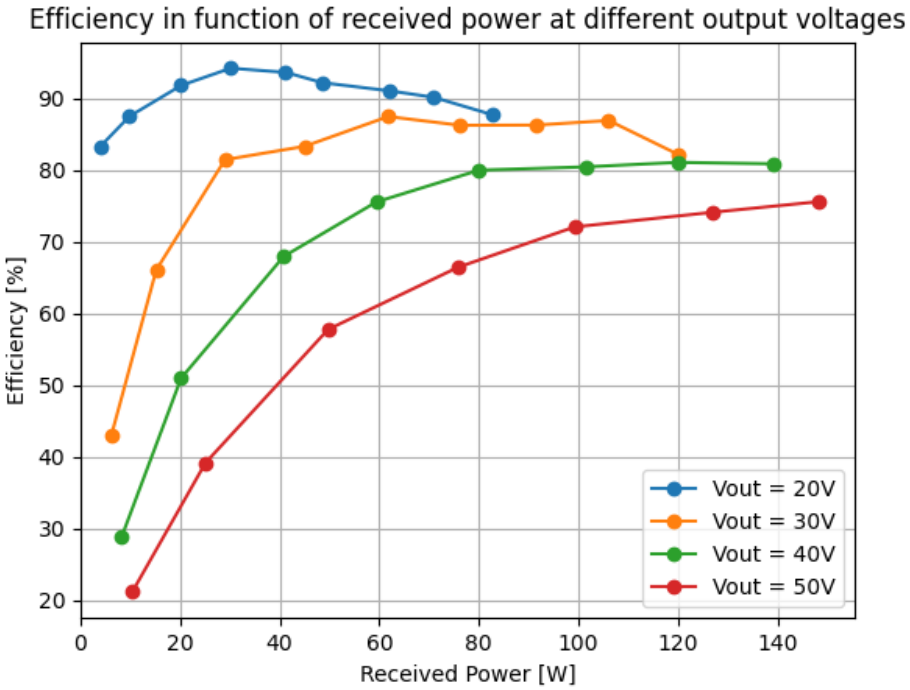

Figure 5.27: DAB efficiency vs power and output voltage

It can be seen in the figure that when the power transfer is performed with a gain bigger than the unity, the efficiency decreases. It can be explained by looking back at the power circle.

If the two source voltages are different, it can be seen that the circle will move along the Y-axis like in Figure 5.28. In this case, $U_2 = 0.8 \cdot U_1$ and the circle center has moved downward. This movement has a great impact on the power transfer. Indeed, the reactive power is permanently reduced, also reducing the losses due to reacting current.

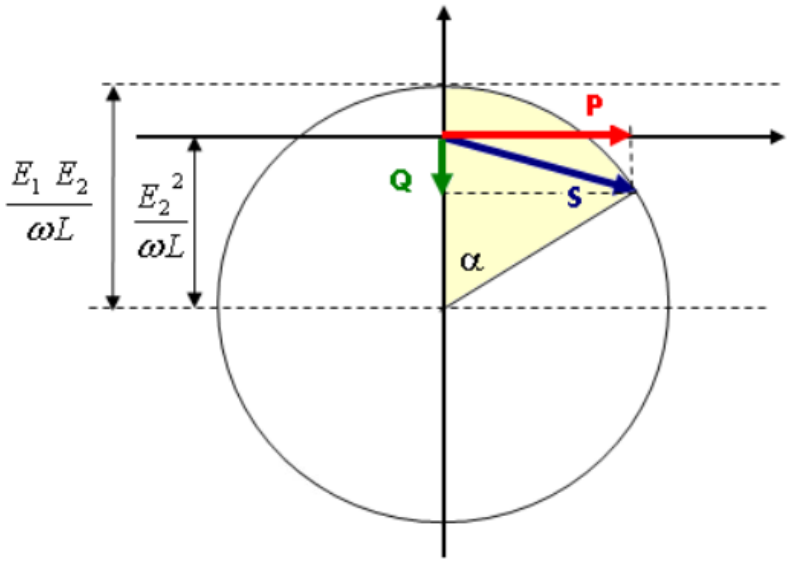

Figure 5.28: Shifted DAB power-circle

In the case where the input voltage is lower than the output voltage, the contrary happens. More reactive power is flowing and the losses are thus greater, lowering the efficiency.

The last test had for objective to analyse the impact of the switching frequency on the power transfer of the DAB without resonance. The efficiency of the transfer in function of the received power has been plotted at different frequencies with bus voltages equals to 20V in Figure 5.29.

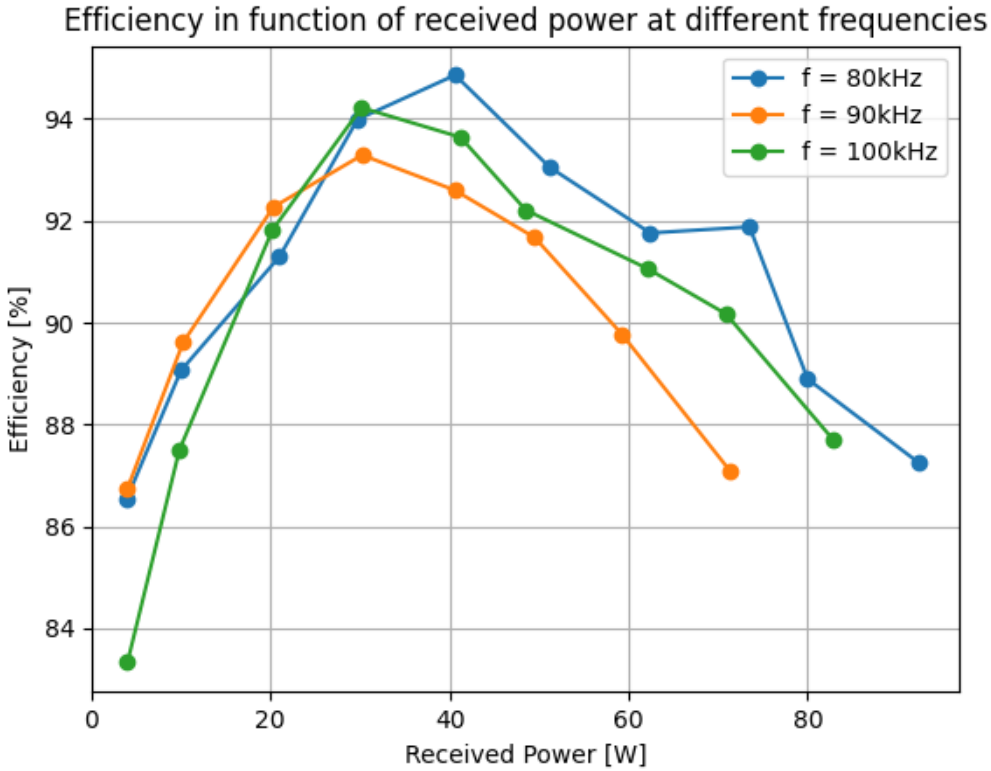

Figure 5.29: DAB efficiency vs switching frequency

It can be seen that they are slight differences in the results at different frequencies. The fact that the efficiency decrease from 80 to 90kHz and increase from 90 to 100kHz seems a little bit weird in a first time.

However, an hypothesis can be that when the frequency decreases, the inductor current increases and the Joule losses and transformer losses become majority. In opposition, when the frequency increases, switching losses becomes more important. No real conclusion can be drawn, this would require a larger range of frequencies to be evaluated and switching losses actively measured with a fast current probe in the mosfet sources.

5.4.2 RDAB

The DAB test setup was renewed with the resonance capacitor installed. In this configuration (with an air gap equal to 3mm), the resonant tank characteristics are the following:

	Leakage inductor	**Resonant capacitor**	**Resonant frequency**
Value	5.037 μH	0.643 μF	88.435 kHz

Table 5.4: Resonance characteristics of the RDAB

The output power in function of the phase shift between the power sources can be plotted like in Figure 5.30.

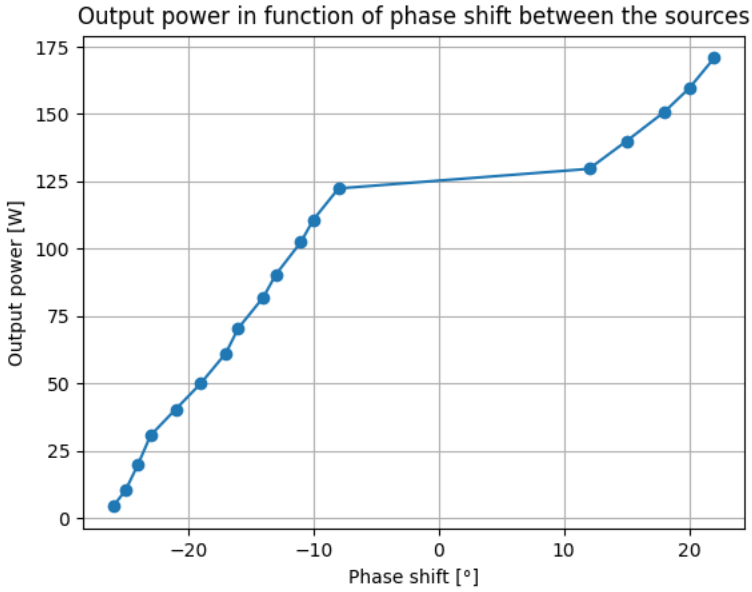

Figure 5.30: RDAB output power vs phase-shift

At first, the results were a little bit disappointing. Indeed, in absence of a voltage source at the receiver side, the power transfer induces a voltage gain at the output due to the resonance. The secondary bridge voltage will thus be bigger than the primary bridge voltage. By looking back again at Figure 5.28, if E_2 is different than E_1, the phasor's amplitude of the active power P is not null when the control signals are in phase.

The result is thus more comprehensive. In the beginning, the phase shift needs to be negative in order to lower the secondary bridge voltage and in the end, the transfer takes back its normal behaviour except around the point where the two signals are in phase. The phase-shift to output power is then as a consequence completely different in RDAB. This is not a problem at all because the complete system requires a closed loop PID control in order to achieve a controlled battery voltage and current.

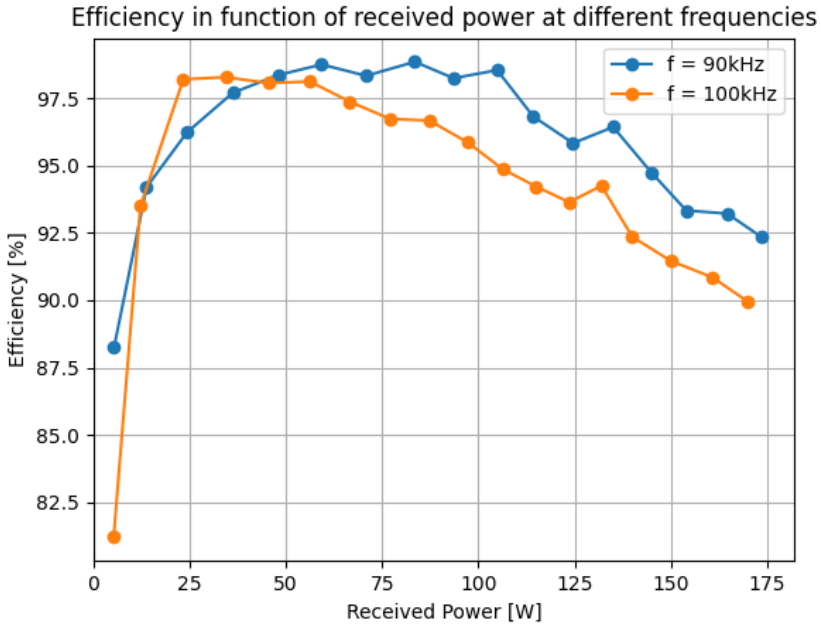

Figure 5.31: RDAB efficiency vs frequency and power

Figure 5.31 shows the efficiency in function of the received power when the bus voltages are equal to 20V with a RDAB at different frequencies. It can be seen that as predicted, the efficiency seems to be better when we are close to the resonant frequency.

Indeed, the resonant frequency is approximately of 88 kHz. There is no 1:1 matching of the switching frequency to the resonance frequency and also a sine wave distortion due to the dead time. Furthermore, the prototype dead-time has been selected relatively high for safety reasons. As seen in Figure 5.25, switching a little bit faster than the resonant frequency allows to perform ZVS and to reduce the switching losses. When the frequency increase, switching frequency walks away from the resonant frequency and the efficiency decreases.

5.4.3 Efficiency comparison

The last Figure 5.32 compares all the topologies.

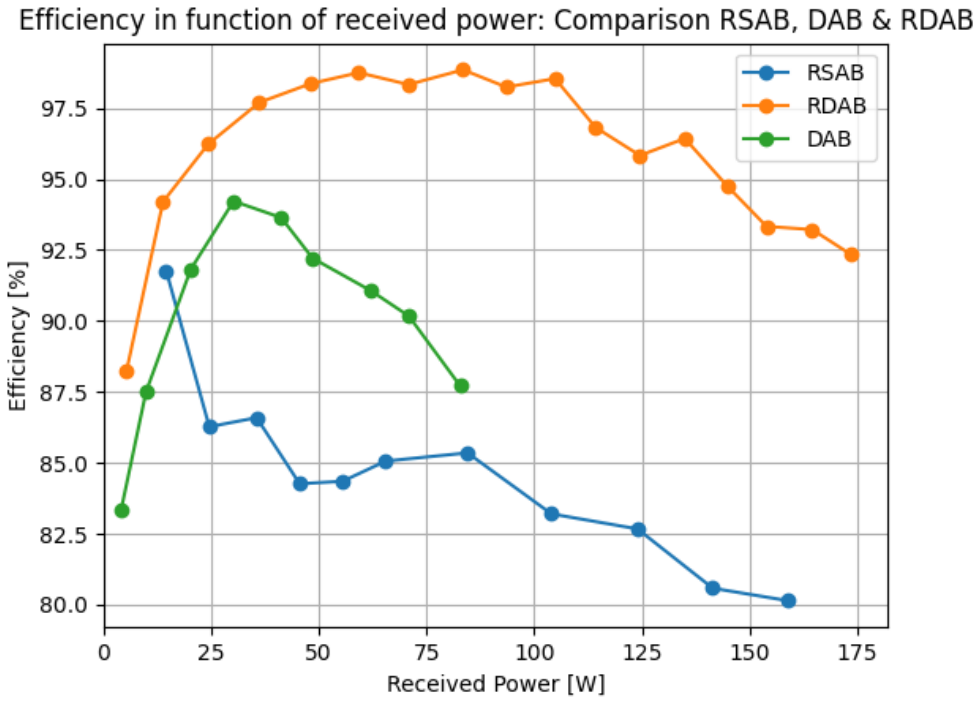

Figure 5.32: Toplogogies efficiencies vs output power

It can be seen that in every case, the DAB is more efficient than the SAB, even in its resonant form. Further, the RDAB is also more efficient than the simple DAB and almost catch up the buck-converters used in this kind of application that can reach 98 to 99% of efficiency. The much lower efficiency of the SAB is also explained though the output bridge setup. Indeed, we are using basic diodes, which are not optimal devices at all, exhibiting a high diode voltage. Better results would have been obtained with dedicated fast-switching schottky diodes.

While the RDAB seems to be the Holy Grail, it exhibits some really annoying drawbacks. The first and not the least is the resonance. Indeed, this kind of circuit is very sensitive to variations, way more complex and needs a lot of work to be tuned and compete the other topologies. For example, transformer to transformer leakage inductance variations along with tuning capacitor value over the full working temperature range can be a challenge.

Moreover, when the battery is in charge, the voltage of the receiving bus is rising. This implies a good closed-loop control of the power transfer, meaning a good control of the switching frequency and phase-shift that will be required to adapt the regulation over the charge / discharge curves. Nevertheless, since a digital closed loop processing and regulation is mandatory for the CCCV regulation, a second closed loop could be introduced in order to modify the switching frequency in order to always achieve the best efficiency.

6 | Conclusion

6.1 Engineering

To conclude this thesis, it is important to recall that the studied solution differs from state of the art on several aspects. The bi-directional behavior of the dual active bridge as well as the resonance in the latter is quite unusual and far from being very widespread. The achievements of this proof-of-concept demonstrated that through organised and sequenced analysis, characterisation, simulations, and practical implementation / tuning, targeted requirements can be fulfilled:

	Wanted	
	Low	**High**
Power transferred [W]	0	200
Main bus voltage [V]	20	50
Battery bus voltage [V]	20	50
Transferred current [A]	0	10
Frequency [kHz]	80	100
Efficiency [%]	20	97

Table 6.1: Proof of concept achievements

In addition to the first step of having a working basic WPT achieved from the simplest SAB architecture, step by step improvements have been introduced in order to be able to raise the complexity in a controlled manner. The thesis milestones where achieved as follows:

- State of the Art analysis;
- Mathematical models ;
- Simulations;
- Transformer characterization and mechanics;
- Characterisation of available components;
- Control and power electronics development and prototyping;
- Practical prototype debugging;
- Improvements;
  - Resonance for efficiency;
  - Dual active bridge;
  - ZVS.
- Prototype characterisation.

However, although the developed solution has several advantages such as a fairly direct and easy control of the transmitted power and matches the requirements, it is far from being complete.

First of all, as discussed in chapter 2.2, only the power part has been addressed in this work. So there is still a lot of work to achieve on the other functions that have not been covered.

Secondly, due to the use of off-the-shelf components such as transformer magnetics, transistor arrays, gate driver, the design is not optimal. For example, the planar transformer magnetics E core had no air-gap and a 3D-printed mechanical holder was designed as workaround to create this gap resulting in less ideal transformer; the transformer ratio has not been tuned for a better system. On the other hand, a breadboard exhibits a non ideal cabling resulting in parasitic inductances and resistances.

In addition, scaling is necessary in order to reach the required power for a space application because for safety reasons, the prototype could not be used with a voltage exceeding 50V and the transferred power could not exceed 200W due to bench instruments current limitations.

As a conclusion, the following subjects could be paths for improvement:

- Adapted dead-time;
- Inductive transfer of the isolated secondary bridge transistors;
- Better components selection;
- Detailed losses measurements;
- Temperature measurements and systems characteristics changes;
- Adapted planar transformer (core size and material, custom air-gap,...);
- Custom optimised dedicated PCB;
- Cost analysis and comparisons;
- System scaling.

6.2 Personal

From a more personal point of view, this work was an opportunity to observe how a more concrete project unfolded from the idea to the design of a functional prototype.

This work turned out to be much more complex than it first appeared. This was a great challenge because without any experience, it is easy to spread out and be lost on the subject instead of focusing on the most important points. So I had to adapt, step back in order to restart on a better basis. I learned the hard way it was mandatory to start with a simpler system and gradually add improvements in order to at the end create a working system.

I realized that simulation work alone is far from sufficient. Even if it makes it possible to better understand and design the system and is essential in order to develop a system, practice remains a concrete and instructive element in order to feel and in-depth understand the system behavior.

Finally, I am particularly grateful to the Thales team who supervised me and allowed me to develop a working prototype in the best conditions. I think that despite the fact that I still have a lot to learn, it has been of great benefit to me and allowed me to improve myself as a future engineer thanks to the many discussions and lessons that I have been able to acquire thanks to them.

Probably the most useful personal lesson I learned is that hard and soft skills must combine in order to achieve something: power is nothing without control!

Appendix

A Further results

A.1 Advanced comparison of WPT technologies

	Electric Field	Magnetic Field		Electromagnetic Field	
	Capacitive Coupling	Inductive Power Transfer	Resonant Inductive Coupling	RF Energy Transfer, Microwaves	Laser Beaming
Range	Short	Short	Mid	Far	Far
Frequency	Hz–MHz	kHz–MHz	kHz–MHz	GHz	>THz
Propagation	Non-radiative	Non-radiative	Non-radiative	Radiative	Radiative
Strength	Very high	Very high	High	Low	High
Multicast	No	No	Yes	Yes	No
Mobility	No	No	Yes	Yes	No
Coupling Device	Metal plate electrodes	Wire coils	Turned wire coils	Parabolic dishes, phased arrays, rectennas	Lasers, photocells, lenses
Safety	Yes	Yes	Yes	Safety constraints may apply	Safety constraints may apply

Figure A.1: Table of comparison between WPT technologies

A.2 Simulation files for the SAB

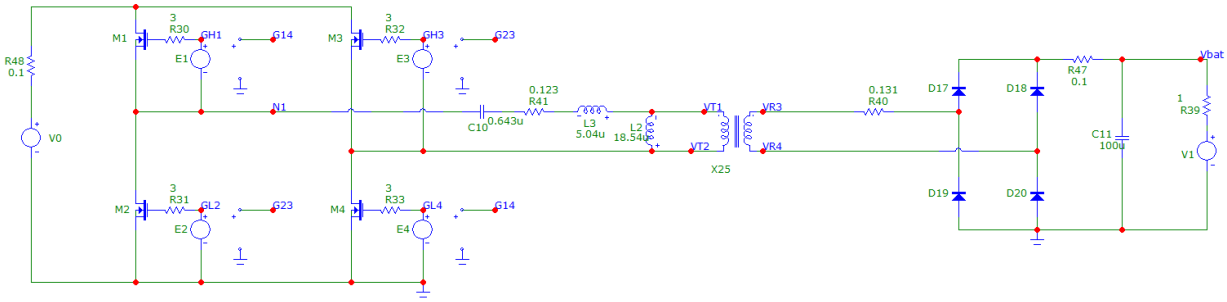

Figure A.2: SAB topology

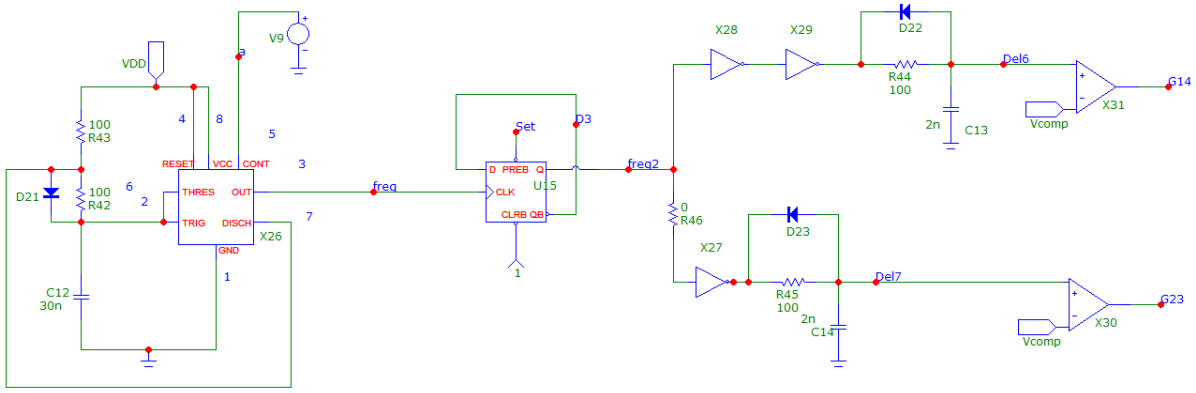

Figure A.3: PWM generation for SAB

A.3 Transformer inductance measurements

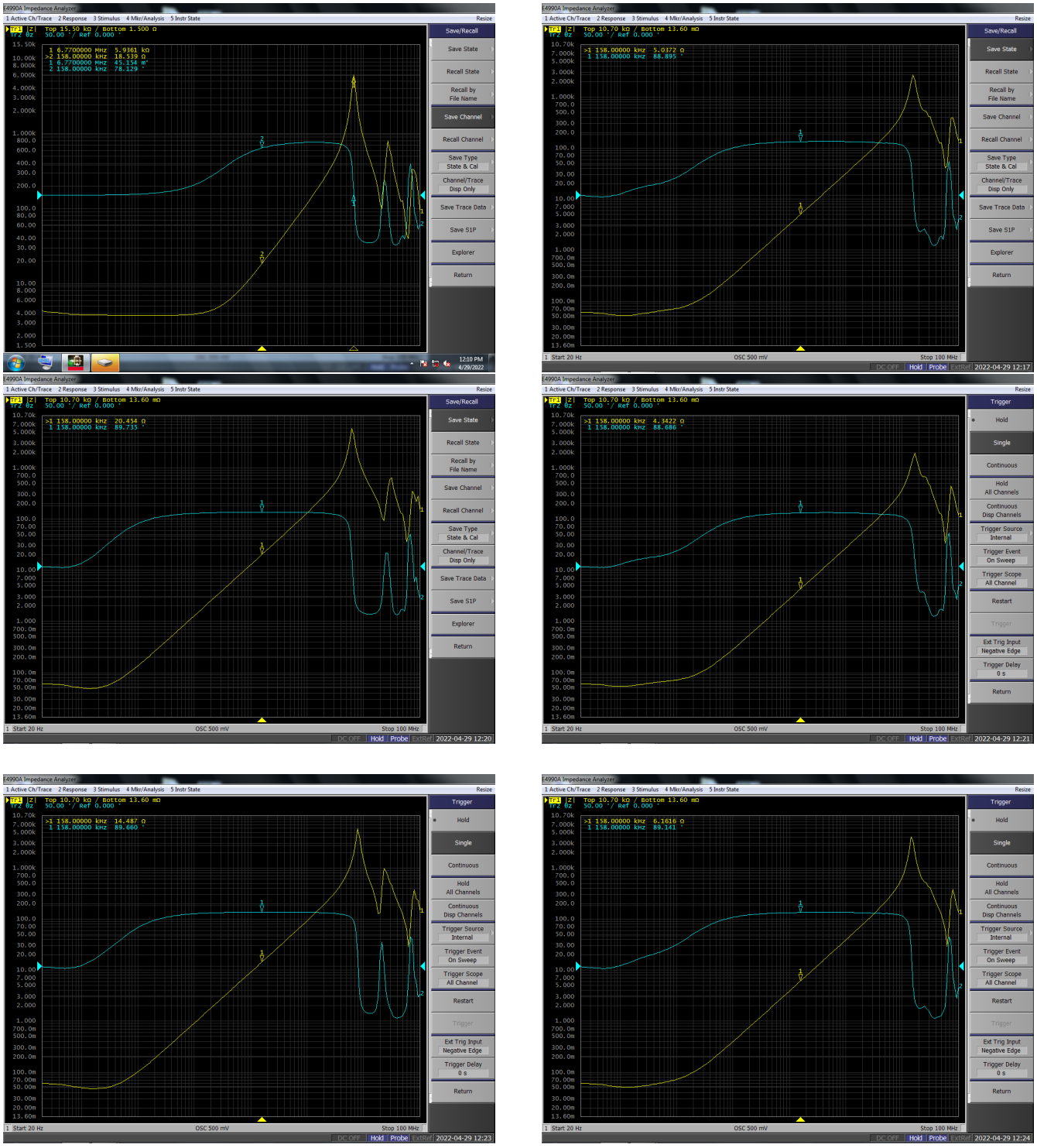

Figure A.4: Inductance measurements with other air gap

A.4 PCB schematic

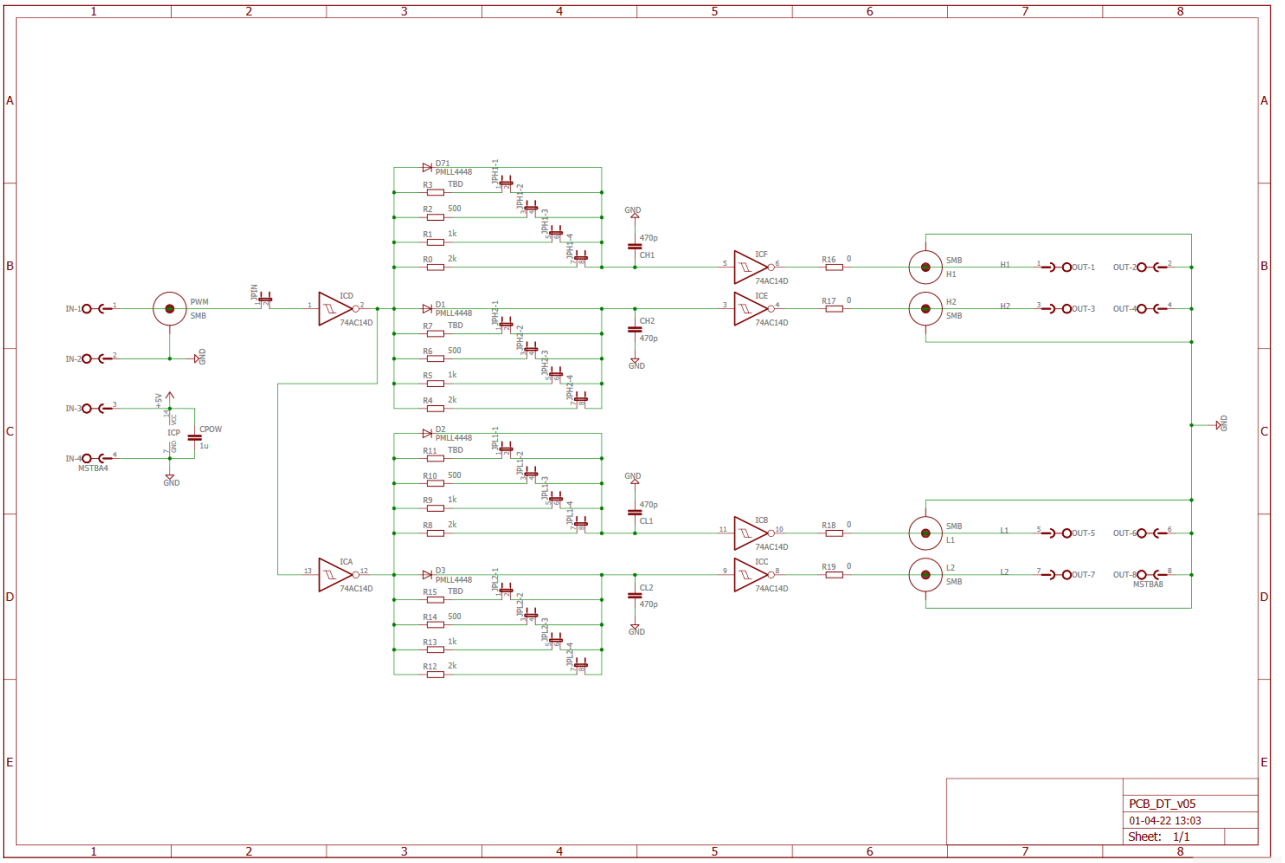

Figure A.5: Schematic of the PCB made by Benjamin Spitaels

A.5 Other prototype tests

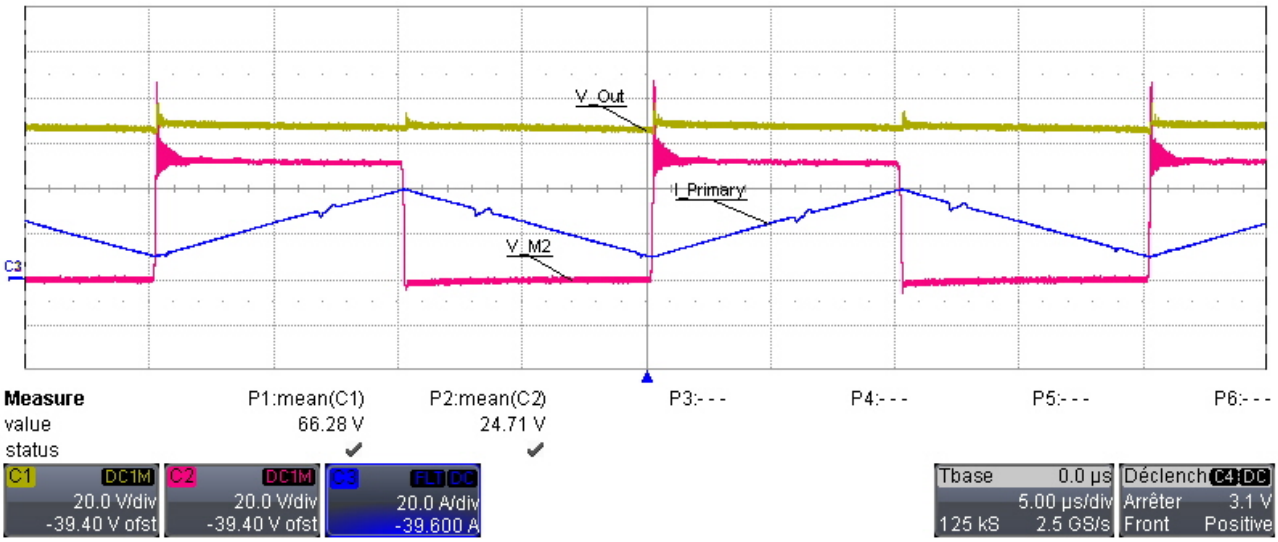

Figure A.6: No load test of the SAB

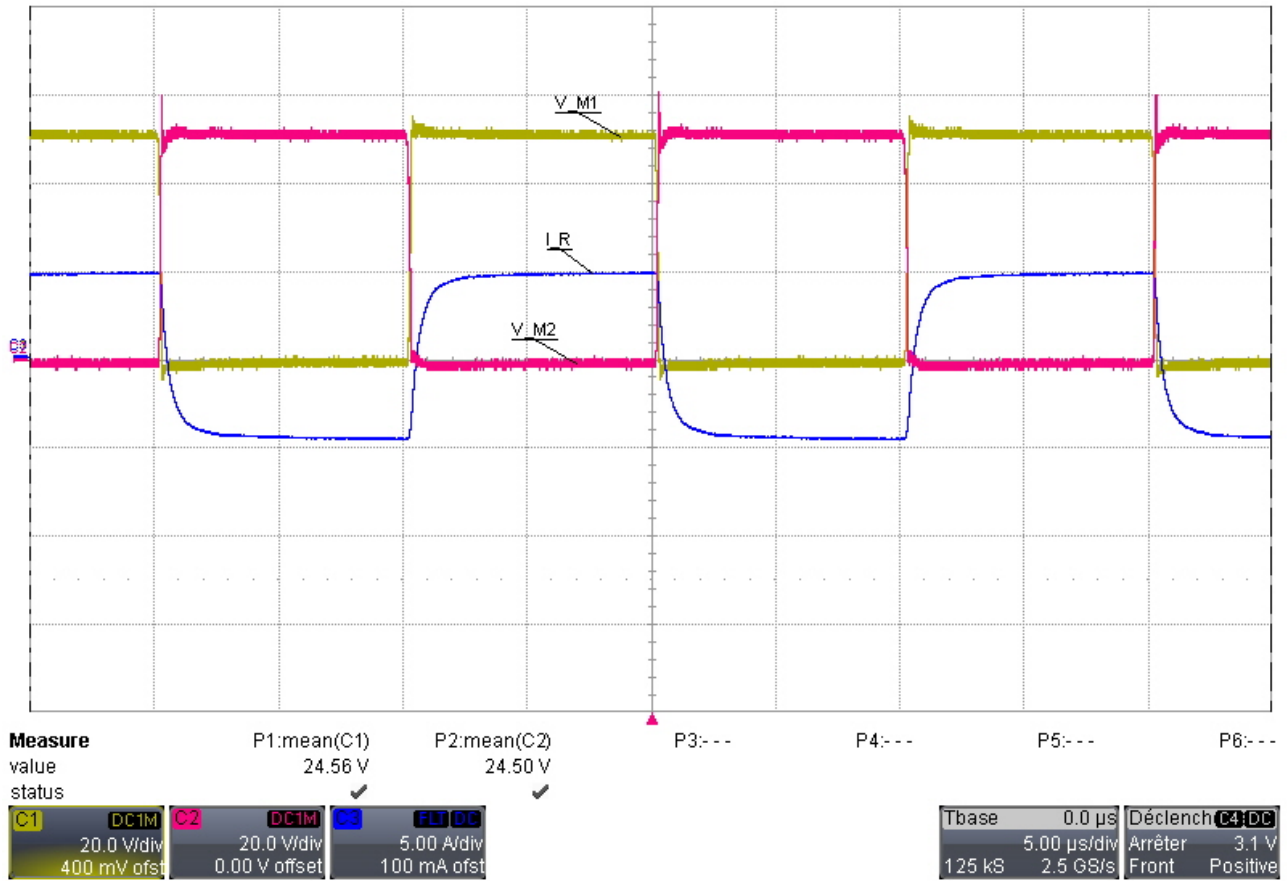

Figure A.7: Loaded test of the SAB

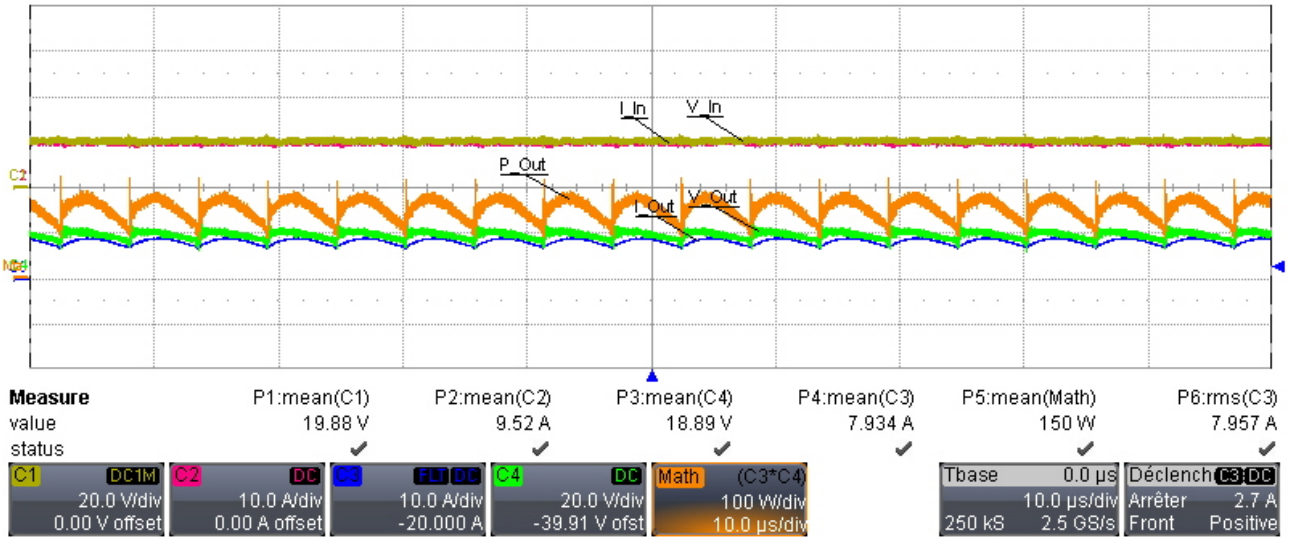

Figure A.8: Output power of the SAB

B Datasheets

B.1 Ferrite material

Core **E64/10/50 + PLT64/50/5**

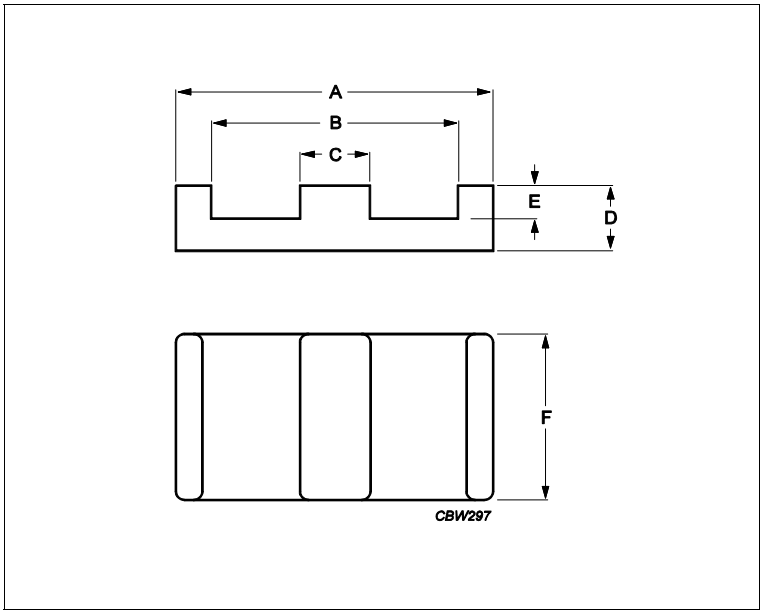

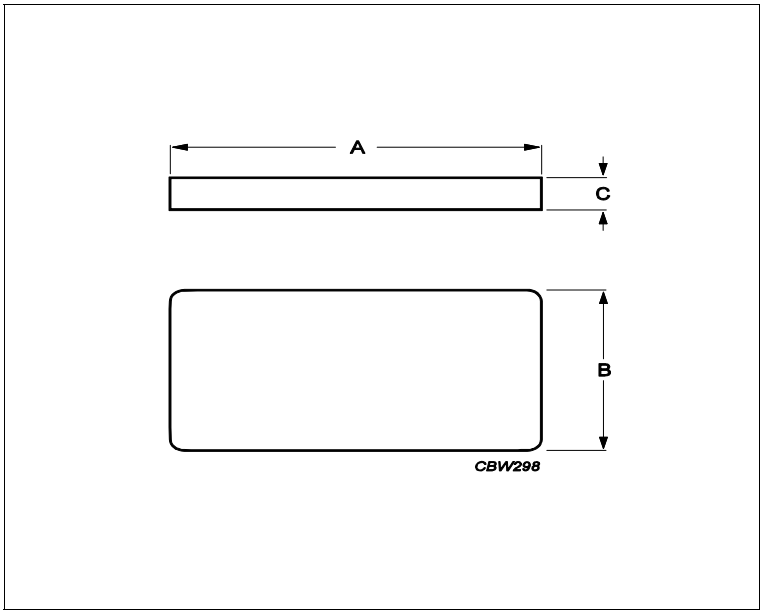

Effective parameters			
	Parameter	**Value**	**Unit**
Σ(I/A)	*core factor (C1)*	0.136	mm^{-1}
Ve	*effective volume*	35500	mm^3
Le	*effective length*	69.7	mm
Ae	*effective area*	519	mm^2
Amin	*minimum area*	519	mm^2
m	*E64/10/50*	≈ 100	g/pcs
m	*PLT64/50/5*	≈ 78	g/pcs

Dimensions for product: E64/10/50						
	Nom	**Tol +**	**Tol -**	**Max**	**Min**	**Unit**
A	64.00	1.30	1.30	65.30	62.70	mm
B	53.80	1.10	1.10	54.90	52.70	mm
C	10.20	0.20	0.20	10.40	10.00	mm
D	10.20	0.13	0.13	10.33	10.07	mm
E	5.10	0.13	0.13	5.23	4.97	mm
F	50.80	1.00	1.00	51.80	49.80	mm
Dimensions for product: PLT64/50/5						
	Nom	**Tol +**	**Tol -**	**Max**	**Min**	**Unit**
A	64.00	1.30	1.30	65.30	62.70	mm
B	50.80	1.00	1.00	51.80	49.80	mm

Core E64/10/50 + PLT64/50/5

Dimensions for product: PLT64/50/5						
	Nom	**Tol +**	**Tol -**	**Max**	**Min**	**Unit**
C	5.08	0.13	0.13	5.21	4.95	mm

Inductance factor				
Material	**Value**	**Tol +**	**Tol -**	**Unit**
3C92	12700	25%	25%	nH/turns²
3C95	18500	25%	25%	nH/turns²
3C96	15050	25%	25%	nH/turns²
3C97	18500	25%	25%	nH/turns²
3F36	9800	25%	25%	nH/turns²
3F4	7500	25%	25%	nH/turns²

Power loss: 3C92				
Measuring conditions			**Max**	**Unit**
100 kHz	200 mT	100 °C	18.000	W/set
Power loss: 3C95				
Measuring conditions			**Max**	**Unit**
100 kHz	200 mT	100 °C	17.000	W/set
100 kHz	200 mT	25 °C	18.000	W/set
Power loss: 3C96				
Measuring conditions			**Max**	**Unit**
100 kHz	200 mT	100 °C	16.000	W/set
400 kHz	50 mT	100 °C	8.200	W/set
Power loss: 3C97				
Measuring conditions			**Max**	**Unit**
100 kHz	200 mT	60 °C	18.000	W/set
100 kHz	200 mT	120 °C	17.000	W/set
100 kHz	200 mT	140 °C	21.000	W/set
Power loss: 3F36				
Measuring conditions			**Max**	**Unit**
500 kHz	50 mT	100 °C	6.500	W/set
500 kHz	100 mT	100 °C	45.000	W/set
Power loss: 3F4				
Measuring conditions			**Max**	**Unit**
1000 kHz	30 mT	100 °C	12.000	W/set
3000 kHz	10 mT	100 °C	19.000	W/set

Bsat					
Measuring conditions			**Material**	**Min**	**Unit**
25 kHz	250 A/m	100 °C	3C92	370	mT
25 kHz	250 A/m	100 °C	3C95	330	mT
25 kHz	250 A/m	100 °C	3C96	340	mT

Core **E64/10/50 + PLT64/50/5**

25 kHz	250 A/m	100 ºC	3C97	330	mT
25 kHz	250 A/m	100 ºC	3F36	340	mT
25 kHz	250 A/m	100 ºC	3F4	330	mT

B.2 Mother board

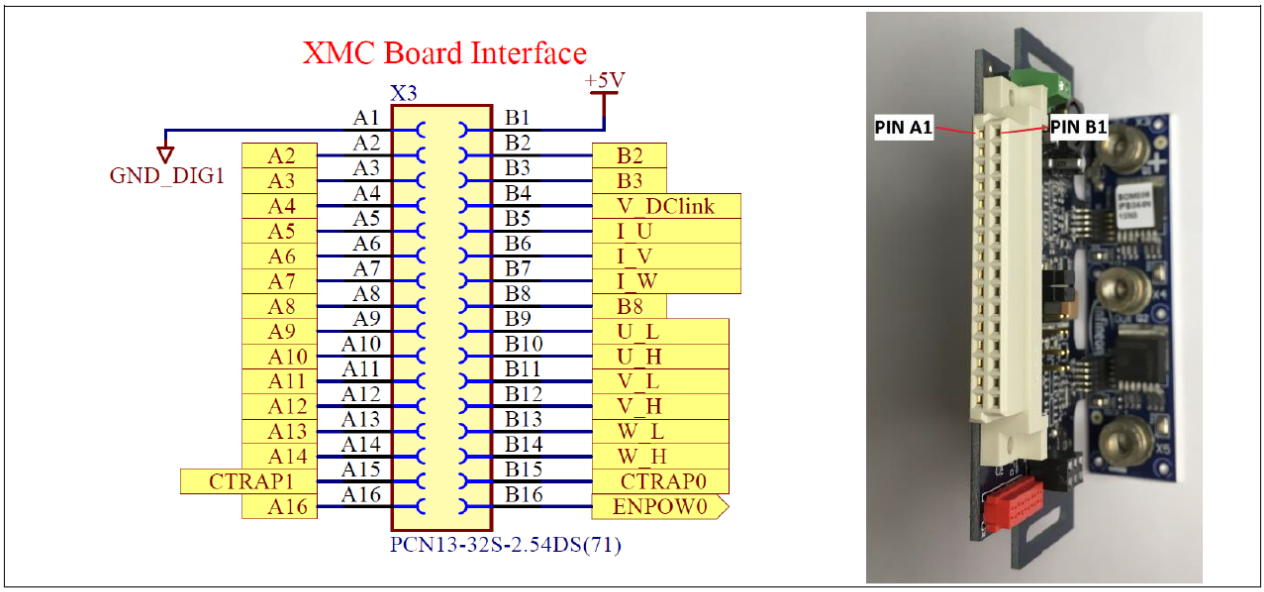

Figure 30 **XMC™ drive card connector pin-out – mother board PCB top view**

Figure B.1: Mother board connectives

B.3 Transistors

OptiMOS™3 Power-Transistor

Features

- N-channel, normal level
- Excellent gate charge x $R_{DS(on)}$ product (FOM)
- Very low on-resistance $R_{DS(on)}$
- 175 °C operating temperature
- Pb-free lead plating; RoHS compliant
- Qualified according to JEDEC[1] for target application
- Halogen-free according to IEC61249-2-21
- Ideal for high-frequency switching and synchronous rectification

Product Summary

V_{DS}	200	V
$R_{DS(on),max\ (TO263)}$	10.7	mΩ
I_D	88	A

RoHS

Halogen-Free

Type	IPB107N20N3 G	IPP110N20N3 G	IPI110N20N3 G
			
Package	PG-TO263-3	PG-TO220-3	PG-TO262-3
Marking	107N20N	110N20N	110N20N

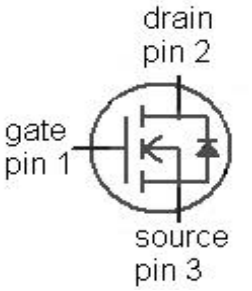

Maximum ratings, at T_j=25 °C, unless otherwise specified

Parameter	**Symbol**	**Conditions**	**Value**	**Unit**
Continuous drain current	I_D	T_C=25 °C	88	A
		T_C=100 °C	63	
Pulsed drain current[2]	$I_{D,pulse}$	T_C=25 °C	352	
Avalanche energy, single pulse	E_{AS}	I_D=80 A, R_{GS}=25 Ω	560	mJ
Reverse diode dv/dt	dv/dt		10	kV/µs
Gate source voltage	V_{GS}		±20	V
Power dissipation	P_{tot}	T_C=25 °C	300	W
Operating and storage temperature	T_j, T_{stg}		-55 ... 175	°C
IEC climatic category; DIN IEC 68-1			55/175/56	

[1] J-STD20 and JESD22

[2] See figure 3

Parameter	Symbol	Conditions	Values			Unit
			min.	typ.	max.	
Thermal characteristics						
Thermal resistance, junction - case	R_{thJC}		-	-	0.5	K/W
Thermal resistance, junction - ambient	R_{thJA}	minimal footprint	-	-	62	
		6 cm2 cooling area[3)]	-	-	40	
Electrical characteristics, at T_j=25 °C, unless otherwise specified						
Static characteristics						
Drain-source breakdown voltage	$V_{(BR)DSS}$	V_{GS}=0 V, I_D=1 mA	200	-	-	V
Gate threshold voltage	$V_{GS(th)}$	V_{DS}=V_{GS}, I_D=270 µA	2	3	4	
Zero gate voltage drain current	I_{DSS}	V_{DS}=160 V, V_{GS}=0 V, T_j=25 °C	-	0.1	1	µA
		V_{DS}=160 V, V_{GS}=0 V, T_j=125 °C	-	10	100	
Gate-source leakage current	I_{GSS}	V_{GS}=20 V, V_{DS}=0 V	-	1	100	nA
Drain-source on-state resistance	$R_{DS(on)}$	V_{GS}=10 V, I_D=88 A, (TO220, TO262)	-	9.9	11	mΩ
		V_{GS}=10 V, I_D=88 A, (TO263)	-	9.6	10.7	
Gate resistance	R_G		-	2.4	-	Ω
Transconductance	g_{fs}	$\|V_{DS}\|>2\|I_D\|R_{DS(on)max}$, I_D=88 A	71	141	-	S

[3)] Device on 40 mm x 40 mm x 1.5 mm epoxy PCB FR4 with 6 cm^2 (one layer, 70 µm thick) copper area for drain connection. PCB is vertical in still air.

Parameter	Symbol	Conditions	Values			Unit
			min.	typ.	max.	
Dynamic characteristics						
Input capacitance	C_{iss}	V_{GS}=0 V, V_{DS}=100 V, f=1 MHz	-	5340	7100	pF
Output capacitance	C_{oss}		-	401	533	
Reverse transfer capacitance	C_{rss}		-	5	-	
Turn-on delay time	$t_{d(on)}$	V_{DD}=100 V, V_{GS}=10 V, I_D=44 A, R_G=1.6 Ω	-	18	-	ns
Rise time	t_r		-	26	-	
Turn-off delay time	$t_{d(off)}$		-	41	-	
Fall time	t_f		-	11	-	
Gate Charge Characteristics[4)]						
Gate to source charge	Q_{gs}	V_{DD}=100 V, I_D=44 A, V_{GS}=0 to 10 V	-	23	-	nC
Gate to drain charge	Q_{gd}		-	8	-	
Switching charge	Q_{sw}		-	15	-	
Gate charge total	Q_g		-	65	87	
Gate plateau voltage	$V_{plateau}$		-	4.4	-	V
Output charge	Q_{oss}	V_{DD}=100 V, V_{GS}=0 V	-	162	216	nC
Reverse Diode						
Diode continous forward current	I_S	T_C=25 °C	-	-	88	A
Diode pulse current	$I_{S,pulse}$		-	-	352	
Diode forward voltage	V_{SD}	V_{GS}=0 V, I_F=88 A, T_j=25 °C	-	1	1.2	V
Reverse recovery time	t_{rr}	V_R=100 V, I_F=44 A, di_F/dt=100 A/µs	-	142		ns
Reverse recovery charge	Q_{rr}		-	640	-	nC

[4)] See figure 16 for gate charge parameter definition

References

[1] Surviving extreme conditions in space. https://www.esa.int/Science_Exploration/Space_Science/Extreme_space/Surviving_extreme_conditons_in_space. [Online; accessed 7-may-2022].

[2] Types of orbits. https://www.esa.int/Enabling_Support/Space_Transportation/Types_of_orbits. [Online; accessed 7-may-2022].

[3] Les satellites. https://metiers-du-spatial.com/missions/. [Online; accessed 7-may-2022].

[4] Deceuleneer Thibaut. Contactless power transfer through a rotating transformer for spatial application, 2016.

[5] Satellite Wiki contributors. Battery. https://www.aero.iitb.ac.in/satelliteWiki/index.php/Battery. [Online; accessed 3-november-2021].

[6] The qi wireless power transfer system power class 0 specification.

[7] Wikipedia contributors. Wireless power transfer. https://en.wikipedia.org/wiki/Wireless_power_transfer. [Online; accessed 20-october-2021].

[8] Minh T. Nguyen, Cuong V. Nguyen, Linh H. Truong, Anh M. Le, Toan V. Quyen, Antonino Masaracchia, and Keith A. Teague. Electromagnetic field based wpt technologies for uavs: A comprehensive survey. *Electronics*, 9(3), 2020.

[9] Ahmad Harb Issa Batarseh. *Power Electronics*. Springer Cham, 2 edition, 2018.

[10] Rupert Gouws Immanuel N. Jiya 1. Overview of power electronic switches: A summary of the past, state-of-the-art and illumination of the future. *micromachines*.

[11] E. Persson N. Mohan, R. Ayyanar. Soft-switching in dc-dc converters: Principles, practical topologies, design techniques, latest developments. [Online; accessed 29-march-2022].

[12] Alberto Rodriguez, Javier Sebastian, Diego G. Lamar, Marta M. Hernando, Iban Ayarzaguena, Igor Larrazabal, David Ortega, Jose M. Bermejo, and Francisco Vazquez. An overall analysis of the static characteristics of the single active bridge converter. *Electronics*, 11(4), 2022.

[13] Rupesh Jha, Mattia Forato, Satya Prakash, Hemant Dashora, and Giuseppe Buja. An analysis-supported design of a single active bridge (sab) converter. *Energies*, 15(2), 2022.

[14] Manish Bhardwaj Lei Song Harish Ramakrishnan, N. Navaneeth Kumar. Bidirectional, dual active bridge reference design for level 3 electric vehicle charging stations. pages 1–30.

[15] Jean-Paul Ferrieux Maximin Blanc, Yves Lembeye. Dual active bridge (dab) pour la conversion continu-continu. *Techniques de L'ingénieur*, pages 1–18.

[16] Abdel-Rahman Sam. Resonant llc converter: Operation and design. *Infineon Technologies North America*, pages 1–12.

[17] Bekemans Marc. Multidirectional tri-acces dc/dc converter. Thales Alenia Space Belgium.

[18] Bekamans Marc. *Convertisseurs DC-DC. LELEC2660-Power Electronics*.

[19] Dehez Bruno. *Rappels des notions de base. LELEC1310-Convertisseurs électromécaniques.*

[20] Cormier Gabriel. *Transformateur.*

[21] What is hysteresis loss: Factors & its applications. `https://www.elprocus.com/what-is-hysteresis-loss-factors-its-applications/`. [Online; accessed 25-May-2022].

[22] Wikipedia contributors. Courants de foucault. `https://fr.wikipedia.org/wiki/Courants_de_Foucault`. [Online; accessed 25-May-2022].

[23] Avaneet Ranjan Anish.K, Rakesh Bute. Litz wire. `https://www.elektrisola.com/fr/Litz-Wire/Info#terminology`. [Online; accessed 3-may-2022].

[24] Yih-Her Yan, Hung-Liang Cheng, Shun-Yu Chan, Yu-Da Chen, and Yong-Nong Chang. Design of an isolated bidirectional symmetric resonant converter. *Applied Sciences*, 10(22), 2020.

[25] Hao-Tang Chang, Tsorng-Juu Liang, and Wei-Chin Yang. Design and implementation of bidirectional dc-dc clllc resonant converter. In *2018 IEEE Energy Conversion Congress and Exposition (ECCE)*, pages 2712–2719, 2018.

[26] Yuanjun Liu, Guiping Du, Xueyi Wang, and Yanxiong Lei. Analysis and design of high-efficiency bidirectional gan-based cllc resonant converter. *Energies*, 12(20), 2019.

[27] Sheng-Yang Yu Manish Bhardwaj. Bidirectional clllc resonant dual active bridge (dab) reference design for hev/ev onboard charger. *Texas Instruments*, pages 1–14.

[28] Resonant circuits and soft switching. *Toshiba*, pages 1–9.

[29] G. Barrere. Measuring transformer coupling factor k. [Online; accessed 13-april-2022].

[30] Bekemans Marc. Caractérisation et identification haute-fréquence du transformateur z2. Belgium Transport.

[31] Avaneet Ranjan Anish.K, Rakesh Bute. Saw tooth wave generator using ne555. `https://www.circuitstoday.com/saw-tooth-wave-generator-using-ne555`. [Online; accessed 27-march-2022].

[32] Haru Matsumoto, Christopher Jones, Holger Klinck, David K. Mellinger, Robert P. Dziak, and Christian Meinig. Tracking beaked whales with a passive acoustic profiler float. 133(2):731.

UNIVERSITÉ CATHOLIQUE DE LOUVAIN
École polytechnique de Louvain
Rue Archimède, 1 bte L6.11.01, 1348 Louvain-la-Neuve, Belgique | **www.uclouvain.be/epl**